'Prajna' - Journal of Pure & Applied Sciences, 16 (2008) 1-8

AN INVESTIGATION ON THE TERMITICIDAL EFFECTS OF CERTAIN WEED PLANTS

Rupal A.Vasant and A.V.R.L. Narasimhacharya
BRD School of Biosciences, Sardar Patel University, Vallabh Vidyanagar-388 120

Abstract

The present study was undertaken to investigate the termiticidal properties of certain plants viz., *Calotropis procera, Ricinus communis, Parthenium hysterophorus* and *Prosopis juliflora.* Chloroform, methanol, petroleum ether, n-hexane, n-butanol and distilled water extracts of the leaves were prepared and for each extract, three concentrations i.e., 0.5%, 1% and 5% were tested using 'no-choice' method with filter paper dipped in respective extracts for 24 and 48h. Of the various extracts tested for mortality of termites, 5% $CHCl_3$ extracts of all the plants were found to be highly effective.

Introduction

Termites are global problem all around the world and especially in tropical areas where relative humidity is higher. As regards the habitats, there are mainly two kinds of termites, viz., the wood dwellers and the ground dwellers. Further, the wood dwellers are categorized as damp wood and dry wood dwellers whereas the ground dwellers are classified as subterranean, mound and carton-nest builders [1].

The most important need of termites is cellulose in their diet. This can be in the form of rotting plants, wood, paper products (especially when non-dyed), and cloth such as rayon and other natural fibers [2]. Termites have enormous potential value to man, in the degradation and bioconversion of lignocelluosic wastes. Termites may have played a more important role in Paleoecology and they continue to play a major role in the functioning of terrestrial ecosystems [3]. The persistent use of chemical termiticides is of environmental concern and has resulted in the need to search for plant-derived compounds as alternative in termite control [4]. Insecticide management practices differ enormously, but there are several problems with their use; they include poisoning, persistence, resistance and re-entry, inappropriate disposal and the secondary effects of environmental degradation and surface and ground water contamination. Termite resistant woods are said to contain alleochemicals such as quinones, flavonoids and terpenoids that possess natural repellent and toxic properties [5, 6]. Use of plant-derived natural products is preferred because of their biodegradability, safety and target-specificity as they do not pollute the environment and are not harmful to animals or to people using them. They are also a very cheap source as control measures. The present study was therefore, undertaken to investigate the termiticidal properties of certain plants viz., *Calotropis procera, Ricinus communis, Parthenium hysterophorus* and *Prosopis juliflora.*

Materials and Methods

Plants

Leaves of *Calotropis procera* (Ait.) R. Br. (F- Asclepidaceae), *Ricinus communis,* L. (F-Euphorbeaceae), *Parthenium hysterophorus* L. (F-Astraceae) *and Prosopis juliflora* (Sw.) DC. (F-Mimosaceae) were collected from areas adjoining and within the departmental premises of BRD School of Biosciences, Satellite Campus, Sardar Patel University. Shade dried leaves of the plants were powdered and used for Soxhlet extraction. Percent yield for each extract is calculated (Table 1). Phytochemical analyses for triterpenoids, steroids, carbohydrates, proteins, flavonoids, tannins, fixed oils and alkaloids were carried out according to standard methods [7] (Table 2).

Animals

Termite workers (Anacanthotermes sps.; F. Hodotermitidae) [8] were collected from two main sites- the Krishna Hospital in Karamsad and a private land in Vadtal road. From the sites termites were collected into plastic boxes in which moistened corrugated card-board pieces were placed to maintain enough moisture level for the survival of termites. These termite boxes were transported and placed in a cool area in the laboratory and were used as stock for the experiments. Periodically, the container was inspected for maintenance of moisture content.

Effect of Plants as Termiticides

Leaf extracts of the aforementioned plants were tested for their termiticidal effects at 3 different concentrations i.e., 0.5, 1 and 5 %. No-choice test was carried out, with moistened extract treated and solvent treated filter paper discs in separate Petri dishes [9] in to which ten worker termites were introduced. Duplicates for each test and control experiments were performed for 24 and 48 h. A hygrostat container was designed (22”X16”X5”) based on the model described by Ahmed [10]. The container is basically a trough made out of perspex (acryllic) glass with vent holes on its sides in to which a perforated tray was placed. In the inner trough, water was placed and the container was closed with a lid. Due to evaporation of water, the whole container would be saturated with moisture. In this saturated chamber, the experimental set up was arranged. To retain moisture in the chamber, a wet paper towel was placed on the inner side of the lid. Finally, the whole chamber was covered with a dark paper to avoid excess light penetration.

Results

The percent mortality of termites exposed to various concentrations of leaf extracts of *Calotropis procera, Ricinus communis, Parthenium hysterophorus* and *Prosopis juliflora* for 24 and 48 h are presented in Tables 3-6.

Discussion

In comparison to chemical termiticides, plant derived products have many advantages in insect pest management strategies. Reports published decades ago had revealed that several wood species possess natural resistance to termite infestations but only a limited number of them have been examined [11, 12]. Phyto-chemical studies on a number of plant species indicated that the leaves contain triterpenoids while the roots and bark contain naphthols and naphtho-quinones [13]. Various plants also have been used to test their efficacy as Termiticides for example, Neem (*Azadirachta indica*) has been used as an insect repellent as it contains triterpenoid- azadirachtin [14, 15]. Several species of Juniper also have been used to test the termiticidal properties [16]. *Lantana camara* leaf extracts have also been shown to possess termiticidal activity [17]. A study on some commercially available formulations of botanical insecticides comprising of cedarwood oil, isoborneol showed significant repellent effects [18]. In the present study, exposure of termites to various concentrations of the extracts made in different solvents indicated that the toxic effects were greater on termite workers at 48 h test duration. The observed termiticidal effects of this no-choice experiment could be because of the presence of different constituents in various extracts.

A highest mortality rate was recorded (85%, 48 h) with 5% chloroform extract of *Calotropis procera*, while with *Ricinus communis, Prosopis juliflora* and *Parthenium hysterophorus* 70, 65 and 45% mortality rates were recorded, respectively. On the other hand, the distilled water extracts of all the plants even at 5% concentration caused low mortality i.e., 15% mortality with extracts of *Calotropis procera, Ricinus communis* and *Prosopis juliflora* and 20% mortality rate with *Parthenium hysterophorus* leaf extracts, after 48 h. With an exposure to 5% methanol extract of all the plants, after 48 hrs a moderate mortality was observed i.e., 25% mortality with *Parthenium hysterophorus*, 30% mortality with *Calotropis procera* and *Ricinus communis* and a 40% mortality with *Prosopis juliflora* leaf extracts. While the 5% butanol extracts of *Calotropis procera* and *Parthenium hysterophorus* showed lower mortality (25 and 30% respectively), a higher mortality rate was recorded for *Ricinus communis* and *Prosopis juliflora* extracts i.e., 45 and 50% respectively. The 5% petroleum ether extracts of *Calotropis procera, Parthenium hysterophorus* and *Ricinus communis* exhibited low mortality rates (20, 25 and 30% respectively) after 48 h while the extracts of *Prosopis juliflora* caused a higher mortality rate (45%). The hexane extracts (5%) of both *Calotropis procera* and *Ricinus communis* revealed a high mortality rate 45 and 50% respectively. On the other hand *Parthenium hysterophorus* and *Prosopis juliflora* leaf extracts caused low mortality rates (25%). In conclusion, a high mortality (more than 45%) was found in the extracts, in which all the secondary metabolites i.e. triterpenoids, flavonoids, tannins and alkaloids were present. Moderate mortality (30-45%) was observed where any of these three: triterpenoids, flavonoids and tannins, alone or in combination were present while low mortality (15-30%) was found when only flavonoids and tannins were present in the extracts. The chloroform extracts were found to be most potent followed by butanol, hexane, petroleum ether, methanol and water. Besides, among the plants tested, *Calotropis procera* exhibited a highest potential source for termiticidal compounds followed by *Ricinus communis*, *Prosopis juliflora* and *Parthenium hysterophorus*.

Acknowledgement

We are thankful to the Head, Department of Biosciences, Sardar Patel University for providing the facilities required for the present work.

References

1. Pearce M.J., Termites. *Biology and Pest Management.* (Cambridge University Press- Cambridge) p.155 (1997)
2. Creffield J.W., *Wood Destroying Insects*: *Wood Borers and termites* (CSIRO Publishing- Melbourne) p.110 (1996)
3. Hall D.O. and De Groot., *Biomass Regenerable Energy*. Ed. Hall D.O and Overend R.P. (John Wiley & Sons- New York) p.3 (1987)
4. Carter F.L., Material and Organisms. **3**, 357-364 (1976)
5. Scheffrahn R.H., Sociobiology. **19**, 257-281 (1991)
6. Carter F.L., Garlo A.M. and Stanely J.B., J. Agric. Food Chem. **26**, 869 (1978)
7. Kokate C.K., Purohit A.P. and Gokhale S.B., *Pharmacognosy* (Nirali Prakashan- Pune) p. 593 (2000)
8. Roonwal M.L., *Termite life and termite Control in Tropical South Asia* (Scientific Publishers- Jodhpur) p.13 (1979)
9. Kulkarni S.K., *Handbook of Experimental Pharmacology* (Vallabh Prakashan- Delhi) p. 172 (1999)

10. Berhan Mahmoud Ahmed., Thesis: *The effects of Boron-treated Timbers against Coptotermes species in Australia*, (The University of Melbourne, Australia) p. 64 (2000)
11. Wolcott G.N., J. Econ. Entomol. **40,**124-129 (1947)
12. Sandermann W., Dietrichs H.H. and Gottwald, H. Holz als Roh Und Werkstoff: European J. Wood and Wood products. **16,** 197-203 (1958)
13. Bhakuni D.S., Satish, S., Shukla and Y.N. Tandon, Phytochemistry **10**, p. 2829-2831(1971)
14. Ascher K.R.S. and J. Meisner. *The Neem Tree*. Ed. Jacobsen. M. (CRS Press-San Francisco) p. 113 (1967)
15. Schumutterer H. Proc. 3rd Int. Neem Conf. Nairobi. p. 351 (1986)
16. Adams R.P., C.A. Mcdaniel and Carter F.L. Biochemical Systematics and Ecology, **16 (5),** 453-456 (1988)
17. Verma R.K. and Verma S.K. Fitoterapia **77**, 466-468 (2006)
18. Blaske V.U. and Hertel H., J. Econ. Entomol. **94**, 1200-1208 (2001)

TABLES

Table 1: Percent yield of the various plant extracts

Plants	$CHCl_3$	CH_3OH	nHexane	nButanol	P. Ether	D/W
Calotropis procera	32.83%	17.77%	5.10%	9.76%	8.23%	13.06%
Ricinus communis	35.48%	22.58%	12.81%	3.31%	6.25%	16.71%
Parthenium hysterophorus	18.30%	10.05%	5.06%	7.01%	3.60%	10.75%
Prosopis juliflora	14.50%	29.65%	3.71%	5.17%	2.17%	9.23%

Table 2: Phytochemical Screening

Plants	Constituents	PE	M	W	H	C	B
Cp	Triterpenoids	+	-	-	+	+++	+
	Steroids	-	+	-	-	+	+
	Carbohydrates	+	+++	+	+	++	+
	Proteins	+	+	+	+	++	+
	Flavonoids	-	-	+	+	+	-
	Tannins	+	+	+	++	+	-
	Fixed oils	++	++	-	+++	+	++
	Alkaloids	+	+	-	-	+	-
Rc	Triterpenoids	+	-	-	+	++	++
	Steroids	+	++	-	+	+	-
	Carbohydrates	+	++	+	+	+	+
	Proteins	+	+	+	+	+	+
	Flavonoids	-	-	+	+	+	+
	Tannins	+	+	+	++	+	+
	Fixed oils	+++	+	-	++	+	+
	Alkaloids	+	+	-	-	+	-
Ph	Triterpenoids	+	+	-	-	+	+
	Steroids	-	+	-	+	+	-
	Carbohydrates	+	+	+	++	+	++
	Proteins	+	+	+	+	+	+
	Flavonoids	-	+	+	+	+	-
	Tannins	+	-	+	+	+	+
	Fixed oils	+	+	-	++	+	+
	Alkaloids	+	+	-	-	+	-
Pj	Triterpenoids	++	+	-	+	+	+
	Steroids	-	+	-	-	+	-
	Carbohydrates	++	++	+	+	+	+
	Proteins	+	+	+	+	+	+
	Flavonoids	+	+	+	-	+	+
	Tannins	+	+	+	+	+	+
	Fixed oils	+	++	-	++	+	+
	Alkaloids	+	+	-	-	-	-

Cp: *Calotropis procera*, Rc: *Ricinus communis*, Ph: *Parthenium hysterophorus*, Pj: *Prosopis juliflora*. PE: petroleum ether, M: methanol, W: water, H: n-hexane, C: Chloroform,B: n-butanol; -: Absent, +: low concentration, ++: high concentration, +++: very high concentration.

Table 3: *Calotropis procera* -% Termite mortality after 24 and 48 h

Solvent	0.5%		1%		5%		Control	
	24 h	48 h	24 h	48 h	24 h	48 h	24 h	48 h
P. ether	5	10	10	15	15	20	0	5
Methanol	5	10	10	15	20	30	0	0
Water	0	5	0	10	10	15	0	5
n-hexane	5	10	15	25	35	45	0	5
Chloroform	20	30	40	55	60	85	0	5
n-butanol	5	10	10	15	20	25	0	0

Table 4: *Ricinus communis* - % Termite mortality after 24 and 48 h

Solvent	0.5%		1%		5%		Control	
	24 h	48 h	24 h	48 h	24 h	48 h	24 h	48 h
P. ether	10	15	15	20	25	30	0	0
Methanol	5	10	10	15	20	30	0	5
Water	0	5	5	10	10	15	0	0
n-hexane	15	20	20	30	35	50	0	5
Chloroform	15	25	25	35	45	70	0	0
n-butanol	10	15	20	30	25	45	0	5

Table 5: *Parthenium hysterophorus* -% Termite mortality after 24 and 48 h

Solvent	0.5%		1%		5%		Control	
	24 h	48 h	24 h	48 h	24 h	48 h	24 h	48 h
P. ether	0	5	5	10	10	25	0	0
Methanol	5	10	15	20	20	25	0	5
Water	0	10	5	15	10	20	0	5
n-hexane	5	10	10	15	15	25	0	5
Chloroform	10	15	20	25	35	45	0	5
n-butanol	10	15	15	25	20	30	0	5

Table 6: *Prosopis juliflora* -% Termite mortality after 24 and 48 h

Solvent	0.5%		1%		5%		Control	
	24 h	48 h	24 h	48 h	24 h	48 h	24 h	48 h
P. ether	10	15	20	25	35	45	0	5
Methanol	10	15	15	25	25	40	0	0
Water	0	5	5	10	10	15	0	0
n-hexane	5	10	10	15	15	25	0	0
Chloroform	20	25	30	40	50	65	0	5
n-butanol	15	20	20	30	40	50	0	5

'Prajna' - Journal of Pure & Applied Sciences, 16 (2008) 9-15

A STUDY ON SEPARATION AND EVALUATION OF MIXED COTTONSEED FATTY ACIDS BY LOW TEMPERATURE CRYSTALLIZATION TECHNIQUE

Sibban Singh
Department of Industrial Chemistry
Institute of Science and Technology for Advanced Studies and Research (ISTAR)
Vallabh Vidyanagar - 388 120

Abstract

The present experimental work deals about the separation of saturated and unsaturated fatty acids prepared from refined cottonseed oil by using low temperature crystallization technique with petroleum solvents like isopropanol, methanol and hexane in the proportion of 1:2 to 1:5 (w/v). The separated fatty acid fractions were characterized by determining their iodine values. It was observed that isopropanol was the most effective solvent for crystallization of the fatty acid. Apart from this the application of low temperature favors the solidification of saturated fatty acids. The liquid fractions were having iodine value as high as 130.2 whereas the lowest iodine value of solid fraction was found to be 31.8.

Key words: Crystallization, cottonseed fatty acids, liquid and solid fraction and isopropanol

Introduction

The diversity and complexity of the mixture of fatty acids prepared from various natural oils has only been fully realized since the development of precise methods of separation and the application of instrumental methods of analysis and identification of such mixture. In the past commonly occurring unsaturated fatty acids have been isolated. In many cases the fatty acid of unusual structure are present in minor amount from a fraction of a percent to no more than 3-5% which may be difficult to separate out them.

Brown and Kolb [1] described about new and more efficient methods for separation and studying fatty acid mixture. He suggested new technique such as distillation of esters, low temperature application using solvent and urea complex formation and lead salt method. Jamieson [2], Jackson and Callen [3], Rebello and Daubert [4] and Cason and Sumrell [5] later found that complete separation of saturated and unsaturated fatty acids was not possible by lead salt method.

The solidification temperature of fatty acids change considerably with the type and degree of unsaturation and thus separation of mixture of saturated and unsaturated fatty acids may become possible. At low temperature, long chain saturated fatty acids which have higher melting points crystallize out and poly unsaturated fatty acids (PUFA) remain in liquid form.

Apart from the cooling, application of solvents to crystallize out saturated fatty acids have several benefits such as:

1) Nucleation and growth are faster, so higher rates of cooling can be used. This favors short crystallization time.
2) Lower viscosity of the liquid leads to easier filtration.
3) Dilution of the fatty acid makes the heat transfer easier and the amount of fatty acid in the entrained liquid smaller.
4) The ability to wash the cake with fresh solvent leads to very low level of entrained material.

The cottonseed oil, the raw material for the present experimental study, has following fatty acid composition [6]:

Sr. No.	**Fatty acids**	**Range (%)**
1.	Myristic	0.1 – 2.3
2.	Palmitic	17 – 39
3.	Stearic	1.0 – 4.0
4.	Oleic	13 – 44
5.	Linoleic	33 – 58
6.	Linolenic	0.1 – 2.1
7.	Arachidic	Traces – 0.5

It is a typical vegetable oil of oleic---linoleic acid group, since unsaturated fatty acids comprise almost 75% of the total fatty acid. It contains about 25% saturated fatty acids to be separated out in the present work by using crystallization technique.

The main objectives of the present study were to prepare the mixed fatty acids from the cottonseed oil and then to crystallize, separate, and evaluate the saturated and unsaturated fatty acids from the mixture at lower temperatures using various organic solvents.

Materials and Methods

Refined cottonseed oil was procured from Anand Regional Co-operative Oilseeds Growers Union Limited (ARCOGUL), Chikhodara, Gujarat. All other chemicals used for analytical work were of A R grade obtained from M/s S.D. Fine Chemicals, Boisar, Maharashtra.

The solvent isopropanol, methanol and hexane were purchased from Chiti-Chem Corporation, Baroda.

The experimental cottonseed oil was first analyzed for Specific gravity Acid value, Saponification value, Iodine value, Refractive index and Unsaponifiable matter by standard AOCS methods [7].

Preparation of mixed fatty acids from cottonseed oil

200 gm of cottonseed oil and 170 ml of 25% alcoholic solution of potassium hydroxide (10% excess) was refluxed for 2--2½ hour for complete saponification of oil. After saponification the excess alcohol was evaporated and at same temperature the distilled water was added to dissolve the soap formed. This solution was further subjected to treat with mineral acid by adding methyl red indicator (2-3 drops) first and then 1:1 sulphuric acid drop wise to split the soap into fatty acid until the pink color observed. The mixed fatty acids float on the surface.

These fatty acids were dissolved in hexane. The hexane layer was collected separately and the mixed cottonseed fatty acid (CSFA) was obtained by evaporating hexane.

Crystallization and Separation of mixed fatty acids

The mixed cottonseed fatty acids (CSFA) and petroleum solvents like methanol, isopropanol and hexane were taken in the ratio of 1:2, 1:3, 1:4 and 1:5 (w/v). These solutions were kept in incubator at three different temperatures i.e. 5^0C, 10^0C and 15^0C to crystallize out the solid fraction of CSFA. At every hour the samples were withdrawn, filtered, dried, weighed and then calculated the percentage of solid CSFA. No appreciable change in the quantity of solid fraction was observed after 5 hours. Therefore, for the further experimental work the crystallization time was fixed as 5 hours. The liquid fractions obtained after filtration, were used to evaporate the solvents. All these solid and liquid fractions thus obtained, were characterized by determining their iodine values.

Results and Discussion

The physico-chemical characteristics of the cottonseed oil are presented in Table 1. The results clearly indicate a typical characteristics of cottonseed oil as compared with the standard values.

For all the solvents the formation of solid crystals increases with time. But after five hours of cooling the growth of crystal was found to be poor as presented in Table 2. Hence the optimum duration for crystallization to separate the solid fraction from the mixed fatty acids obtained from cottonseed oil in the present work was considered to be five hours.

The crystallization of mixed fatty acids by using methanol at different temperatures with varying the quantity of methanol were studied and the iodine values of solid fraction of fatty acids were determined as represented in Table 3. It is clear from the table that at lower temperature the crystallization of fatty acids were higher but their iodine value were lower whereas the iodine value of liquid fractions were higher at low temperature. The results from the table also depicts that as the solvent proportion increases the solidification of fatty acids decreases for all temperatures selected for the crystallization. So lower solvent ratio preferably can be used on large scale production. Moreover, the distillation cost is reduced too.

Table 4 shows the crystallization of fatty acids by using isopropanol as a solvent. It is clear from the table that the trend in changes in crystallization behavior and iodine value is similar to that observed with methanol. However, the yield of solid fatty acid at 5^0C and 10^0C temperature are lower to that provided by methanol. Apart from this the iodine value of solid fraction is lower and that of liquid fractions is comparatively higher to that provided by methanol. It shows that the performance of isopropanol is better than methanol.

The crystallization and evaluation was also studied by hexane and the results are depicted in Table 5. The results indicate that the quantity of solid fatty acids obtained is higher than those provided by other two solvents. Also the iodine value of solid fractions is comparatively higher than that of liquid fraction showing poor crystallizing efficiency.

Therefore, the study reveals that the isopropanol is most suitable solvent for crystallization of fatty acids obtained from cottonseed oil. Also higher the iodine value of separated fatty acid by isopropanol may be a suitable raw material for medium oil alkyd preparation. However, the solid fraction of fatty acids having lower iodine value can be used for soap manufacture.

Acknowledgement

Author is thankful to Director, ISTAR, Vallabh Vidyanagar for providing all facilities in the laboratory to complete the experimental works.

References

1. Brown J.B. and Kolb D.K. in *Progress in the chemistry of oils and other lipids* Vol. III R.T. Holman, W.O. Lundberg, and T. Malkin, eds. Pergamon Press, New York, 1955, pp 57 – 94
2. Jamieson G.E., *Vegetables Fats and Oils*, 2nd edn. Reinhold, New York, 1943, p – 407

3. Jackson F.L. and Callen J.E., *J. Am. Oil Chemists' Soc.*, **28** 61–65 (1951)
4. Rebello D. and Daubert B.F., *J. Am. Oil Chemists' Soc.*, **28** 183–185 (1951)
5. Cason J. and Sumrell G., *J. Org. Chem.*, **16** 1193–1197 (1951)
6. Lynn A., Jone C. and Clay King, in *Bailey's Industrial Oils and Fats Products Vol. 2*, 5th edn., edited by Y.H. Hui, John Wiley and Sons, New York, 1996
7. *Official and Tentative Methods of the American Oils Chemists' Society,* edited by W.F. Link, AOCS, Champaign, IL, 1976 Vol. 1

TABLES

Table 1: Physico-chemical Characteristics of Experimental Cottonseed Oil

Sr. No.	Characteristics	Value	Standard value
1.	Specific Gravity at 20^0C	0.915	0.914—0.917
2.	Acid value	1.1	1—10
3.	Iodine value	110.5	103 –112
4.	Saponification value	193.2	189—198
5.	Unsaponifiable matter	0.53	0.3—0.7
6.	Refractive index at 25^0C	1.4649	1.468—1.472

Table 2: Effect of crystallizationa time on separation of fatty acids (mixed fatty acids:solvent = 1:3, w/v)

Solvents	**Percentage of solid fatty acids crystallized as a function of time (hrs)**						
	1.0	**2.0**	**3.0**	**4.0**	**5.0**	**6.0**	**7.0**
Isopropanol	12.3	16.4	21.6	24.8	25.5	25.8	26.2
Methanol	10.5	14.8	18.3	23.2	26.3	26.7	27.1
Hexane	11.2	15.0	18.9	23.9	26.6	27.0	27.3

a-crystallization was carried out at 5^0C.

Table 3: Crystallization and Evaluation[a] of mixed fatty acids using Methanol

Tempera-ture (^{O}C)	Fatty acid: Solvent ratio (w/v)	Yield of fatty acid fraction (%)		Iodine value	
		Solid	Liquid	Solid fraction	Liquid fraction
5	1:2	30.6	69.4	51.2	120.9
	1:3	29.2	70.8	50.0	122.6
	1:4	28.0	72.0	48.9	124.3
	1:5	27.5	72.5	47.6	126.8
10	1:2	27.9	72.1	56.5	117.7
	1:3	26.3	73.7	55.1	119.0
	1:4	24.6	75.4	53.9	120.6
	1:5	23.4	76.6	52.4	121.7
15	1:2	21.2	78.8	61.3	107.4
	1:3	19.9	80.1	59.8	110.5
	1:4	17.6	82.4	59.0	112.1
	1:5	17.1	82.9	57.8	116.9

a-average of two determinations with the variation up to ± 0.5%.

Table 4: Crystallization and Evaluationa of mixed fatty acids using Isopropanol

Tempera-ture (^{O}C)	Fatty acid: Solvent ratio (w/v)	Yield of fatty acid fraction (%)		Iodine value	
		Solid	Liquid	Solid fraction	Liquid fraction
5	1:2	27.3	78.7	35.6	124.3
	1:3	26.1	73.9	33.8	126.4
	1:4	25.5	74.5	32.2	127.0
	1:5	24.2	75.8	31.8	130.2
10	1:2	26.7	73.3	42.9	121.1
	1:3	25.5	74.5	40.1	123.3
	1:4	24.4	75.6	38.2	125.8
	1:5	23.8	76.2	35.7	126.3
15	1:2	26.8	73.2	52.5	117.7
	1:3	25.5	74.5	50.1	120.3
	1:4	24.4	75.6	48.3	122.4
	1:5	23.9	76.1	47.4	125.6

a-average of two determinations with the variation up to ± 0.5%.

Table 5: Crystallization and Evaluationa of mixed fatty acid using Hexane

Temperature (^{O}C)	Fatty acid: Solvent ratio (w/v)	Yield of fatty acid fraction (%)		Iodine value	
		Solid	Liquid	Solid fraction	Liquid fraction
5	1:2	33.3	66.7	72.4	112.3
	1:3	31.2	68.8	70.5	113.6
	1:4	29.9	70.1	67.7	115.0
	1:5	28.8	71.2	65.8	117.2
10	1:2	28.3	71.7	80.4	110.8
	1:3	26.6	73.4	78.1	112.4
	1:4	23.8	76.2	76.0	113.5
	1:5	20.4	79.6	74.1	116.4
15	1:2	21.4	78.6	91.2	110.3
	1:3	20.2	79.8	88.5	112.8
	1:4	19.1	81.9	84.2	113.5
	1:5	18.3	82.7	83.5	115.8

a-average of two determinations with the variation up to ± 0.5%.

'Prajna' - Journal of Pure & Applied Sciences, 16 (2008) 16-29

CASHEW NUT SHELL LIQUID RESIN COMPOSITES REINFORCED BY SAWDUST AND WOOD FLAKE

Anurag L. Emanuel and Vijay Kumar Sinha*
Bhailalbhai & Bhikabhai Institute of Technology, P.O Box 3, Mota Bazar, Vallabh Vidyanagar-388 120
*Industrial Chemistry Department, V.P. & R.P.T.P. Science College, Vallabh Vidyanagar-388 120

Abstract

Cashew nut shell liquid (CNSL) is a by-product of cashew nut processing industry and is a potential natural alternative to chemically derived phenol. It was reacted with formaline to form Resol type phenolic resins, which is further used to prepare composites using natural fibers such as wood flakes and sawdust as reinforcing agents. The Resol resin was characterized by FTIR spectroscopy. The molecular mass was determined using GPC. The composites prepared using the Resol resin as matrix and sawdust and wood flakes as reinforcing agents were tested for their mechanical properties viz. Rockwell hardness, Izod-Impact Strength, flexural strength, flexural modulus and chemical resistance.

Keywords: CNSL, Formalin, sawdust, wood flake, composite.

Introduction

Over the last few decades, there has been considerable development in the field of composite materials. Today modern composite materials constitute a significant proportion of the engineering materials ranging from everyday products to sophisticated niche applications. Lightweight corrosion resistance materials such as fiber-reinforced composites could provide an important contribution to the safe economical development of resources for structural applications. If renewable resources can be used for preparation of composites then it has many added advantages ranging form cost effectiveness to proper management and reduction in industrial wastes and byproducts.

Composites are materials with superior properties for example glass fiber composites, which made possible the construction of structures, which are lightweight yet very strong [1]. Recently however, questions have been raised on toxic and carcinogenetic nature of some of the synthetic fibers currently in use. Glass fiber and silica carbide whiskers are being associated with some forms of cancer of the lung. Blue asbestos is well known to promote cancer of the lungs when inhaled. Kevlar, Glass and Carbon fiber reinforced composites are widely use for high-tech applications and are very expensive and unsuitable for low-tech applications. The increase in cost and effect on environment due to synthetic fibers have forced the scientist and engineers to synthesize new materials and composites which besides having their needed specific physical properties [2, 3, 4] are cost effective as well as environmentally friendly [5]. The natural fiber can replace the synthetic fibers in the areas where high strength and stiffness are not the primary requirement [6]. The use of Natural fibers over synthetic fibers as reinforcements in resin matrix has gained momentum in last decade [7, 8, 9].

Plastics such as polyester, phenolic and epoxy have been successfully reinforced with some plant fibers to produce composites that are suitable for general structural applications, housing and panels for the construction industry [10, 11, 12, 13]. Plant fibers are renewable and biodegradable natural cellulosic materials. They are also light compared to other synthetic fibers and have desirable mechanical properties. In addition, they are cost-effective, environmentally friendly, non-toxic and are abundantly available [14]. Along with these advantages there are certain disadvantages like they absorb moisture easily, they are attacked by micro-organisms and insects who fed on cellulose, thus causing bio-degradation, also they get delaminated with time [15]. Sawdust and Wood flakes are lignocellulosic fibers. Significant advances have been made by number of researchers in this field [16, 17]. Sawdust and wood flakes are abundantly available at a very low cost as they are waste product of wood cutting and furniture industry. This makes them potential source of naturally occurring reinforcing agents in composites preparation.

The other economical route is to use alternative cheap polymeric material without compromising the properties of composites. Plant based chemical compounds exist which are suitable for the manufacture of composites matrices and most extensively studied of these natural substances is Cashew nut shell liquid (CNSL). CNSL is a byproduct of Cashew nut processing industry [18, 19]. CNSL is essentially a mixture of phenolics extracted from the shells of the cashew nut and is a good natural alternative to chemically derived phenol. It can react with formaldehyde in presence of basic catalyst by condensation polymerization reaction to give CNSL formaldehyde polymer [20, 21, 22]. It is also know that CNSL has a very good insecticidal property. Raw CNSL has been used for many years for protecting furniture against certain species of ants and other insects [23, 24].

The above literature survey encouraged us to use sawdust and wood flakes as reinforcing agents in manufacture of composites. CNSL-formaldehyde (Resol type) resin was taken as matrix. Both the reinforcing agents and the resin used are abundantly available and are economically very cheap. The main aim of this work is to prepare low cost composites with reasonably good mechanical properties, which can be used where high strength and stiffness are not of primary importance.

Experimental:

Material:

The basic chemicals used for the experimental purpose were of laboratory grade. Raw CNSL procured form Vellow Chem. Industry, Vitthal Udyognagar, Gujarat, was according to Indian standards IS-840-1964. The specifications are given in Table: 1. The free phenol content of CNSL was estimated in laboratory [25]. The free phenol available to react with formaldehyde in raw CNSL was found to be 21%. Formaldehyde in the form of 37% formalin was obtained from S.D. fine chemicals. Liquor ammonia was used as catalyst. Solvents and chemicals used for the synthesis purpose were of laboratory grade and were used after routine purification.

Table 1 : Physico-chemical Characteristics of Experimental Cottonseed Oil

Sr. No.	Properties	Value
1.	Specific gravity, 30°C	0.950-0.970
2.	Viscosity at 30°C, centipoises	550
3.	Moisture content (% by weight)	1.0
4.	Matter soluble in toluene (% by weight)	1.0
5.	Loss in weight on heating (% by weight)	2.0
6.	Ash content (% by weight)	1.0
7.	Iodine value	
	Wijis method	270
	Catalytic method	375
8.	Polymerization time in minutes	4

Synthesis of Resin

Synthesis of Resol type resin was carried out using CNSL, formaldehyde as starting materials and liquor ammonia as catalyst. The ratio of free phenol and formaldehyde was kept 0.8:1 and 5% liquor ammonia was taken.

The raw material was taken in a round bottom flask equipped with a reflux condenser a thermometer pocket and a mechanical stirrer. The reaction mass was heated slowly and maintained at reflux temperature. Viscosity of the reaction mass steadily increased as the reaction progressed. After 2 hours water formed due to condensation reaction was removed under vacuum. After complete removal, the temperature was again raised slowly until it reached 230°C. It was maintained at this temperature until 18"-21" long threads of resin were obtained. The resin at this point was of dark reddish brown color. The mass was cooled down and stored in an airtight container. Formation of resin was confirmed by spectral analysis (FTIR) and the molecular mass was determined by the help of gel-permeation chromatography (GPC).

Reaction Scheme

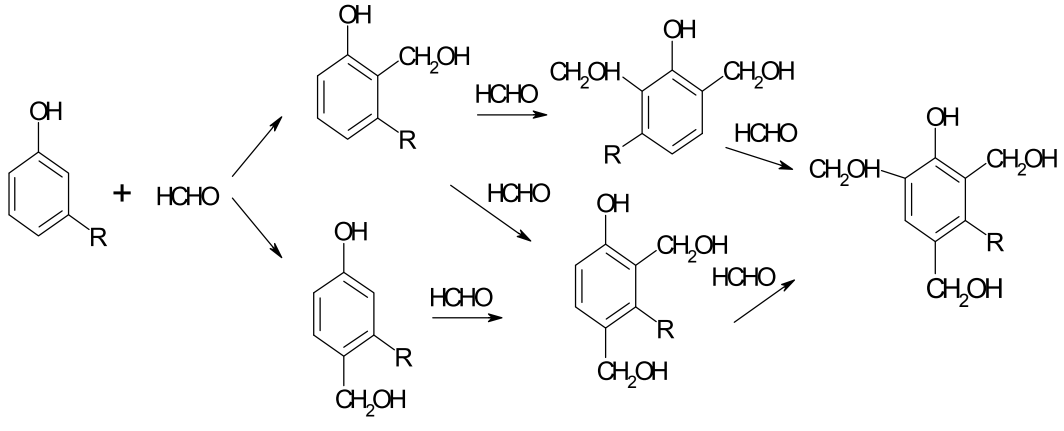

The Cardanol in CNSL which is essentially a phenol will take part in the reaction. The condensation reaction of Cardanol with formaldehyde using base catalyst will initially give a mixture of o- and p-methylol Cardanol, which being more reactive than cardanol will result in formation of di- and trimethylol derivatives.

The methylol groups undergo self-condensation to form polynuclear compounds in which phenolic nuclei are linked by methylene groups. The product obtained by the condensation reaction of Cardanol with formaldehyde using base catalyst will give a complex mixture of mono and polynuclear Cardanol with methylene bridges. The structure of such a component can be represented as:

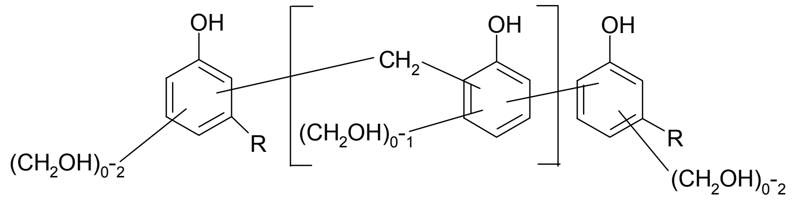

Where R stands for,

$C_{15}H_{31}$ =

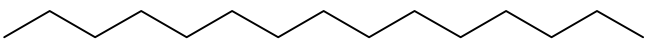

$C_{15}H_{29}$ =

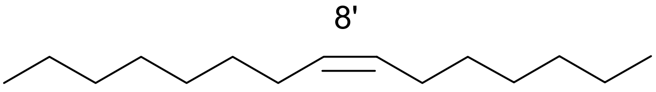

$C_{15}H_{27}$ =

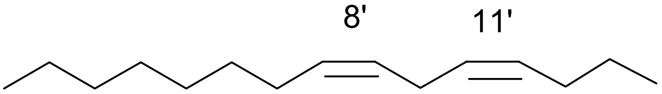

$C_{15}H_{25}$ =

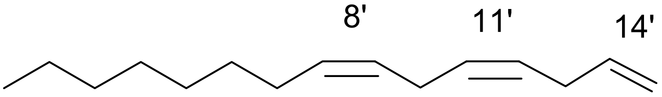

Preparation of Composites

Composites were prepared using resol type CNSL-formaldehyde resin as matrix and sawdust and wood flakes as reinforcing agents. Compression moulding machine was used for fabrication of composites. A mould was designed for preparing composites. The dimensions of the composites prepared were 100mm X 200mm X 10mm.

For preparing composites, sawdust and wood flakes were mixed with the CNSL-formaldehyde (Resol) resin in different substrates to resin ratios. Acetone was taken as diluent and the mixture was kept overnight, so that proper absorption of the resin by the substrates takes place. For Resol composites, the temperature was kept 190°C for 1 hour and the pressure of 70 Kg/cm^2 was applied. The resin got heat cured. It was then cooled under pressure and cured composites were taken out for testing.

Measurements:

The mechanical and chemical tests of the prepared composites were conducted according to ASTM methods as listed below using five test specimens for each test.

Flexural Strength and Flexural Modulus Test

The flexural strength is the ability of the material to withstand bending forces applied perpendicular to the longitudinal axis. The stress induced due to flexural load is combination of compressive and tensile stresses. ASTM D-790 procedure was used to measure the flexural strength of the composites using Universal Instron testing machine model no.1111. The crosshead speed was 100 mm/min.

For Flexural test, the dimensions were as follows:

- Length = 120 mm

- Width = 20 mm
- Thickness = 10 mm
- Support Span = 75 mm

Flexural strength = $3PL / 2bd^2$

Where,

P = Breaking load (Kg)
L = Support span (mm)
b = width of the specimen (mm)
d = thickness of the specimen (mm)

Flexural modulus can be determined by using the following equation:

Flexural modulus = $PL^3 / 4bd^3y$

Where,

P = Breaking load (Kg)
L = Support span (mm)
b = width of the specimen (mm)
d = thickness of the specimen (mm)
y = beam deflection (mm)

Hardness Testing

Hardness is defined as resistance of material against permanent deformation. The Rockwell hardness was measured according to ASTM D-785. The sample size was 25mm X 25mm and the hardness was measured using hardness tester TSE testing machine.

Impact Testing

Impact resistance is ability of a material to resist breaking under shock loading or ability to resist the fracture under stress applied at high speed. The impact properties indicate toughness of material. The tests were carried out according to ASTM D-265.

For Izod impact strength the dimensions were as follows:

- Length = 75 mm
- Width = 10 mm
- Thickness = 10 mm
- Depth of Notch = 2 mm

Chemical Resistance:

ASTM D 543-67 procedure was used to measure the chemical resistance property of the composite specimen.

Results and Discussion:

The results obtained after testing the composites for their mechanical properties are shown in the tables. The results of Resol resin based sawdust composites are shown in Table: 2 and wood flake composites are shown in Table: 3.

Reaction Conditions:

CNSL being a phenolic material reacts with formaldehyde at 90-95°C. The reaction is a condensation polymerization and water is formed as a byproduct. The reaction takes two hrs to complete and viscosity of the reaction mass steadily increases. Water formed and the unreacted formaldehyde if any should be removed from the reaction mass. If not removed excessive foaming occurs which is difficult to control as the temperature is raised above 100°C. Moreover, if unreacted formaldehyde is present then it will result in gelling/ curing of the resin as the temperature is raised especially in Resol type resin. Therefore, water and unreacted formaldehyde should be removed completely before raising the temperature of the reaction mass above 100°C. After complete removal, the temperature is again raised to 230°C and maintained until 18"- 20" long resin threads are obtained. During the whole process the reaction mass should be continuously stirred to evenly distribute heat. If not done, it will result in localized heating and reaction mass will start bumping, finally resulting in gelling of the reaction mass.

Resin Analysis:

The characterization of resin was done by using Fourier Transform Infrared Spectroscopy (FTIR). IR spectrum of CNSL based Resol resin is shown in Figure-1. The band in the region 3300-3400 cm^{-1} indicates the presence of hydroxyl group. The peaks at 3010 cm^{-1} and 2920 cm^{-1} are assigned to C-H stretching and Methylene stretching respectively. The peaks at 1587 cm^{-1} and 1620 cm^{-1} is due to the vibration of the aromatic -C=C- linkages. The peak at 1452 cm^{-1} is due to bending vibration of $-CH_2$. The peak at 1094 cm^{-1} is due to the in plane C-H bending of phenyl ring. The presence of band at 911 cm^{-1} is due to a trans double bond in aliphatic side chains of cardanol moiety. The peak at 721 cm^{-1} is due to the meta substituted aromatic benzene ring.

The molecular weight of the resin was confirmed using GPC (Figure-2). The number average (Mn) molecular weight was found to be 3985. The weight average (Mw) molecular weight was found to be 11071. The peak molecular weight PMwt was found to be 12029.

Figures to be taken from Word

cm^{-1}

Figures to be taken from Word

Composite Testing and Comparison:

Here our main aim was to prepare composites from renewable resources, which are commercially compatible as well as economical. The composites prepared using Resol resin as the matrix and sawdust and wood flakes as the reinforcing material were tested for their mechanical properties and chemical resistance. The results of mechanical properties of sawdust composites are shown in the Table: 2 and results of wood flake composite are shown in the Table: 3. Teak wood was tested under identical conditions and the results are shown in Table: 4. The results obtained were compared with the sawdust and wood flake composites.

Table 2: Mechanical properties of Resol based Sawdust composites

% Resin	Rockwell hardness	Izod Impact Strength (joule/cm)	Flexural Load (Kg)	Flexural Strength (MPa)	Flexural Modulus (MPa)
30%	7	0.237	10.1	5.68	106.51
40%	15	0.650	27.3	15.35	287.90
50%	18	0.712	27.9	15.69	294.23
60%	18	0.712	28.4	15.97	299.50

Table: 3 Mechanical properties of Resol based Wood flakes composites

% Resin	Rockwell hardness	Izod Impact Strength (joule/cm)	Flexural Load (Kg)	Flexural Strength (MPa)	Flexural Modulus (MPa)
30%	16	1.712	21.9	12.31	230.95
40%	22	1.850	35.1	19.74	370.16
50%	27	1.887	37.4	21.03	394.42
60%	27	1.887	37.5	21.09	395.47

Table: 4 Mechanical properties of Teak wood:

Property tested	Result obtained
Rockwell hardness	5
Izod Impact Strength (joule/cm)	1.85
Flexural Load (Kg)	36.2
Flexural Strength (MPa)	20.36
Flexural Modulus (MPa)	381.79

On comparing the sawdust composites with teak wood, they showed better hardness but lacked in Izod impact strength and showed poor load bearing properties. On increasing the resin percentage, improvement in mechanical properties was observed, but still the impact strength and load-bearing property was lower than that of teak wood. However, sawdust composites showed better surface hardness even at lower resin ratios. Sawdust composites also showed poor mechanical properties compared to wood flake composites. Their hardness and flexural strength were lower which can be clearly seen from the Figure-4 and Figure-5 respectively.

Figure-4 Graphical comparision of hardness of Sawdust and woodflake comospites

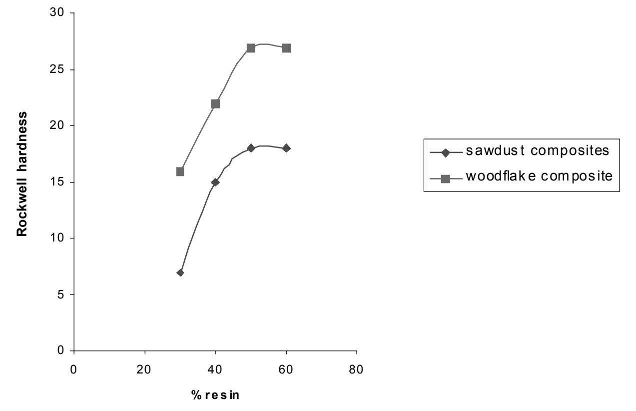

Figure-5 Graphical comparision of flexural strength of sawdust and woodflake compsoites

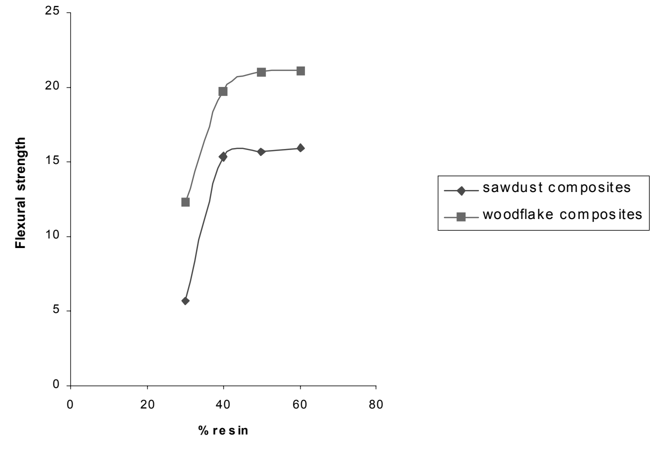

On comparing the wood flake composites with teak wood at lower resin ratio they showed better hardness but lower impact and load bearing property. However, as the resin ratio was increased they showed better results than the teak wood. At 50% resin ratio and above they showed better hardness, better impact strength, and better load bearing properties than teak wood.

All the composites were tested for their chemical resistance. They were unaffected by common organic solvent, concentrated mineral acids (25% V/V) and water. But, showed little increase in weight about (1-2.5%) because of moisture absorbing properties of the natural fibers. When immersed in 25% NaOH solution little swelling of the composites was observed and weight increased by 6-8%, but no delamination was noticed. Wood flake composites gained more weight compared to sawdust composites.

Conclusion:

Resol type resins, prepared using Cashew nut shell liquid (CNSL) can be used to prepare composites having competitive mechanical properties at low cost. Natural fibers such as sawdust and wood flakes, which are waste products of woodcutting and furniture industry and are abundantly available at a very low cost, can be used effectively as reinforcing agents for composite manufacture. From the study of mechanical properties of these composites, it can said that composites prepared from renewable natural resources definitely can replace wood in some applications. They can also be used effectively in low-tech applications where high strength and stiffness is not the major concern. In such applications natural fiber composites can replace synthetic fibers and there by making it more economical and environment friendly.

Acknowledgement

The authors are gratefully thankful to the Principal, V.P. & R.P.T.P. Science College and Head of the Industrial Chemistry Department for providing laboratory facilities.

References

1. Thomason J.L., Schoolenberg G.E. 'An investigation of glass fiber polypropylene interface strength and its effect on composite properties', Composites. 25A, 197-203, 1994
2. Budiansky B., Hutchinson W., Evans A.G. 'Matrix Fracture in fiber reinforced ceramics', J. Mech. Phys. Solids. 34, 167, 1986
3. Nomura S., Chou T.W. 'Bounds of Effective Thermal Conductivity of Short-Fiber Composites', J. Comp. Mat 14, 120, 1980

4. Kakson C., Kubat J. Cellulose in polymer composites. In: Samen L., de Ruvo, Seferis J.C, Stark E.B, editors. Composite systems from natural and synthetic polymer. Amsterdam: Elsevrier, 1986

5. Sreekala M.S., 'Oil palm fibers: Morphology, chemical compositions, surface modification and mechanical properties', J. Appl. Polym. Sci. 66, 821-835, 1997

6. Roe P.J. and Ansell M.P. 'Jute reinforced polyester composites', Material Science, 20, 4015, 1985

7. Stephen G.K., John A.H., Phillip A.W. 'Impact performance of phenolics composites following thermal exposure', J. Appl. Polym. Sci. 67, 349, 1998

8. Bishop G.R., Sheard P.A., 'Fire resistance composites for structural sections', Compos Struct. 21, 85, 1992

9. Jack Vinson. R., Chou T.W. 'Composite Material and their Uses in Structures (Chapter 2) Applied Science Publication Ltd, London pp.35-46, 1975

10. Bisanda E.T.N. and Ansell M.P. 'Properties of Sisal - CNSL composites' Journal of Material Science, Vol. 27, p. 1690-1700, 1992

11. Mwaikambo L.Y. and Basinda E.T.N., 'The performance of cotton-kapok fabric polyester composites', Polymer Testing, Vol. 18. p. 181-198, 1999

12. Owolabi O., Czvikovszky T. and Kovacs I. 'Coconut fiber reinforced thermosetting plastics', Journal of Applied Polymer Science, Vol. 30, p.1827-1836, 1985

13. Satyanarayana K.G., Sukumaran K., Kulkarni A.G., Pillai S.G.K., and Rohatgi P.K., Composite Structures. Ed. Marshall, I.H.; p.535-548, Applied Science, London, U.K, 1983

14. Mwaikambo L.Y. and Ansell M.P., 'Hemp fiber reinforced cashew nut shell liquid composites', Composites Science and Technology, 63, 1297-1305, 2003

15. Gassan J., Bledzki A.K., 'Effect of moisture content on the properties of silanised jute-epoxy composites', Polym. Comp. 18(2): 179-84, 1997

16. Woodhams R.T., Thomas G., Rogers D.K., 'Wood fibers as reinforcing fillers for polyolefins', Polym. Eng. Sci. 24:1166, 1984

17. Bataille P., Ricard L., Sappieha S., 'Effect of cellulose in polypropylene composites', Polym. Comp. 10(2):103-8, 1989

18. Pillot J.P., Vanthanh M.D.M., Gerval J. and Dunoques J., Eur. Polym. J. 25(3), 285, 1989

19. Prodi R., De Castro P., Malorgio G.A. 'The world cashew economy', Bologna: Marino Cantelli Printing House, 1994
20. Sahoo S.K., Swain S.K. and Lenka S., 'Polymers from renewable resourses: V: Synthesis and characterization of resins derived from CNSL', J. Appl. Polym. Sci., 54, 10, pp1413-1421, 1994
21. Sahoo S.K., Swain S.K. and Lenka S., 'Polymers from renewable resourses: VI: Synthesis and characterization of resins derived from CNSL', J. Appl. Polym. Sci., 233, 1, pp 1-13
22. Mahanwar P.A., Kale D.D., 1996: 'Effect of Cashew nut Shell liquid (CNSL) on properties of phenolic resins', J. Appl. Polym. Sci., 61(12), 2107-2111, 2003
23. Mwalongo G.C.J., Mkayula L.L., Dawson Andoh B., Mubofu E.B., Shields J. and Mwingira B., 'Preventing termite attack: environmentally friendly chemical combinations of cashew nut shell liquid, sulfited wattle tannin and copper(II) chloride', Green Chem., 1, 13-16, 1999
24. Gowari V.S. and Saxena M., 'Protection of bamboo surfaces by CNSL based coatings', Indian J. Chem. Technol., 3, 145-149, 1997
25. Vogel's Textbook of Quantitative Chemical Analysis. 5th Edition. Determination of Phenol. Chapter 10 - Titrimetric Analysis. pp. 408-409

'Prajna' - Journal of Pure & Applied Sciences, 16 (2008) 30-36

KNOWLEDGE SCOUTING IN E-LEARNING SYSTEMS USING SEMANTIC AGENTS

Priti Sajja and Manish Sharda*
Department of Computer Science, Sardar Patel University, Vallabh Vidyanagar - 388 120
*SEMCOM College, Sardar Patel University, Vallabh Vidyanagar - 388 120

Abstract

The education has taken a giant leap and paradigm shift from class room learning to e-learning to semantic tutoring. Our attempt in this research is to identify the problem with class room learning, to find the feasibility of e-learning system using semantic tutors, to pin point barriers and concerns of the students aspiring to go for e-learning using semantic tutors.

The research attempts to identify, evaluate and present the outcomes of the study undertaken using standard techniques and statistical tools. We propose a model for semantic e-learning and future implications for the further research in the area.

Keywords: E-Learning, Semantic tutor, Semantic Tutoring, F2F (Face-to-Face) Learning

Introduction

Electronic learning or eLearning is a general term used to refer to computer-enhanced learning. It is used interchangeably in so many contexts that it is critical to be clear what one means when one speaks of 'eLearning' [06].

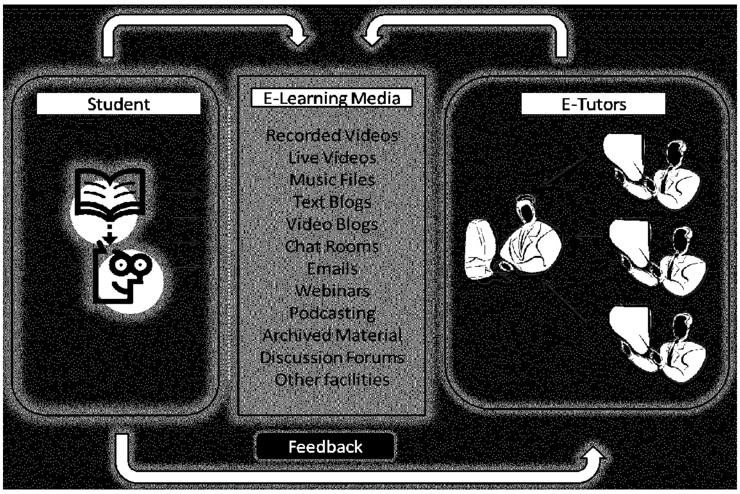

Figure 1: e-Learning System in Web 2.0

E-Learning lessons are generally designed to guide students through information or to help students perform in specific tasks. Information based e-Learning content communicates information to the student. Communication technologies used in e-learning are generally categorized as asynchronous or synchronous. Asynchronous activities use technologies such as blogs, wikis, and discussion boards. The idea here is that participants may engage in the exchange of ideas or information without the dependency of other participant's involvement at the same time. Email is also asynchronous in that mail can be sent or received without having both the participants' involvement at the same time [02].

Synchronous activities involve the exchange of ideas and information with one or more participants during the same period of time. A face to face discussion is an example of synchronous communications. Synchronous activities occur with all participants joining in at once, as with an online chat session or a virtual classroom or meeting.

Knowledge Scouting in E-learning System using Semantic Agents

Knowledge scouting in semantic web handles elicitation, analysis and transfer of knowledge almost simultaneously [01]. The emphasis is on the development of knowledge base systems that give straight set of rules from examples or samples of knowledge acquired interactively from the domain expert. This saves money, time and energy for the knowledge engineer.

Major challenges in implementing of knowledge scouting framework in semantic web are [05]:

- Extracting hidden knowledge from unstructured and structured data
- Knowledge fusion over heterogeneous data sources
- Ontology sharing
- Building user-friendly semantic web applications
- Security, privacy, and reputation in semantic web services
- Quality of Service (QoS)
- Query and optimization models for semantic web

All processes are related somehow to domain ontology. Since ontology is a domain model, it contains a set of domain axioms which are used for deriving new information - that is the task of an inference engine.

The framework shown in figure 2 is an attempt to meet above challenges using semantic technologies:

a. Firstly, identify types of knowledge sources, which could be treated in the knowledge capturing phase like expert knowledge, legacy (rule -base) systems, metadata repositories, documents, etc [04].

b. Then decide about knowledge repository, which is a relational database organized in a way that enables efficient storing and access to RDF metadata. This repository can be seen as a RDF repository. The RDF metadata model is based upon the idea of making statements about resources in the form of subject-predicate-object expressions, called triples in RDF terminology. For example, in the English language statement 'New York has the postal abbreviation NY', 'New York' would be the subject, 'has the postal abbreviation' the predicate and 'NY' the object [08].

Encoded as an RDF triple, the subject and predicate would have to be resources named by URIs. The object could be a resource or literal element. For example, in the Notation_3 form of RDF, the statement might look like:

<urn:states:New%20York> <http://purl.org/dc/terms/alternative> "NY" .

c. Now the knowledge processing component enables efficient manipulation with the stored knowledge, especially graph-based processing for the knowledge represented in the form of rules, e.g. deriving dependency graph or consistency checking [05].

Figure 2: Knowledge Scouting in e-Learning Systems using Semantic Agents

d. Knowledge sharing is realized by searching for rules that satisfy the query conditions. In the RDF repository rules are represented as reified RDF statements and while in RDF any statement is considered to be an assertion, we can view an RDF repository as a set of ground assertions in the form (subject, predicate, object). For example, RDF triples can be written with XML tags as,

[resource]	[property]	[value]
The Cake	Is	Chocolate
[subject]	[predicate]	[object]

They are often conceptualized graphically as:

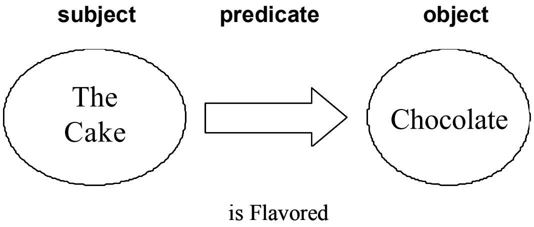

Rules are also related to domain ontology [10], which contains domain axioms used for deriving new assertions. Therefore the searching is realized as an inferencing process.

e. In that way querying for a problem can result in a composition of documents, which cover problem solving. SPARQL is an RDF query language; its name is a recursive acronym that stands for SPARQL Protocol and RDF Query Language. SPARQL allows for a query to consist of triple patterns, conjunctions, disjunctions, and optional patterns [09].

The computer doesn't really understand information the way a human can, but it has enough information to make logical connections and decisions.

Survey and Findings

The survey was conducted to check the operational feasibility for "Knowledge Scouting in e-Learning Systems using Semantic tutors". The respondents were selected on the basis of following criteria:

- Student should be having a computer and/or laptop with Internet access
- Student accesses internet for at least 4 hrs per day in college, home or cyber cafe
- Under Graduate & Post Graduate students with knowledge of semantic technologies

Methodology

- The primary data was collected from the respondents using digital close ended structured questionnaire.
- The secondary data was collected from various journals, books, articles and magazines.

- The sample size was 86 respondents which include 48 male and 38 female students.
- Purposive sampling scheme was adopted to select the respondents.
- Statistical tools like chi square test, percentage analysis and descriptive statistics were used for the analysis.

Hypothesis

Our hypothesis that we propose for the study are as mentioned as under:

1. Null Hypothesis (H_0): There is no relationship between gender and preference to study the subjects online with the help of semantic tutor.
2. Null Hypothesis (H_0): There is no relationship between gender and likings to study the compulsory, electives and both subjects online with the help of semantic tutor.
3. Null Hypothesis (H_0): There is no relationship between gender and kind of subjects that is management, technical and both, available for online study with the help of semantic tutor.
4. Null Hypothesis (H_0): There is no relationship between gender and readiness to go for e-learning with the help of semantic tutor.

Findings

The following findings were derived from the survey on statistical analysis:

1. The null hypothesis that there is no relationship between gender and preference to study the subjects online with the help of semantic tutor is accepted at 5% level of significance and 1 degree of freedom. The calculated value of chi-square is 0.037 and the critical value is 3.841.
2. The null hypothesis that there is no relationship between gender and likings to study the compulsory, electives and both subjects online with the help of semantic tutor is accepted at 5% level of significance and 2 degree of freedom. The calculated value of chi-square is 1.84 and the critical value is 5.991.
3. The null hypothesis that there is no relationship between gender and kind of subjects available for online study with the help of semantic tutor is accepted at 5% level of significance and 2 degree of freedom. The calculated value of chi-square is 0.070 and the critical value is 5.991.
4. The average number of hour's students want to spend on e-learning with the help of semantic tutor is 2.60 hours with standard deviation of 0.94 hours. The median number of hours is 2 hours.

5. The null hypothesis that there is no relationship between gender and readiness to go for e-learning with the help of semantic tutor is accepted at 5% level of significance and 2 degree of freedom. The calculated value of chi-square is 2.86 and the critical value is 5.991.
6. 50 % respondents strongly agree that semantic tutoring can enhance and improve knowledge sharing.
7. 36.05 % respondents strongly agree that semantic tutor can improve study success.
8. 41.86 % respondents rate semantic tutoring system highly effective compared to class room learning.
9. 29 % respondents pin pointed that inflexible timings and 29 % respondents pin pointed slow learning as the major problems with class room learning.
10. 26.74 % respondents selected flexible timings as the major advantage of semantic tutoring over class room learning.
11. 36.05 % respondents opted that knowledge sharing amongst classmates is very low in class room learning.

Challenges and Concerns in Semantic Tutoring

Along with the attraction of easy access to semantic tutors, several factors mitigate the value of online instruction [07]:

a. Outsourcing teacher's jobs from the community: Rather than creating teaching expertise in a local environment, online tutoring encourages displacement of instruction outside of a student's location and social group.

b. Separation of student from group problem solving with peers: Many problems in communities and the working world are solved with "team effort". Learning how to solve problems and resolve peer conflicts is a central part of socialization. Semantic tutoring encourages faceless communication with what may be an entirely unknown group [03].

c. Almost all potential students live in countries already providing schooling, often without cost. Semantic tutoring is expensive, yet while a state has a commitment to education, an online tutor's commitment is limited to continued payment.

Conclusion and Future Implications

Besides, semantic tutoring can be one of the most exciting enhancements to contemporary education. Semantic tutoring is neither right for all students nor right for all the faculties, but it will frequently meet the needs of both for an exciting, high-quality learning experience.

As with any instructional mode, the quality of online courses varies, but the potential-often met and still expanding-is on a par and in some respects even better than with the traditional F2F mode. Admittedly, it is up to future research to support or reject the impressions we have reported in this paper. The important point, however, is that semantic tutoring can be done well, and the demand for it is such that we all have to work to make it better.

References

1. Sajja P S, Manish Sharda. *Knowledge Scouting- An Out of Box Thinking and Acting*, Journal of Management, Sardar Patel University, Vol. 9, Pg. 80-86 (2007)
2. Brusilovsky, P. *Adaptive hypermedia: From intelligent tutoring systems to Web-based education* (Invited talk). In: G. Gauthier, C. Frasson and K. VanLehn (eds.) Intelligent Tutoring Systems. Lecture Notes in Computer Science, Vol. 1839, Berlin: Springer Verlag, pp. 1-7. (2000)
3. Lytras M., Pouloudi A., Poulymenakou A. *Dynamic e-Learning setting through advanced semantics: The value justification of a knowledge management oriented metadata schema.* International Journal of e-Learning, 1(4), 49-61 (2002)
4. Nenad Stojanovic, Siegfried Handschuh. *"A Framework for Knowledge Management on the Semantic Web"*, The Eleventh International WWW Conference, USA, (2002)
5. Warren, Paul, *"Knowledge Management and the Semantic Web: From Scenario to Technology"*, IEEE Intelligent Systems, January/February, pp 53-59 (2006)
6. http://en.www.wikipedia.org/e-learning
7. www.technologysource.org
8. http://en.wikipedia.org/wiki/Resource_Description_Framework
9. http://en.wikipedia.org/wiki/SPARQL
10. http://www.w3.org/TR/owl-guide/

'Prajna' - Journal of Pure & Applied Sciences, 16 (2008) 37-40

PERFORMANCE COMPARISION OF GLUCOSE BIOSENSORS BASED UPON DIFFERENT POLYMER MATRICES

U.B. Trivedi and D. Lakshminarayana
Department of Electronics, Sardar Patel University, Vallabh Vidyanagar - 388 120

Abstract

Amperometric glucose biosensors, based upon the immobilization of glucose oxidase enzyme, have been fabricated. Three different biosensors have been developed by immobilizing the enzyme in the polymer matrices of a unique combination of Poly carbamoylsulphonate (PCS) + Polyethylenemine (PEI) and electrodeposited Polypyrrole (PPy) and Poly *o*-phenylenediamine (PPD). The performance of the biosensor based on the PCS+PEI polymer matrix has been found to be better than that of the biosensors based on the electrodeposited polymers of PPy and PPD. The results obtained during the comparative study are presented.

Introduction

Improvement of "life quality" is one of the most important objectives of global research efforts dealing with any area of Science and Technology. The quality of life is closely linked to the detection and control of diseases, food quality and safety, and quality of our environment. For example, diabetic patients as well as non-diabetics need regular blood sugar level monitoring and control. The authors reported in their previous communication [1], about the fabrication of an enzyme based low cost, portable and disposable type of glucose biosensor. The biosensor was found to exhibit reasonably good performance in the detection of glucose concentration in human blood samples and soft drinks. The designed and fabricated amperometric glucose biosensor [1] was based on the immobilization of glucose oxidase (GOD) in a polymer matrix of Polyethylenemine (PEI) and Poly carbamoylsulphonate (PCS) hydrogel. However, a variety of conducting and non-conducting polymeric membranes can, in principle, be utilized for the purpose of enzyme immobilization [2-5].

In the present investigation, the authors report the fabrication of the glucose oxidase enzyme based glucose biosensors by utilizing the polymers of Polypyrrole (PPy) and Poly o-phenylenediamine (PPD). Accordingly, the performance of the Pt/PCS+PEI/GOD glucose biosensor system has now been compared with that of the Pt/PPy/GOD and Pt/PPD/GOD glucose biosensor systems, and the results are presented here.

Experimental

I. Immobilization of GOD in PCS+PEI polymer matrix: The details regarding the chemicals, reagents, enzyme immobilization, fabrication of transducer and biosensor operation have been already reported earlier [1].

II. Immobilization of GOD in PPy polymer membrane: A two step procedure as described by Trojanowicz *et al.* [5] was applied for the preparation of PPy layers. A first layer of Polypyrrole was obtained by electropolymerization using 0.1M KCl solution in a potentiostatic condition at +850mV against Standard Calomel Electrode (SCE) which, in turn, resulted in a yellow transparent layer. The process was performed for about 30-40 seconds. Then after 8 minutes, a conditioning was performed in a 5mM hydrogen peroxide solution. Later, an electropolymerization was performed again from solution containing 200-1000Uml^{-1} GOD leading to the immobilization of enzyme. The electro polymerization was performed for about 5 minutes.

III. Immobilization of GOD in PPD polymer membrane: The electropolymerization procedure descried by Trojanowicz *et al.* [1] was again adopted for the preparation of PPD layers. Initially, the polymer layer without enzyme was electro polymerized for 1 minute from a deoxygenated solution of monomer in 0.2M acetate buffer of pH 5.2 at +750mV. Then, the enzyme 200Uml^{-1} GOD was added to this solution and electro polymerization was continued for 5 to 15 minutes resulting in the formation of a colourless transparent film on the electrode surface. Thus, the enzyme was immobilized with PPD.

Results and Discussion

Figure 1 shows the calibration plots for glucose biosensors obtained by the immobilization of GOD in the three different polymers namely, PPy, PPD and PCS+PEI. The Figure clearly indicates the higher detection sensitivity of the biosensor fabricated with PCS+ PEI compared to PPy and PPD. In the present investigation, instead of the normal one step procedure of polymer layer formation, a two step procedure was utilized for the PPy and PPD polymerization. The results obtained suggest that a preliminary covering of the surface of the platinum tip with a thin layer of polymer (PPy, PPD) without enzyme is very advantageous for the reproducible formation of an enzyme containing polymer layer. The stability of the response was found to improve upon conditioning the Pt/PPy/GOD and Pt/PPD/GOD electrodes. An oxidative conditioning of PPy has been found to stabilize the amperometric response.

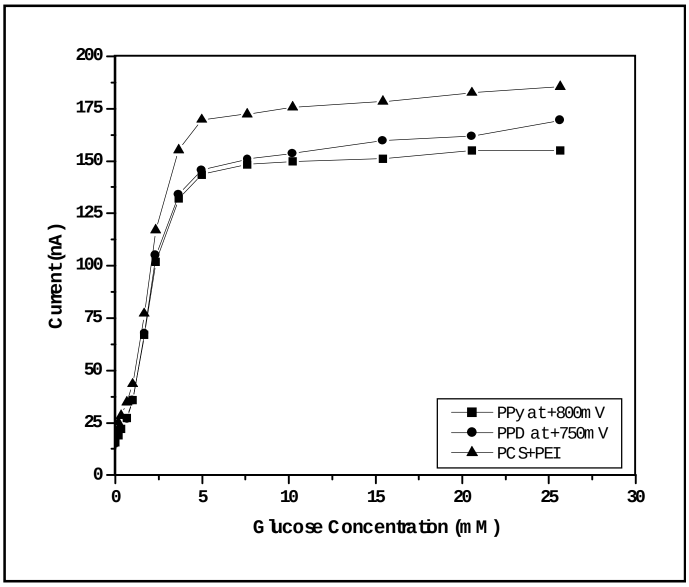

Figure 1: Calibration plot for glucose biosensor.

In the present investigation, the performance of the glucose biosensor with PCS+PEI polymer matrix has been found to be superior compared to the glucose biosensors fabricated with electropolymerized PPy and PPD polymers matrices. In addition to the better amperometric current response, the PCS+PEI polymer matrix has also been found to provide only a very negligible amount of enzyme bleeding out of the sensor structure.

The glucose detection limits obtained in the present investigation with the different polymer membrane based biosensor systems of Pt/PCS+PEI/GOD, Pt/PPy/GOD and Pt/PPD/GOD are 0.20 to 0.35 μM, 0.30 to 0.40 μM, and 0.25 to 0.40 μM respectively. Similarly, the response times obtained for the PCS+PEI, PPy and PPD based systems are 18-25 sec, 25-35 sec and 23-38 sec. The sensitivity value of 0.68 nA/μM ±0.13 of the PCS+PEI based system is also found to be better than that of the values obtained for PPy and PPD systems.

The advantageous rate of response of a glucose biosensor with PPD polymer in comparison to a Pt/PPy/GOD sensor has already been reported [6]. The rapidly growing literature on the enzyme based biosensors has given rise to numerous controversial opinions and interpretations about the mechanism of immobilization, polymerization, the role of polymer matrix in electron transfer in biocatalytic processes, stability of the obtained layers etc. [7-8]. In the present investigation, the results indicate that the PCS+PEI polymer matrix offers a better performance in comparison with that offered by electro polymerized PPy and PPD polymers. In the case of electrochemical polymerization of PPy and PPD, a suitable monomer is oxidized in the presence of the enzyme. The enzyme is accordingly confined to a layer adjacent to the electrode. However, the unique combination of hydrophilic PCS and the conducting polymer of PEI yielded a more workable hydrogel membrane for the enzyme based glucose biosensor operation. The combination of PCS hydrogel and the layer forming PEI might have offered a better enzyme entrapment instead of the layer only type of entrapment by other polymers.

Conclusions

Glucose biosensors based upon polymer matrices of PCS+PEI, PPy and PPD have been developed and their performances have been compared. It is found that the unique PCS+PEI based system offers superior sensor response.

References

1. U.B. Trivedi, D. Lakshminsrayana, I.L. Kothari, K.K. Makhija and H.N. Kapse, 'Prajna'- Journal of Pure & Applied Sciences, 15 (2007) 42
2. V. Saxena and B.D. Malhotra, Curr. Appl. Phys., 3 (2003) 293
3. S. Cosnier, Biosens. Bioelectron., 14 (1999) 443
4. Miao Yuqing, Chen Jianrong and Wu Xiaohua, Trends in Biotechnology, 22 (2004) 227
5. M. Trojanowicz, O. Geschke, T. Krawczynski vel Krawczyk and K. Cammann, Sensors and Actuators, B28 (1995) 191
6. C. Malitesta, F. Palmisano, L. Torsi and P. G. Zambonin, Anal. Chem., 62(1990) 2735
7. P.N. Bartlett and R.G. Whitaker, J. Electroanal. Chem, 224 (1987) 37
8. L. Coche-Guerente, A. Deronzier, P. Mailley and J.C. Moutet, Anal. Chim. Acta, 289 (1994) 143

'Prajna' - Journal of Pure & Applied Sciences, 16 (2008) 41-49

EFFICIENCY OF DETERGENTS ON COTTON, POLYESTER AND COTTON-POLYESTER BLEND

Namrita Kola

P.G. Department of Home Science, Sardar Patel University, Vallabh Vidyanagar-388 120

Abstract

Proper cleaning of clothes is one of the important aspects to be considered for increasing their life. Soil gets accumulated on textiles, which needs to be cleaned for reuse ability. There are vast varieties of detergents for laundry use available in the market, these consist of regular detergents, detergents with added ingredients like whitening agents, enzymes, oxy-agents etc., and so to select the right type based on performance and price is of much importance. The present study was mainly to study few varieties for their efficiency in detergency on artificially soiled cotton, polyester and cotton-polyester blend. Cleaning efficiency of detergent was determined by comparing light reflected from soiled and washed samples, with a reflectance meter. Soil was more readily removed from cotton fabrics due to their hydrophilic nature. The best results were obtained with detergents having added enzymes, though regular detergents were also good soil removers.

Introduction

Soiling of textiles is a very common and natural phenomenon. It normally occurs by three processes: direct soiling, transfer soiling and electrostatic soiling [1]. One of the most important problems in maintaining clothes clean and with satisfactory appearance is the removal of soil accumulated during wear, handling and storage. Soiling is influenced by nature of fabric, especially its hydrophilic/hydrophobic property. Since soil contains oils and grease, oleophilic fabrics are more difficult to clean (Nair [2]).

All fabrics and garments used for domestic purpose are laundered frequently to remove deposited soil to maintain them fresh and clean. Laundering practices used for a fabric greatly affect its life and performance (Mahale and Vastrad, [3]). Cleaning of clothes becomes necessary to make them last long and appear pleasant, bright and colourful. Importance of clean clothes was realized long back, and clothes have been washed and cleaned since the clothes have been in use. Earlier natural products like aritha and white clay were used for laundering then came the use of soaps. Now detergents have replaced soaps in laundering.

Detergents are substances that clean soiled surfaces, and usually are synthetic. Different chemicals make up the detergents, including a basic cleaning agent called a surfactant or surface-active agent, which lowers the surface tension of water and allow dirt and grease on clothing to be removed. Other ingredients added are builders (inorganic and organic), anti deposition agents to keep soil suspended, sodium silicate to protect aluminum pots and pans, optical brighteners for white effect, corrosion inhibitors etc. (Trotman [4]).

The detergent solution penetrates between the soil particle and the fiber, forms a thin film over the soil and transports it to the wash liquor from the surface of the fabric. The action of detergent is simple but factors that influence detergency are many and so the study of detergency is complex. Dave and Das [5] have listed various factors that effect detergency. They are: wetting, adsorption, surface and interfacial tension, emulsification and dispersion power, age of bath prior to washing, nature of soil, amount of soil, age of soil, composition of water, concentration of detergent, washing temperature, degree of mechanical action, duration of treatment, type of fabric etc.

Many studies have been reported on soiling and soil removal from textiles, some of them that are of direct significance have been abstracted. Cameron and Brown [6] evaluated the effectiveness of 42 detergents; 11-non-phospate containing powdered detergents, 12-phosphate containing powdered detergents, 11 unbuilt liquid detergents and 8 built liquid detergents, of varying formulations, in cleaning a standard soiled fabric in water of varying hardness. Powdered detergents were found to be significantly affected only at very high water hardness levels. There was no significant difference between washing in warm and hot water for liquid detergents, except for a melaleua oil based detergent which performed significantly better in hot water. Increasing water hardness had no significant effect on liquid detergents. Powdered detergents performed better than liquid detergents in cleaning the standard soiled fabric. While no one detergent was significantly better than the others, in general, washing with detergents that contained phosphates did give somewhat better results in warm water. Detergents that combined bleach as an additive did not result in whiter fabric.

Effects of detergent type and water temperature on soil removal on cotton fabric was studied by Bubl [7]. In six university laboratories, white cotton fabric was repeatedly soiled with a synthetic sebum and clay and laundered in home-type equipment. Two built nonionic detergents were used at 30° and 50° C. After 24 treatments, evidence of a build up of soil on all samples was obtained from the increase in extraction oil and ash content. The mean percentages of total soil removed varied among the laboratories. Clay soil was removed more readily than oily soil. More soil was removed by laundering at 50° C than at 30° C. The regular detergent had better detersive action than the cold-water detergent. Water temperature was more important than detergent type in soil removal. Re-deposition of soil onto unsoiled laundered fabrics was negligible.

Detergent considerations for consumers were studied by Cameron [8]. The effectiveness (ability to whiten) of six consumer laundry detergents, three powder and three liquids, was tested using a standard procedure. Assessment of each detergents ability to clean (ability to remove stain, thus whiten) a standard soiled cloth in six different cold-water samples was evaluated. Two of the detergents, one powder and one liquid, were new laundry products designed to function in cold water. Results were based on a standardized procedure using laundro-meter treatment and reflectance colorimeter testing. Although no one detergent was very effective in whitening, the differences in the detergents were significant when compared to the original standard soiled cloth. In addition, when laundering this particular standard soiled cloth (carbon black/olive oil) in cold water, neither of the new cold water detergents were better at cleaning (whitening) the samples than the detergents without bleach-containing detergents, and in fact, the powdered detergent with bleach performed the best in each of the tests in this study. The liquid detergent with bleach was best in comparison to other liquid detergents in only half of the tests performed.

Today the market is flooded with wide varieties of detergents with different ingredients and advertisements, which are at times misleading the consumer. A common housewife is at times in a dilemma and is not able to decide upon the right detergent in terms of money spent and results obtained. Detergents with special ingredients are costly but it is important to know how effective these ingredients are in soil removal for which the detergents are high priced. More over there is a general assumption that with increasing amounts of detergents the efficiency of cleaning will go up. Garments and household textiles these days mainly are of cotton, polyester and blends of cotton-polyester. With these basis the present study was planned to evaluate common types of detergents on artificially soiled white cotton, polyester and cotton-polyester fabrics.

Methodology

(1) Classification of detergents: The local market was surveyed and advertisements were interpreted to find out the various types of detergents (as detergent manufacturers do not mention the ingredients in the detergent). It was observed that mostly all detergents could be classified into four classes: (a) Regular (b) with whitening agents (c) with enzymes and (d) with oxy agents. For convenience these detergents have been classed as DR, DW, DE and DO respectively in the study.

(2) Fabrics used: White cotton (100%), polyester (100%) and cotton-polyester (68:32) fabrics were purchased from the local market. The fiber was identified using AATCC test method No. 20-1976; fabric count and fabric weight was determined as per method given by Booth [9].

(3) Preparation of the fabric: The three fabrics were scoured to remove starch with 2 gms./lit. soap solution, M:L=1:30, for 30 minutes at boil.

(4) Soil preparation and soiling: Study was done with artificial soiling. 1% soil solution was prepared by mixing the required ingredients as given in table no.1. Fifty-one samples of 5x5 cm were cut from each fabric and soiled in a steel cylinder with lid. Diameter of the cylinder was 7.26 cm and height 8 cm. The amount of soil used for soiling was based on the weight of the fabric. At a time only three samples were soiled. Along with the samples and soil, 10 steel balls were put in the cylinder. The cylinder was continuously agitated for 8 to 10 minutes in all directions by holding it in both hands. Out of the 51 samples, 3 were used, as control and remaining were washed with four types of detergents in four different concentrations. All soiled samples were preserved separately in plastic bags.

(5) Washing: For washing four different types of detergents were purchased from the local market as per classification and dissolved in tap water to make four concentrations: 0.25%, 0.5%, 0.75% and 1%. Washing was done in semi-automatic Videocon (top loading) washing machine for 8 minutes with additional load of dummy fabric. All samples were rinsed, dried and ironed flat.

(6) Determination of soil removal: To evaluate which samples were better cleaned, reflectance of all the samples was determined for which light meter was used. The setting up of the light source, sensor, sample was as given in figure 1. A cardboard box with lid was covered with black paper from inside. The light source was an electric lamp of 6 volts with a lens to obtain a straight beam of light. On the lid of the box 1 sq. cm hole was made for the light to fall on the sample. The sample was placed inside the box at an angle of 45° . The light sensor received the reflected light from the sample. The sensor was attached to a digital lux meter, which directly gave the readings. The reflected light was noted (in lux) and average of three readings was taken.

Results

The main objective of the present study was to evaluate few types of detergents for their cleaning property on artificially soiled cotton, polyester and cotton-polyester blend.

(1) Preliminary information and classification of detergents: The market consists of different brands of laundry detergents and each one claimed to have any number of special qualities. Looking at the qualities the detergents were classified into four classes: (a) Regular (DR) - without any special ingredient, these were cheapest of all (b) with whitening agent (DW) - promising that the detergent will make the laundry

whiter than white, usually containing optical brighteners, these were costlier than regular ones (c) with enzymes (DE) - claiming addition of enzymes for removal of biological stains like grass and blood. Enzymes used are protease combined with amylase (d) with oxy agents (DO) - claiming to contain special oxidizers, which have active oxygen to give bleaching effect. The detergent may contain sodium per carbonate or sodium per borate. There was not much price difference between DE and DO types of detergents.

(2) Preliminary information of fabrics used: The fiber content, fabric count, weave and fabric weight of the three fabrics is given in table no. 2.

(3) Effect of soiling: Scoured and unsoiled samples were evaluated for whiteness. The blend fabric appeared whitest of all where 116.3 lux light was reflected followed by cotton and polyester which were recorded at 111.1 and 100 lux respectively. After soiling in 1% soil, the reflectance of fabric was determined (average of three readings), these samples were control samples (table no. 3). Almost all samples appeared equally dirty. As soil was applied by impact with the help of steel balls. Cooke [10], has pointed out that soil particles are irregular in shape. The contact between soil particle and fiber increases when the particle is deformed on impact and more nearly conforms to the fiber surface. This means that pressure on the soil particles that cause deformation of soil particle as per the fiber surface will increase soiling. The samples were soiled with pressure when the soiling cylinder was agitated with steel balls.

(4) Cleaning efficiency of detergent: As expected from a detergent, all detergents studied had cleaning ability, but their efficiency varied, also cleaning efficiency varied from fabric to fabric. (table no. 3). As the samples were heavily soiled (1%) none of the detergents was capable of bringing back the original whiteness in one wash cycle, without soaking, at room temperature even at 1% detergent concentration. As pointed out by Bubl [7] water temperature is more important in soil removal than detergent type. As the concentration of the detergent increased, the cleaning efficiency of all detergents improved, but the improvement was not very drastic.

Cotton fabrics were better cleaned by all detergents because of its hydrophilic nature. Polyester was better cleaned by regular detergents and detergents with oxy-agents, while cotton-polyester blend were better cleaned by detergents with whitening agents and enzymes. Amongst all the detergents, detergents with enzymes (DE) showed best cleaning efficiency. Detergents containing oxy-agents (bleaches) did not result in whiter fabric as has been also reported by Cameron and Brown [6].

As home laundry consists of variety of fabrics that are cleaned at a time, the best cleaning results can be obtained by detergents with added enzymes. Where cost is to be considered, regular detergents are also equally good. Heavily soiled fabric should be washed more than one time at low detergent concentration rather than using more detergent in one wash cycle.

Conclusions

Cotton fabrics loose soil more readily than polyester and cotton-polyester. Regular detergents are efficient enough in cleaning power. Though detergents with enzymes are better cleaners, they are costly also. With increase in concentration of detergent, cleaning efficiency increases, but the increase is very less. Heavily soiled fabrics cannot be cleaned in one wash at 1% detergent concentration at room temperature without soaking. Washing needs to be done at higher temperature for better efficiency of detergent especially where oily soil is present. It is better to use low concentration of detergent and increase the wash cycles for heavily soiled fabrics.

References

1. Kissa E., *Handbook of fiber Science and Technology*, (Marcel Dekker Inc., New York) Vol. 2, p 211 (1984)
2. Nair G.P., Colourage, **51**(8), 41-46 (2004)
3. Mahale G. and Vastrad, Textile dyer and printer, **2**(1), 22-24 (1995)
4. Trotman E.R., *Textile scouring and bleaching* (B.I. Publications Pvt. Ltd., New Delhi) p 56-73 (1993)
5. Dave M. and Das M., J. of Text. Chemists and Colourists, **8**(3), 29 (1983)
6. Cameron B.A. and Brown D.M., J. of consumer studies and home economics, **19**(1) 85-97 (1995)
7. Bubl J.L., Text. Res. J, **40**(7), 637-643 (1970)
8. Cameron B.A., Family and Consumer Sci. Res. J, **36**(2), 151-162 (2007)
9. Booth J.E., *Principles of Textile Testing* (3rd ed.) (Newness Butterworths, London) p 210-215, 229-231 (1996)
10. Cooke T.F., J. of Text. Chem. and Colourists, **10**(2), 31-33 (1987)

Table 1: Ingredients of artificial soil

Ingredients	Amount
Oleic acid	32 ml
Coconut oil	28ml
Paraffin oil	20ml
Mineral oil	20ml
Carbon Black	1gm
	100ml

Table 2: Preliminary information of fabrics used

Fabric No.	Fiber content	Weave	Count (per sq. inch)	Weight in gms (per sq. mt.)
F1	Cotton	Plain	92x46	250
F2	Polyester	Plain	96x83	220
F3	Cotton-polyester (68:32)	Plain	108x62	150

Table 3: Reflected light index (lux) from scoured, soiled and washed samples

Fabric	Scoured	soiled	Washed with detergents of various concentrations															
			DR				DW				DE				DO			
			0.25%	0.5%	0.75%	1%	0.25%	0.5%	0.75%	1%	0.25%	0.5%	0.75%	1%	0.25%	0.5%	0.75%	1%
F1	111.1	26.3	40.6 (14.3)	41.6 (15.3)	42.6 (16.3)	45 (18.7)	48.6 (22.3)	49 (22.7)	50.3 (24)	50.3 (23)	50 (23.7)	51 (24.7)	51.3 (25)	53 (26.7)	47 (26.7)	48 (21.7)	48.6 (22.3)	49 (22.7)
F2	100	24	36.6 (12.6)	37.6 (13.6)	41 (17)	44.6 (19.6)	40.3 (16.3)	40.6 (16.6)	41 (17)	42 (18)	41 (17)	42.6 (18.6)	43 (19)	44.6 (20.6)	38.6 (14.6)	40 (16)	41.3 (17.3)	42 (18)
F3	116.3	25.5	33.6 (8.1)	33.8 (8.3)	34.6 (9.1)	36 (10.5)	45 (19.5)	46.2 (20.5)	49 (23.5)	47.3 (21.8)	44 (18.5)	47 (21.5)	48.6 (23.1)	50 (24.5)	36.3 (10.8)	38 (12.5)	39 (13.5)	42 (16.5)

Values in brackets are the difference between washed and soiled reflectance

Figure 1: Arrangement of light, sample and sensor to determine reflectance

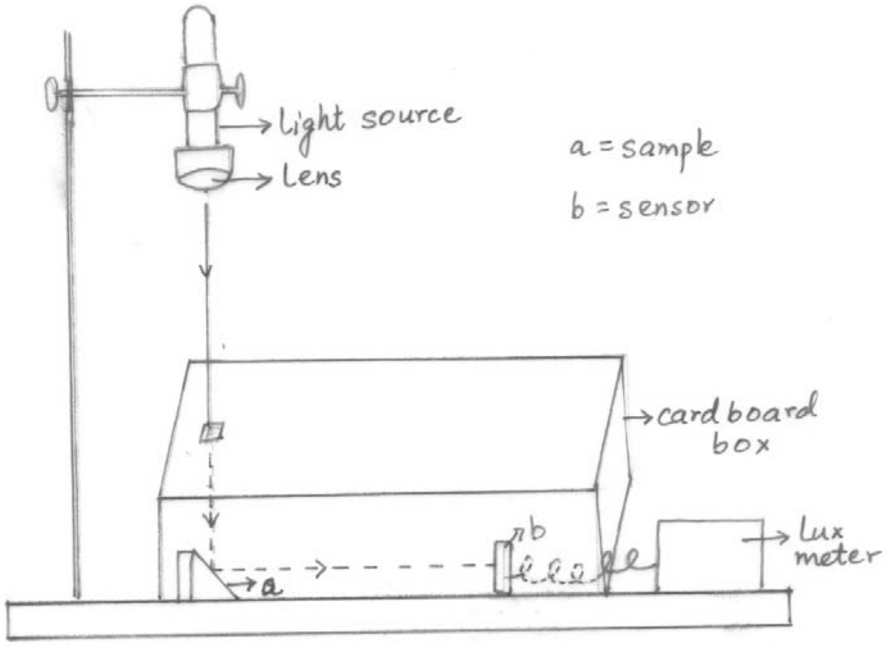

'Prajna' - Journal of Pure & Applied Sciences, 16 (2008) 50-53

A COMPARATIVE STUDY OF NATURAL CLEANING AGENTS AND SYNTHETIC DETERGENT FOR ITS CLEANING EFFICIENCY

Madhu Sharan
Department of Clothing & Textile, Faculty of Family and Community Science
The Maharaja Sayajirao University of Baroda, Vadodara

Abstract

Hundreds of thousands of tones of detergent with a value of billion of rupees are used annually in India. The production, use and disposal of such a large amount of chemicals is bound to have an adverse impact on the environment.There is a need to find out eco-friendly substitute as detergent is an indispensable part of the human life. Aritha and Shikakai have been used since antiquity for washing of ornaments and hair. Today also it is being used as additives to some compounds for the washing. The properties of Aritha and Shikakai were studied systematically for their cleaning efficiency and found to be effective.

Introduction

Detergents, used by almost every urban household, have the distinction of being one of the most successful income generating products for the companies who manufacture them. Their penetration in the rural areas is also increasing at an accelerated pace (1). It is an indispensable part of Human life. But its effluent is posing problems as all the chemicals used are not biodegradable. Some of these impacts include pollution of water sources, depletion of natural resources, concentration of heavy metals, the localized effects of chemical ingredients on biodiversity and toxicity to animals (2).

There is a need to find out substitute to reduce these adverse impacts. The natural cleaning agents can be an answer to this. Though, these are used in some formulations of detergents and shampoos (3). But neither its % content is known nor it has been used as a product itself.

Here is an attempt to study Aritha and Shikakai as a laundry reagent and compared with the properties of synthetic detergent.

Materials and Methods

Five commercially available fabrics (cotton, wool, cotswool, polyester cotton and polyester) were used. The preliminary data of these fabrics were determined as per standard procedures (4).

Aritha and Shikakai were used as natural cleaning agents and Teepol as detergent.

Extraction from Aritha and Shikakai: 500 grams of Aritha and Shikakai was soaked in 1000 ml of warm water for 12 hrs separately. It was then boiled for 30-40 min. Solution was strained using muslin cloth. Extract was made to 1000 ml residue (kernels and skin) was separated and weighed. Extract in 5% conc. was made and used for the work. The related properties studied were (5):

pH	:	by pH scale
Surface tension	:	by no. of drops method
Wetting time	:	by drop method
Percent wettability	:	by centrifuge method
Emulsifying power	:	by measuring the emulsified layer
Foaming power	:	by measuring foam formation & stability.

The washing was done in fabricated wash wheel for 15 min at room temperature keeping M:L ratio 1:30. Assessment of the samples was done with the value on gray scale (4).

Results and Discussion

The preliminary data of the fabrics used is given in Table 1.

Table 1: Preliminary Data of the Fabrics Used

Sr. No.	Fibre %		Fabric Count	Wt/unit area (gm/sq.cm.)	Weave
1	Cotton	100	46x56	82.4	Plain
2	Wool	100	66x102	68.6	Twill
3	Cotswool	100	54x84	128.0	Twill
4	Polyester cotton	60-40	42x66	76.8	Plain
5	Polyester	100	48x62	72.0	Plain

The properties of the cleaning agents studied are given in Table 2.

Table 2: Preliminary Data of the Cleaning Agents Used

Sr. No.	Properties	Reagent		
		Aritha	Shikakai	Teepol
1	pH	6.0	7.9	7.6
2	Surface tension	.31	.34	.25
3	Wetting time	180	190	1
4	Foaming power	20.0	6.2	18.2
5	Emulsifying power	57.2	14.3	28.6

pH of the shikakai was alkaline quite similar to detergent whereas aritha showed acidic (6.0) pH (Table 2).

Relative surface tension of aritha and shikakai was slightly more than the detergent (Table 2). Wetting time for detergent was lowest followed by aritha and shikakai. Aritha showed good percentage wettability and emulsifying power. Therefore owing to these properties aritha and shikakai can be used as laundry reagents.

Cleaning Efficiency

Cleaning efficiency of the solution was affected by the fabric to be washed. The results are given in the Table 3.

Table 3: % Cleaning Efficiency of Reagents

Sr. No.	Fabric	Laundry Reagent		
		Aritha	Shikakai	Teepol
1	Cotton	43.7	62.5	62.5
2	Wool	71.4	64.2	64.2
3	Cotswool	64.2	64.2	57.1
4	Polyester cotton	55.5	66.6	66.6
5	Polyester	66.6	77.7	77.7

For cotton, cotswool and polyester cotton fabric shikakai, for wool and cotswool aritha and for cotton, polyester and polyester cotton teepol and shikakai gave better results.

Therefore it was seen that amongst the natural cleaning agents aritha proved to be better for wool and cotswool. Wool fiber absorbs and retain more the cleaning solution because of its percent wettability and hydrophilic nature (6). Hydrophillicity indicates the polar portion of the molecules is repelled which is supported by lower surface tension and thus assist in cleaning action of the solution (7). Aritha being amphoteric in nature works for cotswool fabric.

Nowadays there is requirement of detergents for washing machines. This needs a reagent which forms less foam. It should have good wettability and takes less time for wetting and less time for washing. Shikakai will prove better for washing machines. The compact detergent produced by combination of natural cleaning agent with detergent will have an added advantages of being eco-friendly (being not 100% chemical), increased cleaning efficiency (cumulative effect) and safe for hands and fabric as compared to detergent. The exact percent combination of natural cleaning agent to the detergent to improve the property will not mislead the consumer.

References

1. Anon, Soaps and detergents for small scale industries, SBP Publication Ltd., Delhi, 11 & 81(2001)
2. Gupta V. and Niscam A., Effect of commercial detergents on functional finishing properties of fabrics, Colourage, Vol. 4, p. 37-40(2004)
3. Ullman's Encyclopedia of industrial chemistry, The wealth of India-raw material Vol. IX Rh-So, 225-227
4. Angappan P. and Gopal Krishnan R., Textile testing, SSM Institute of textile technology, 351-352(2002)
5. Saville B.P., Physical testing of textiles, (Woodhead-Cambridge) p.180 (1999)
6. Seema Y., Textbook of textile and laundry, Anmol Publication Pvt. Ltd., Delhi, p.129-148 (1997)
7. Upadek H. and King P., Detergent trends and environmental compatibility, The Indian textile journal, 18-26 (May 1992)

'Prajna' - Journal of Pure & Applied Sciences, 16 (2008) 54-60

AVAILABILITY OF NUTRIENTS FROM PREPROCESSED AND PROCESSED MOTHBEAN (Phaseslus aconitifolius Jacq)

Harshada J. Shah

Department of Biochemistry, M.B. Patel Science College, C.E. Society, Anand - 388 001

Abstract

Varieties of cooking procedures are used at home. Choice of the method directly affects the nutrient intake of the family and the individual. The present study was planned to study the alteration in the nutritive value of Moth bean during soaking, germination and cooking. The specific processes studied were soaking, soaking and pressure cooking, soaking and microwave cooking, germination, germination and pressure cooking as well as germination and microwave cooking.

The results of the study indicate that processes like soaking and germination increased the vitamin contents of the grains. Grains when cooked for eating purpose these vitamins level decreases. Pressure cooking seemed to retain higher amount of the nutrients compared to microwave cooking except for riboflavin content. The study indicates that the traditional cooking method is better for the preservation of nutrients compare to advanced and rapid microwave cooking.

Introduction

Food processing covers simple treatment applied to food in the kitchen. Treatments applied renders the food more appetizing, attractive and digestible (Chopra et al 1978).

Soaking and germination are the processing methods generally carried out prior to cooking for most of the legumes. Soaking, germination and sprouting are the three processes which are associated with the development of the sprout. These bring out desirable changes in dry seed grains and legumes. In the dry state they lack in several vital nutrients. The process of sprouting increases the quantity of vitamins several fold. They contain a full spectrum of minerals, which undergo significant changes. Sprouted grains are a major source of food proteins.

Legumes are generally cooked for consumption to increase palatability. Studies reviewed indicate increases in nutrients on germination, but very selected work is found on availability of nutrients after cooking. Varieties of the cooking procedures are used at home. Choice of the method directly affects the nutrient intake of the family (Miloslav1986). Soaking the beans in water before cooking shortens the cooking time. The cooking time for dried beans may also be shortened by pressure cooking. Considering all these aspects the present study was planned to assess the alteration in the nutritive value of Moth bean due to soaking, germination and cooking. The processes studied were soaking, soaking and pressure cooking, soaking and microwave cooking, germination, germination and pressure cooking as well as germination and microwave cooking.

Methods and Materials

Mothbean was procured from the local market, cleaned and immature grains were removed.

Raw grains: Sound legumes were weighed and crushed for analysis to obtain the initial value.

Soaked legumes: Sound legumes were weighed and soaked in separate containers with measured amounts of distilled water for six hours (Madanpal et al 1995).

Germinated legumes: Soaked seeds were transferred to a glass bowl, covered with a lid and allowed to germinate under moist conditions for 24 hrs.

Soaked and germinated seeds were cooked using the Pressure cooker and the Microwave oven.

Pressure cooking of soaked legumes: Soaked legumes were seasoned with 2% ground nut oil and kept in glass container. To this 20 ml of water was added and legumes were cooked using the pressure cooker.

Pressure cooking of germinated legumes: germinated legumes was seasoned with 2% ground nut oil. The legume were transferred to a glass container. To this 20 ml of water was added and legumes were pressure cooked using pressure cooker.

Microwave cooking of soaked legumes: legumes were seasoned with 2% ground nut oil and kept in a glass container. To 100 gram of soaked legumes, 50ml of water was added and cooked in a glass container using the microwave oven for 10 min.

Microwave cooking of germinated legumes: legumes were seasoned with 2% ground nut oil and kept in a glass container. Per 100 gram of germinated legumes, 50ml of water was added and cooked using the microwave oven for 10 min.

All the legumes were freshly analyzed by standard methods. Chemical analysis were carried out using standard methods:

Protein (Total nitrogen Oser and Hawks 1956 * 6.25), Moisture (AOAC 1984), Lipid (AOAC 1984), Iron (Ramsay et.al.1954), Calcium (Morris 1958), Phosphorous (Fiske and Subbarow 1925), Thiamine and riboflavin (AOAC 1984), Vitamin "C" (AAVC 1951).

Results and Discussion

Protein and fat content of the Mothbean were studied for raw, soaked, soaked and pressure cooked, soaked and microwave cooked, germinated, germinated and pressure cooked as well as for germinated and microwave cooked products.

Study indicates a significant ($p>0.005$) decrease in the protein content on soaking. The decrease in protein in agreement with Youssef et al (1987), which may be due to leaching out of water soluble proteins. Mostafa et al (1987) reported a loss in non-protein nitrogen on soaking. On germination of soaked grain the protein content indicates a non-significant increase compared to raw. Cooking of the soaked and germinated seeds leads to a non-significant decrease on pressure cooking but a significant ($p>0.005$) decrease on microwave cooking ($p>0.1$) for germinated and ($p>0.005$) for soaked grains respectively. Observations indicate that pressure cooking is better than microwave cooking to retain the protein. The loss in protein on cooking is in agreement with Aliya et al (1981). The decrease in protein was higher on microwave cooking compared to pressure cooking ($p>0.05$). These results are presented in Fig -1.

Fat content of raw Mothbean increases by 12% on soaking which further increases and finally indicates a 22.6% increase ($p>0.025$) on germination. Increase in fat on germination is also reported by Ahmad et al (1982). As the legumes was seasoned with 2% ground nut oil prior to the cooking 2 % fat remained present. Result of this study is presented in Fig - 2.

Soaking and germination both the processes found to increase the vitamins content. Soaking of the dry grains showed significant increase ($p>0.005$) for vitamin C which further increased significantly on germination ($p>0.005$). Increases in vitamin C on germination is reported by Kylen (1975) and Maggie and Field (1981) which may be due to synthesis from reducing sugar. Vitamin C content of the grain decreases on cooking due to its oxidative and heat sensitive nature, which is related to values reported by Ajay et al (1980) and Sree Ramula (1983). The decrease in vitamin C content was higher on microwave cooking ($p>0.005$) compared to pressure cooking ($p>0.025$). Naveeda and Prakash (2006) reported that microwave cooking caused 36-57% reduction of ascorbic acid while pressure cooking caused 10-30% loss. Fig - 3 represents these changes.

Thiamin content of the dry grains showed a significant increase ($p>0.05$) on soaking which further increased significantly on germination ($p>0.005$). Cooking of the mothbean leads to a loss in thiamin content. The decrease was higher on microwave cooking ($p>0.05$) compared to pressure cooking ($p>0.2$). Fig - 4 represents these observations.

Riboflavin content of the dry grains showed a significant increase ($p>0.005$) on soaking which further increased significantly on germination ($p>0.0005$). Cooking of mothbean leads to loss in riboflavin content. The decrease was non-significant for soaked grains but significant for germinated grains ($p > 0.01$) on microwave cooking ($p > 0.005$) and on pressure cooking ($p > 0.025$). Fig - 5 represents these results.

The result of this study indicates that processes such as soaking and germination increased the vitamin content of the grains. When grains were cooked for eating purpose these vitamin levels decreased. Pressure cooking seemed to retain higher amount of nutrients compared to microwave cooking except for riboflavin indicating that traditional cooking was better for the preservation of nutrients than microwave cooking.

Acknowledgement

The author acknowledges the guidance of Dr. S.S. Sail for this work. The present research work was carried out at the Postgraduate Department of Home Science, Sardar Patel University, Vallabh Vidyanagar-388 120

References

1. AAVC (American Association of vitamin Chemist). Methods in Vitamin Assay, II ed., Inter science publisher Inc. NewYork (1951)
2. Ahmad Rafic,. Mahdy El. Laila A. and Sabaiy El. Effect of germination on nitrogenious constitutants, protein fractions invitro seeds. Fd. Chem. 1982. **8**, 253-63 (1982)
3. Ajay, Oderinde and Osibanibo. Vitamin C losses in cooked fresh vegetables. Fd. Chem. **5**, 243-47 (1980)
4. Aliya S. and Geervani P. An assessment of the protein quality and vitamin B contents of commenly used fermented products of legumes and millets. J. of Sc. Fd. Agri. **32**, 837 – 42 (1981)
5. AOAC. Official Methods of Analysis of Association of Official Agricultural Chemists. Ed. Williams S. 14th ed. Virginia, USA (1984)
6. Chopra Kiran, Chopra A.K. and Bhat C.M. Protein quality of chapattis prepared from high yielding varieties of wheat. J. Res. P.A.U. XV **4,** 478-80 (1978)
7. Fisk R.H. and Subbarow Y. Colourimetric determination of phosphorus. J. Biol. Chem. **66**, 375 – 400 (1925)
8. Kylen A.M. and Mc. Grandy R.M. Nutrients in seeds and sprouts of alfalfa, lentils, mungbeans and Soyabeans. J. Food. Sci. **40**, 1008 – 9 (1975)
9. Maggie May and Field M.L. Nutritive value of corn and corn fermented after germination. J. Food Sci. **460**, 1069 – 73 (1981)

10. Madan Pal, Aruna Sharma and Sen Gupta. Effect of UV radiation on germination and seedling growth in Mungbean. Ind. J. Plant Physiology. xxxviii: **4** , 293-97 (1995)
11. Miloslav Rechcigl. Hand book of nutritive value for processed food. Vol. 1, CRC Press Inc. Third edition (1986)
12. Morris S. Jacobs. The chemical analysis of food and food products. III edi. Robert Kinger Publishing Co. Inc. (1958)
13. Mostafa M., M. Rahma E.H. and Rady A.H. Chemical and nutritional changes in soya bean during germination. Fd. Chem. **23**, 257-75 (1987)
14. Naveeda Khatoon and Jamuna Prakash. The effects of germination on the cooking quality and nutrient retention in pressure and microwave-cooked Bengalgram, greengram and horsegram. Food Chemistry. **97, 1**, 115-121 (2006)
15. Oser B. and Hawks B. Physiological chemistry, 13 edi. T.M.H. Publishing company Ltd., New Delhi (1956)
16. Ramsay W.R. Colourimetric determination of iron. J. of Biol. Chem. **53,** 227 – 79 (1954)
17. Sree Ramula N. and Motomuem C.D. Effect of cooking on nutritive value of common food plants of Tanzania (1983) (1) vitamin C in some of wide green vegetables. Fd. Chem.**3,** 205-10 (1954)
18. Youssef M.M., Abd M.H., Aal E.L., Laila A., Shekib E.L. and Ziena H.M. Effect of dehulling, soaking and germination on the chemical composition, minerals and protein of the fala bean. Fd. Chem. **23,**129-38 (1987)

Fig. 1: Changes in protein (gm%) content of mothbean

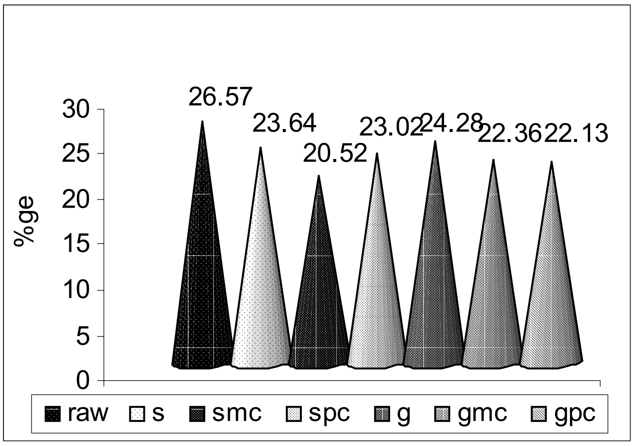

Fig. 2: Changes in fat (g%) content of mothbean

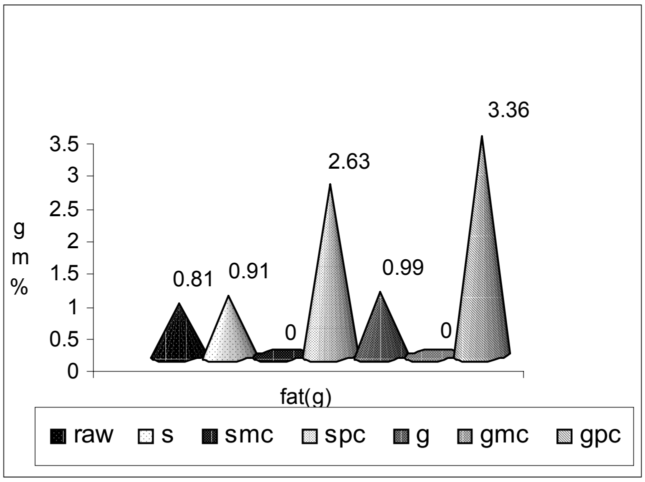

Fig. 3: Changes in Vitamin C (mg%) content of mothbean

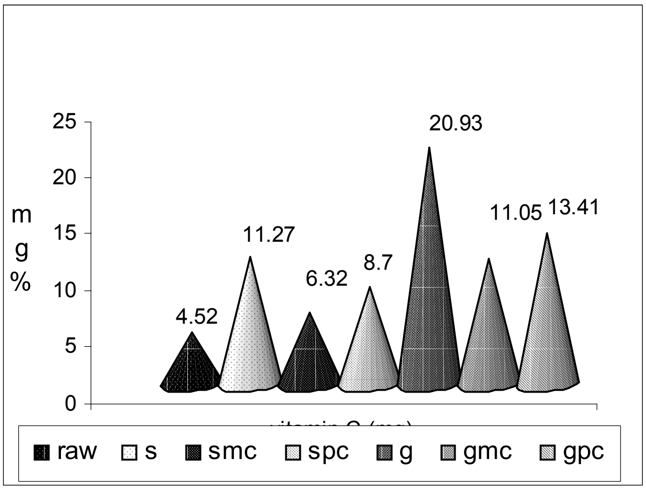

Fig. 4: Changes in Thiamin (mg%) content of mothbean

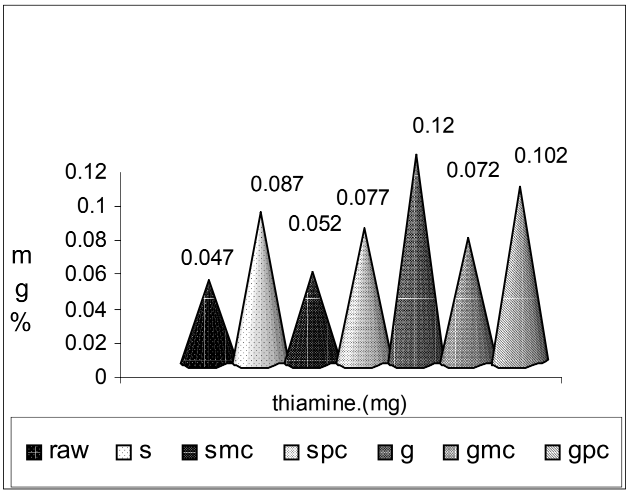

Fig. 5 Changes in Riboflavin (mg%) content of mothbean

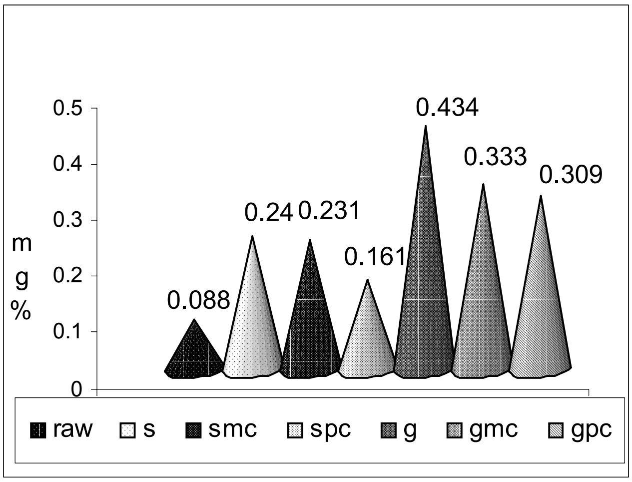

'Prajna' - Journal of Pure & Applied Sciences, 16 (2008) 61-69

A NOVEL METHOD OF IMPACT MODIFICATION OF THERMOSETTING MATRICES USING ELASTOMERS IN REACTIVE/NON REACTIVE PROCESSES IN JUTE FIBRE COMPOSITES

Umesh Bhimani, Rajnikant Malsana and Neetha John
Plastics Technology Department, Institute of Science & Technology for Advanced Studies &
Research (ISTAR) - C.L. Patel Center for Science & Technology
Vallabh Vidyanagar - 388 120

Abstract

Thermosetting plastics materials posses low impact strength compared to other plastics materials. Elastomer based toughening system was adopted for these materials. Natural rubber and nitrile rubber were used as toughening agents. The matrices were phenol formaldehyde, epoxy and unsaturated polyester resin. All are modified by the rubbers and jute fibre composites were prepared. Mechanical properties were estimated for the composites and found to superior than the unmodified matrices.

Introduction

Successful rubber toughening imparts greater ductility, improved crack resistance and impact strength to the material (1-5). The toughening is achieved by a small loss in stiffness of the material and without a large effect on its thermal stability (6, 7).

In toughening of plastics, polystyrene is the first that was tried and high impact polystyrene (HIPS) was prepared. Styrene acrylonitrile (SAN), Acrylonitrile butadiene styrene (ABS), polymethyl methacrylate (PMMA) etc. comes next to that. They all come under purely engineering plastics. Thermosets like epoxy resin are also toughened now a days (8-10).

In brittle material like thermosets plastics the molecular mobility in the glassy state is low and the poly chains are unable to undergo large scale molecular motion in response to rapidly applied external stresses or impacts (11). Several different routers are used for the preparation of rubber toughened polymers. The formations of crosslinked rubbery regions by phase separation during the polymerization are widely accepted in the toughening of phenol formaldehyde (12). The structure of the material obtained by this route depends on the chemical and physical changes that occur during the polymerization process (13, 14).

Present work deals with toughening of thermosetting materials like phenol formaldehyde resin, unsaturated polyester resin and epoxy resin with rubbers like natural rubber and nitrile rubber.

Experimental

Materials Used:

Phenol, formaldehyde, xylene, toluene, methanol are laboratory grade.

Unsaturated polyester, commercial grades supplied by Krishna Polymers, Anand.

Epoxy resin, epoxy equivalent 200 was commercial grade, supplied by Sympol, Ahmedabad.

Unsaturated Polyester resin (UPE), general purpose and epoxy resin were commercial resins widely used to make composites.

Epoxy resin was cured with Tri ethyl tetra amine (TETA) in molar ratios.

UPE resin was cured with Methyl ethyl ketone peroxide-1% (MEKP) and cobalt octate-0.1%.

Natural rubber (NR), ISNR-5, ML(1+4) at 100^0 C 85 was supplied by RRII, Kottayam, Nitrile rubber (NBR), ML(1+4) at 100^0 C 45, acrylonitrile content 33 % was supplied by Apar Polymers Ltd.

Jute fibre was commercial grade.

Experimental Techniques:

Preparation of Rubber solution:

Rubber was masticated to reduce the molecular weight using a Laboratory scale two roll mill (6x12 inch). In the two roll mill a temperature of 50-60^0 C was kept. It was then dissolved in toluene. The solution was stirred and kept in air tight containers. This rubber solution was used for further blending.

Modification of PF resin (Reactive method):

Phenol and formaldehyde were mixed and oxalic acid is used as catalyst. This solution was mixed with rubber solution in the reactor vessel by adding drop wise with continuous stirring. Temperature given was kept between 90-100^0 C. Stirring continued until and a homogeneous mass was obtained with sufficient viscosity. This mixture of phenol formaldehyde with rubber was used for composite preparation. Different ratios of rubber were used to prepare jute fibre composites.

Modification of UPE and Epoxy resin (Solution blending):

In unsaturated polyester resin (General purpose) and epoxy resin (EEW: 200) were commercial resin available which were used in composites preparations. Solution stage mixing was used to mix with rubber. Solutions of UPE and epoxy in xylene (10%) was mixed with rubber solutions in different ratios and used for composite preparation.

Composite preparation:

The resin to jute fiber ratio was 60/40. In every composites 6-7 plies of jute fibre were taken. The curing agents for the resins were mixed. The resin was diluted by solvents like toluene/xylene and applied on each layer of fiber and allowed to dry. The plies were then kept in a compression molding machine without applying any pressure. Sheets were prepared and specimens were cut using cutting machines.

Testing:

a) Impact strength: Test specimens were prepared for Izod impact test. Specimens were kept vertical in cantilever position and pendulum load was used to strike it. The energy required for breaking the specimens was recorded. Using the thickness of the specimen impact energy was also calculated and reported in J/mm. This test was conducted as per ASTM D 256***.

*******ASTM: American Standards for Testing Materials. The most popular testing standards used world wide, published and revised periodically. This is available for all materials and "D" section is for plastics/Rubber/Polymers etc. The standard used in this was published in 2004.*

b) Flexural strength and modulus: Rectangular pieces were cut out of the sheets and flexural strength was measured using universal testing machine. Three point bending technique was followed in this test. This test was performed as per ASTM D 790.

c) Rockwell hardness: Sheets specimens were taken for estimating Rockwell hardness in L scale as per ASTM D 785.

d) Surface and volume resistivity: The surface and volume resistivity of the compression-moulded compounds were determined using a mega ohmmeter. The test was conducted as per ASTM D 257.

e) Chemical resistance: The effect of chemicals on the compounds was estimated in different mediums NaOH and H_2SO_4. Specimens were immersed in the chemicals for 24 hours at room temperature. The test was performed as per ASTM D 543.

Results and Discussion

Figure 1, 2 & 3 show the impact strength of jute fibre composites made of phenolic, unsaturated polyester and epoxy resin respectively modified by rubbers like natural rubber and nitrile rubber.

As the amount of rubber increases the impact strength increases. The effect is same for phenolic, UPE and epoxy matrices in which impact strength is increasing for the composites. Impact strength is increasing because of the toughening effect of rubbers in the composites.

Rubber particles will be acting as stress concentration points and absorb the shock or impact which saves the matrix from a brittle failure [15, 16].

In this case the type of toughening was shear yielding in which rubber particles absorb and yield to the maximum before failure [16]. When concentration of rubber increases impact strength increases. This behaviour is found to be similar in both types of rubbers irrespective of the polarity. Due to toughening 100% increase in impact strength was observed. Out of two rubbers natural rubber shows superior effect than nitrile rubber because of its higher elongation, tensile strength and flexibility.

Figure 4 & 5 shows the flexural strength and modulus respectively of the phenolic composites. As the rubber content increases flexural modulus and flexural strength decreases. This is due the presence of low modulus member in the matrices. This behaviour is similar in all the other composites also. Similar effects are shown in figure 6-9 in UPE and Epoxy resin composites.

Rockwell Hardness results are shown in Figure 10. The hardness values are found to be decreasing as the rubber content increases. This is due the lower hardness of rubber components.

Volume resistivity and surface resistivity values are shown in Figure 11 and 12. As rubber content increases resistvity decreases slightly. This may be due to the effect of rubber on making the composites less resistance to current passage.

Chemical resistance of the composites is shown in the Table 1. The chemical resistance of these composites was found to be very good. The weight changes are very negligible which is superior compared to conventional composites without rubber.

Table1: Chemical Resistance of the Composites with 1x1 cm size (area)

Sample (With 4% rubber)	**Weight change in HCl (1N), mg**	**Weight change in NaOH (1N), mg**
PF without rubber	0.061	0.061
PF – NR (with rubber)	0.049	0.059
PF- NBR (with rubber)	0.005	0.013
Epoxy (without rubber)	0.05	0.05
Epoxy –NR (with rubber)	0.049	0.05
Epoxy- NBR (with rubber)	0.005	0.013
UPE (without rubber)	0.03	0.03
UPE – NR (with rubber)	0.012	0.016
UPE- NBR (with rubber)	0.019	0.023

Conclusions

Generally thermosetting, polymers show very low toughness. The thermosetting matrices like phenolic, epoxy, UPE are modified with rubber. This technique is used to improve the impact strength but shows marginal reduction in flexural properties and Rockwell hardness due to the presence of rubber. In this study two rubber were used and out of this natural rubber was found to be giving higher properties than nitrile rubber. Chemical resistances of the compounds are superior to unmodified composites. This method of Toughening of thermosetting matrices is found to be very effective. The amounts of rubber required were very small. The technique used are very simple and thus can easily be commercialized.

References

1. R.F. Boyer, Encycl. Polymn. Sci. Technol, 13: 392, 1982
2. D.J. Angier, Rubb. Chem. Technol, 36: 1164, 1965
3. J.D. Moore, Polymer, 12: 478, 1971
4. A.M. Donald, J. Appl. Polym. Sci. 27: 478, 1971
5. Y. Okamoto, Polymn. Eng. Sci. 33(24), 1606, 1993
6. C.B. Bucknal, Polymer, 6437, 1965
7. C.B. Bucknal, Polymer Blends, Academic Press, New York, p-99, 1978
8. S. Miles and S. Rostami, Multi component systems, Longman Scientific & Technical, p-149, 1992
9. W. Lees, Adhesives in Engineering Design, Springer-Verlag, Berlin, 1984
10. A.J. Kinloch, Developments in Adhesives, Vol. 2, Applied Science Publishers, London, 1981
11. L.T. Manzione, J.K. Gilham and C.A. McPherson, J. Appl. Polym. Sci. 26, 907 (1981)
12. J.A. Sayre, R.A. Assink and R.R. Lagasse, Polymer, 22, 87 (1981)
13. J.K. Gillham, SPE Ann. Tech. Conf. 38, 268 (1980)
14. C.B. Bucknall and T. Yoshii, Br. Polymn. J, 10, 53 (1978)
15. A.Y. Coren and R. Patel, Rubber Chem. Technol, 1993, 56, 1045-1060
16. G.O. Shonaike and G.P. Simon, Polymer Blends and Alloys, 1999, Marcel Dekker, New York

FIGURES

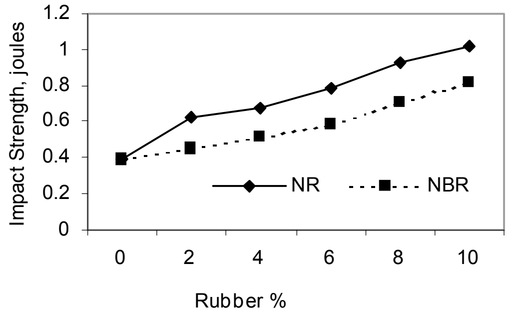

Figure 1 Impact Strength PF resin with rubber

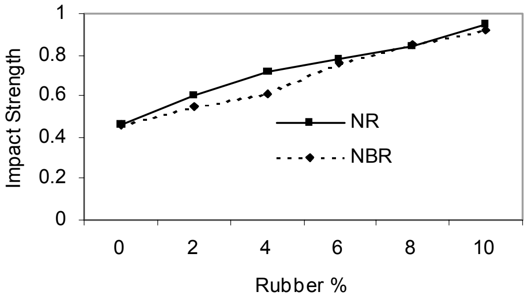

Figure 2 Impact Strength of Epoxy resin with rubber

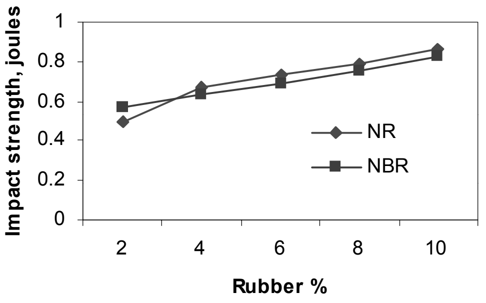

Figure 3 Impcat strength of UPE with rubber

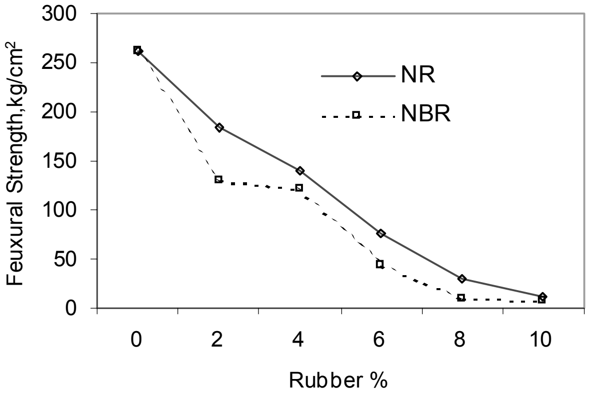

Figure 4 Flexural Strength of PF with rubber

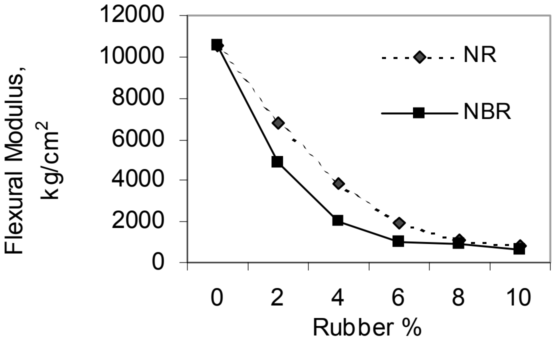

Figure 5 Flexural Modulus of PF with rubber

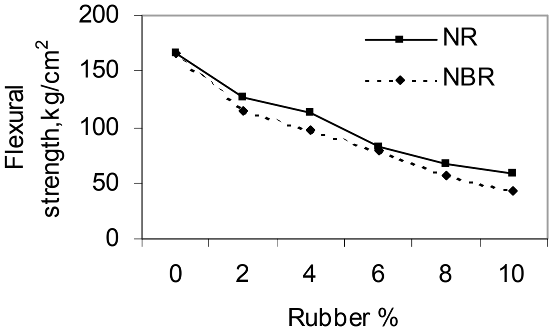

Figure 6 Flexural Strength of Epoxy resin with rubber

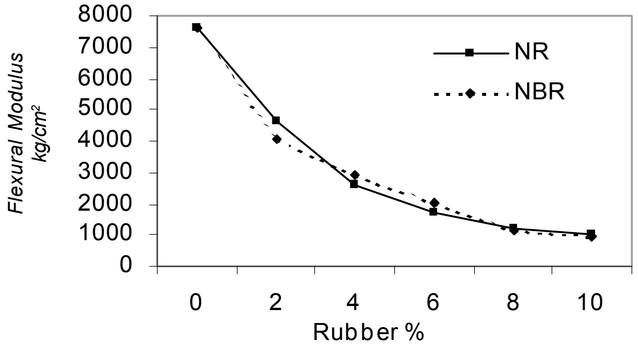

Figure 7 Flexural Modulus of Epoxy resin with rubber

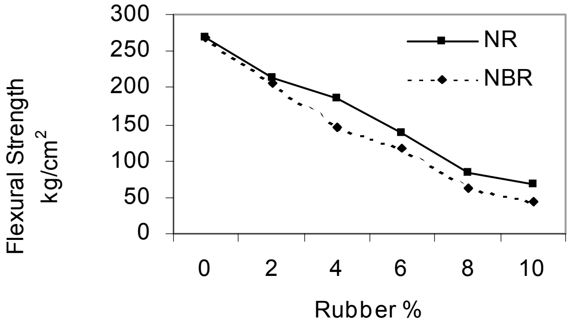

Figure 8 Effect of rubber in Flexural Strength polyester matrix

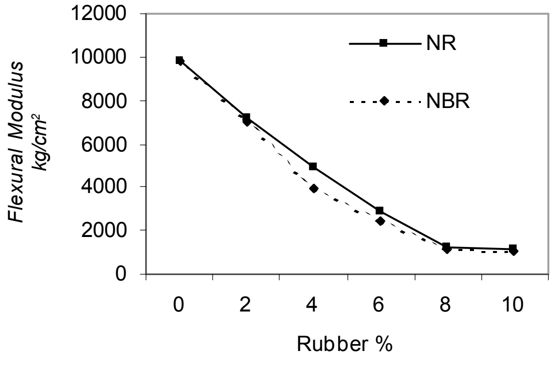

Figure 9 Flexural Modulus of Polyester with rubber

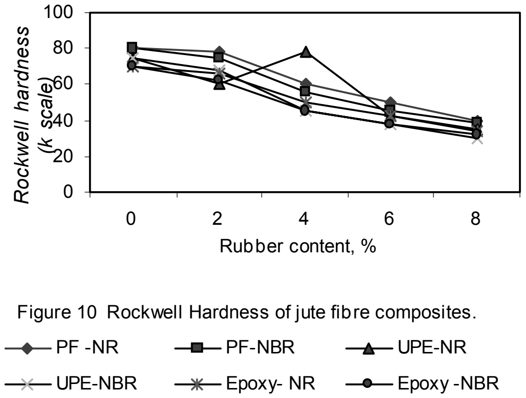

Figure 10 Rockwell Hardness of jute fibre composites.

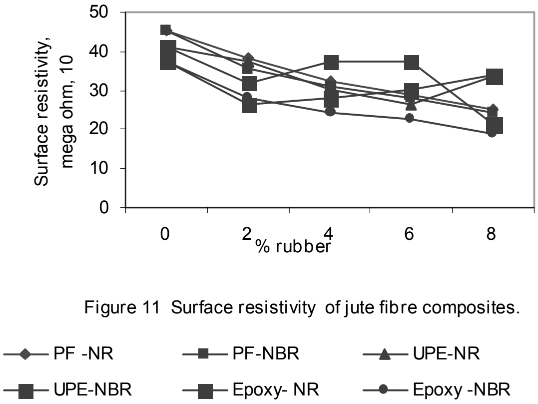

Figure 11 Surface resistivity of jute fibre composites.

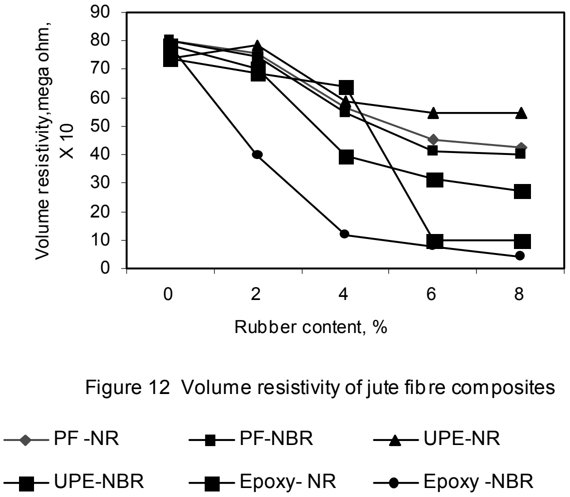

Figure 12 Volume resistivity of jute fibre composites

'Prajna' - Journal of Pure & Applied Sciences, 16 (2008) 70-79

A STUDY OF SQUEEZE FILM BEHAVIOR IN ANNULAR PLATES LUBRICATED WITH MAGNETIC FLUID

R.M. Patel G.M. Deheri* and H.C. Patel**
Department of Mathematics, Gujarat Arts and Science College, Ahmedabad - 380 006
*Department of Mathematics, Sardar Patel University, Vallabh Vidyanagar - 388 120
**Department of Mathematics, Government Engineering College, Patan

Abstract

Efforts have been made to study the behavior of squeeze film formed by magnetic fluid between curved annular plates considering the curvature of a secant form to represent the film thickness. The Reynolds' equation is solved and the expressions for performance characteristics such as pressure, load carrying capacity and response time are derived. The results are presented in graphical form. It is observed that all these above characteristics register increase with increasing magnetization parameter. Furthermore the performance of bearing with magnetic fluid lubricant is relatively better than that with the conventional lubricant.

Key words: Magnetic fluid, Squeeze film, annular plate, Reynolds equation, load carrying capacity.

Introduction

The behavior of the squeeze film between various geometrical configurations of flat surfaces was analyzed by Archibald [1]. Hays [2] presented the squeeze film phenomenon between curved plates considering curvature of the sine form and keeping minimum film thickness as constant. Murti [3] discussed the behavior of the squeeze film trapped between curved circular plates describing the film thickness by an expression of exponential function. He based his analysis on the assumption that the central film thickness instead of minimum film thickness as assumed by Hays, was kept constant. Following the analysis of Murti, Gupta and Vora [4] studied the squeeze film behavior between curved annular plates. In all the above studies the lower plate was considered to be flat. The squeeze film behavior between porous annular disks has been analyzed by Wu [5] for irrotational disks. This analysis was extended by Gupta and Sinha [6] by considering the effect of the axial current. Ting [7] simplified the analysis [6] considerably taking only the lower disk to be rotating. All the above studies considered conventional lubricant. Verma [8] and Agrawal [9-10] investigated the application of a magnetic fluid as a lubricant. Subsequently Bhat and Deheri [11] analyzed the squeeze film between porous annular disks using a magnetic fluid lubricant with the external magnetic field oblique to the lower disk. Also Bhat and Deheri [12] analyzed the magnetic fluid based squeeze film in curved porous circular disks. In these articles it has been observed that the performance of the bearing working with a magnetic fluid was better than that with a conventional lubricant. However, the plates were taken to be flat.

In practice, the flatness of the plates does not endure owing to elastic, thermal and uneven wear effects. With this end in view Bhat and Deheri [13] studied the effects of magnetic fluid lubricant on the configurations of Ajwaliya [14]. Recently Patel and Deheri [15] studied the magnetic fluid based squeeze film between two curved plates lying along the surface determined by secant functions rather than the surfaces being determined by exponential functions as assumed in [13] and [14]. Further works regarding the behavior of squeeze film in curved plates have been carried out in ([16], [17], [18]). Here we propose to study the problem of Ajwaliya [14] in the presence of a magnetic fluid, wherein, the plates lie along the surfaces determined by secant function.

Analysis

The configuration of the bearing is as shown in figure 1. We assume the upper plate lying along the surface given by

$$z = h_0 [\text{ Sec } (Br^2)]; \; b \le r \le a$$

approaching with normal velocity $\dot{h}_0 = \frac{dh_0}{dt}$ to the lower plate lying along the surface

$$z = h_0 [\text{ Sec } (Cr^2) - 1]; \; b \le r \le a$$

where B and C are the curvature parameters governing the curvature of the two surfaces respectively (h_0 is the central distance between the film thickness) (C.f. [10], [14]).

The film thickness h(r) is defined as

$$h(r) = h_0 [\text{ Sec } (Br^2) - \text{Sec } (Cr^2) + 1]; \; b \le r \le a$$

Introducing the dimensionless quantities

$$\bar{h} = h / h_0, \qquad R = r / a, \qquad \alpha = b / a.$$

$$\mu^* = \frac{\mu_0 \; \bar{\mu} \; h_0^3}{\mu \; \dot{h}_0} .$$

we obtain the dimensionless film thickness

$$\bar{h} = [\text{ Sec } (\bar{B}R^2) - \text{ Sec } (\bar{C}R^2) + 1] \qquad \dots (1)$$

wherein $\bar{B}$ and $\bar{C}$ are the dimensionless curvature parameters defined by $\bar{B} = Ba^2$ and $\bar{C} = Ca^2$. Concerned Reynolds' equation governing the film pressure is obtained as [C.f. (13), (14)]

$$\frac{d}{dr}\left[r h^3 \frac{d}{dr}\{ p - 0.5\, \mu_0\, \bar{\mu}\, H^2 \}\right] = 12\, \mu\, \dot{h}_0\, r \qquad \dots (2)$$

where $H^2 = (a - r)(r - b)$; $b \le r \le a$, μ is the fluid viscosity, $\bar{\mu}$ represents the magnetic susceptibility, μ_0 stands for the permeability of the free space and the inclination ϕ of the external magnetic field with the lower disk is represented as in [13]. Integrating (2) with boundary conditions $p = 0$ at $r = a$ and $p = 0$ at $r = b$, we get the dimensionless pressure P as

$$P = -\frac{h_0^3\, p}{\mu a^2 \dot{h}_0} = 0.5\, \mu^* (1 - R)(R - \alpha) - 6\int_{\alpha}^{R} \frac{R}{\bar{h}^3}\, dR + \frac{6\int_{\alpha}^{1} (R / \bar{h}^3)\, dR \int_{\alpha}^{R} (1 / R\, \bar{h}^3)\, dR}{\int_{\alpha}^{1} (1 / R\, \bar{h}^3)\, dR} \qquad \dots (3)$$

The load carrying capacity W is obtained from the relation

$$W = 2\pi \int_{b}^{a} r\, p(r)\, dr$$

The dimensionless load carrying capacity is given by

$$\bar{W} = -\frac{W h_0^3}{2\, \pi\, \mu\, a^4\, \dot{h}_0}$$

$$= (\mu^* / 24)(1 - \alpha^2)(1 - \alpha)^2 + 3\int_{\alpha}^{1} \frac{R^3}{\bar{h}^3}\, dR - \frac{3\left[\int_{\alpha}^{1} (R / \bar{h}^3)\, dR\right]^2}{\int_{\alpha}^{1} (1 / R\, \bar{h}^3)\, dR} \qquad \dots (4)$$

The response time in the dimensionless form becomes

$$\Delta T = \frac{\Delta t \, W \, h_0^2}{\pi \, \mu \, a^4} = \left[(1 / \bar{h}_2^2) - (1 / \bar{h}_1^2) \right] (\mu^* / 24)(1 - \alpha^2)(1 - \alpha)^2 \, \bar{W} \quad \ldots (5)$$

where

$h_1 = h_1 / h_0$, $\bar{h}_2 = h_2 / h_0$.

Results and Discussion

Expressions for pressure, load carrying capacity and response time in dimensionless form are presented in equations (3), (4) and (5) respectively. These three equations make it clear that the increase in pressure, load carrying capacity and response time in the present case are $(\mu^* / 2)\ (1 - R)\ (R - \alpha)$, $(\mu^* / 24)\ (1 - \alpha^2)\ (1 - \alpha)^2$ and $(1 / \bar{h}_2^2 - 1/ \bar{h}_1^2)\ (\mu^* / 24)\ (1 - \alpha^2)\ (1 - \alpha)^2$ respectively. All these tend to increase with increasing values of magnetic parameter μ^* For the sake of comparison the ranges of the parameters are chosen as in [15]. The computed values of dimensionless pressure, load carrying capacity and response time are presented in graphical form.

In figure 2 we have the pressure distribution with respect to the magnetization parameter μ^*. This figure reveals that the pressure increases with increasing μ^*.

Figure 3 presents the variation of load carrying capacity with respect to μ^*. The graph suggests that increasing values of μ^* cause increased load carrying capacity. Further a comparison with the conventional lubricant indicates that the bearing performance gets improved here (C.f. [14]).

Figure 4 depicts the variation of response time with respect to μ^*. Here it is observed that increasing values of μ^* cause increase in the response time.

Variation of pressure and load carrying capacity with respect to the curvature parameter of the upper plate is presented in figures 5 and 6 respectively. It is interesting to note that in these figures a symmetric nature in the distribution of pressure and load carrying capacity is manifest.

Lastly figures 7 and 8 give the distribution of pressure and load carrying capacity with respect to the lower plate's curvature parameter respectively. Here also the symmetrical nature persists so far as the distribution of pressure and load is concerned. Further, a comparative study on the effect of the curvature parameters indicates that the trends are reversed in nature. In addition, a comparison of figures 6 and 8 suggests that the effect of lower plate's curvature parameter is little better than the effect of the curvature parameter of the upper plate.

Conclusion

The study clearly underlines that the performance of the bearing with a magnetic fluid lubricant is considerably better than that of a conventional lubricant. The symmetrical nature is observed in the distribution of load with respect to the curvature parameter makes it all the more interesting from the industrial point of view. For a more better performance of the bearing one can suitably adjust (increasing / decreasing) the curvature parameters of both plates.

Acknowledgement

The authors acknowledge the critical and in-depth remarks and comments of the referee. Two of the authors would like to thank UGC for the funding of U. G. C. major research project (U. G. C. F. No. 32-143/2006 (SR) - "Magnetic fluid based rough bearings") under which this investigation has been carried out.

References

1. Archibald, F.R., "Load capacity and time relations for squeeze films", ASME, D, 78, (1956) p. 29
2. Hays, D.F., "Squeeze films for rectangular plates", ASME, D, 58, (1963) p. 243
3. Murti, P.R.K. "Squeeze films in curved circular plates", ASME, JLT, Vol. 97, (1975) p. 650
4. Gupta, J.L. and Vora, K.H. "Analysis of squeeze film between curved annular plates", J. Lubr. Technol. 102, (1980), 48
5. Wu, H., "Squeeze film behavior for porous annular disks", J. Lubr. Technol., Vol. 92, (1970) pp. 593-596
6. Gupta, J.L. and Sinha, P.C., "Axial current induced pinch effect on the squeeze film behavior for porous annular disks", J. Lubr. Technol., Vol. 97(1), (1975) pp. 130-133
7. Ting, L.L., "Engagement behavior of lubricated porous annular disks", Wear, Vol. 34, (1975) pp. 159-182
8. Verma, P.D.S., "Magnetic fluid-based squeeze film", Int. J. Engg. Sci. 24(3), (1986) p. 395

9. Agrawal, V.K., "Magnetic-fluid-based porous inclined slider bearing", Wear, 107, (1986) pp. 133-139
10. Agrawal, V.K., "Magnetohydrodynamiczne lozysko slizgwe w stycznym polu magnetycznym", Rozprawy Inzynierskie, Vol. 18(1), (1970) pp. 45-53
11. Bhat, M.V. and Deheri, G.M., "Squeeze film behavior in porous annular disks lubricated with magnetic fluids", Wear, Vol. 151, (1991) p. 123
12. Bhat, M.V. and Deheri, G.M., "Magnetic fluid based squeeze film in porous circular disks", Journal of Magnetism and Magnetic Materials, Vol.127, (1993) pp. 159-162
13. Bhat, M.V. and Deheri, G.M., "Magnetic fluid-based squeeze film between two curved circular plates", Bull. Cal. Math. Soc. 85, (1993) p. 521
14. Ajwaliya, M.B., On certain theoretical aspects of Lubrication, Ph.D. thesis, S.P. University, V.V. Nagar (1984)
15. Patel, R.M. and Deheri, G.M., "Magnetic fluid based squeeze film between two curved plates lying along the surfaces determined by secant functions", Journal Engineering and Materials Sciences, Vol. 9, (2002) p. 45
16. Patel, R.M. and Deheri, G.M., "A study on the behavior of squeeze film between annular plates", South East Asian Journal of Mathematics and Mathematical Sciences, Vol. 3(2), (2005) p. 73
17. Patel, R.M., Deheri, G.M. and Patel H.C., "Squeeze film behavior in annular plates lubricated with magnetic fluid", To appear in ADIT Journal of Engineering, (2008)
18. Deheri, G.M., Patel, R.M. and Abhangi, N.D., Magnetic fluid based squeeze film behavior between transversely rough curved plates, CIST 2008 5th China International Symposium on Tribology and ITS-IFToMM 2008 1st International Tribology Symposium of IFToMM, Beijing

FIGURES

Figure 1: Bearing Configuration

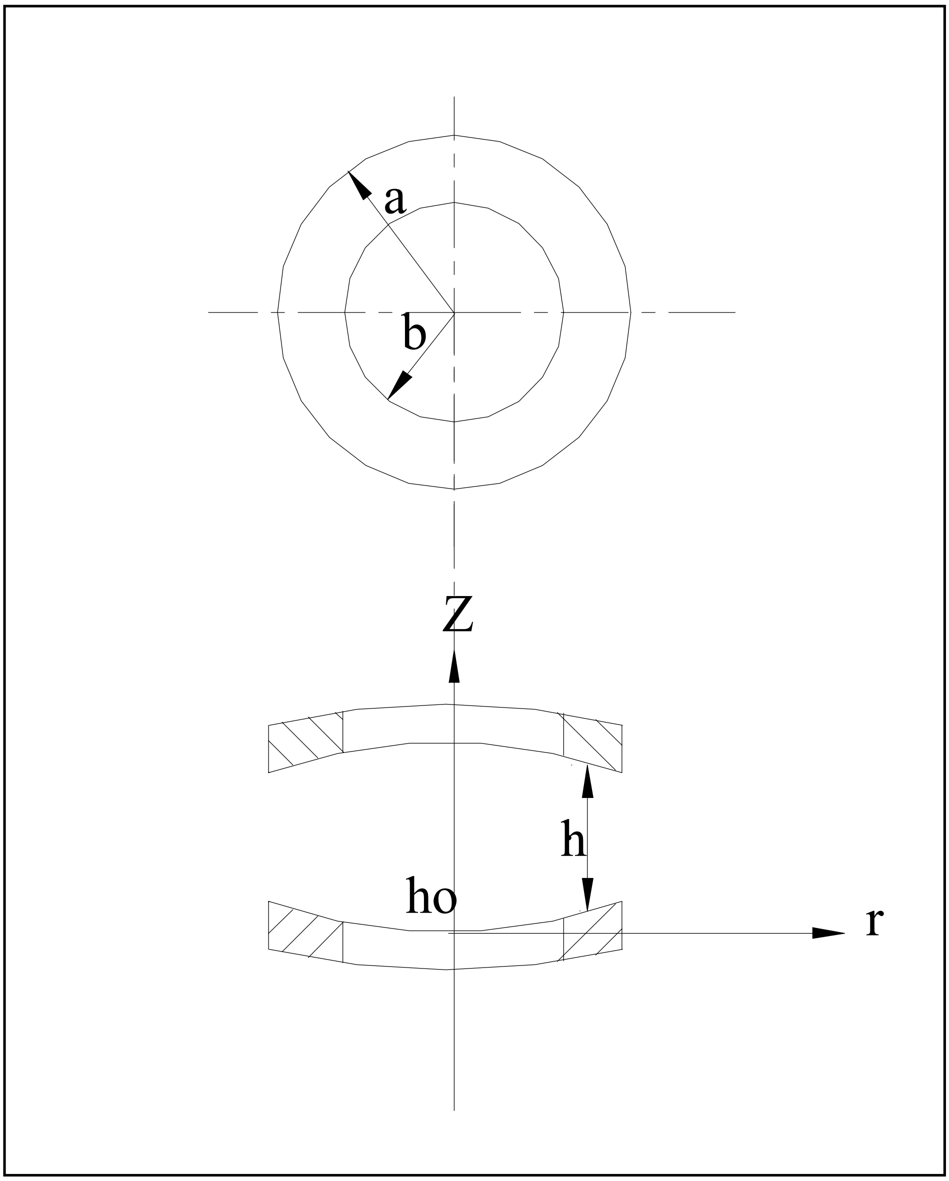

Figure 2: Variation of pressure with respect to μ*

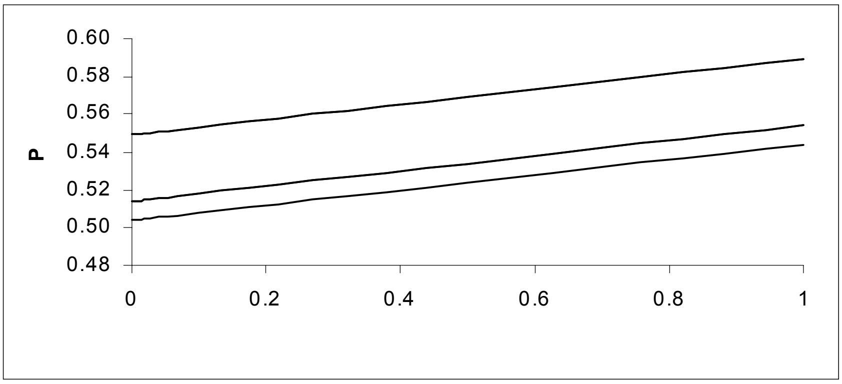

Figure 3: Variation of load carrying capacity with respect to μ*

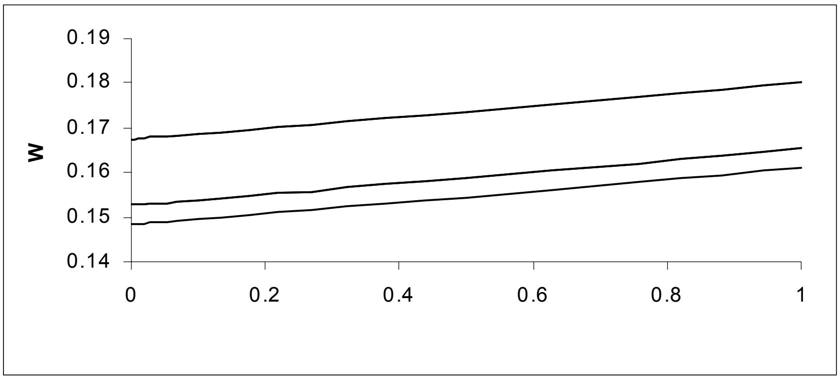

Figure 4: Variation of response time with respect to μ*

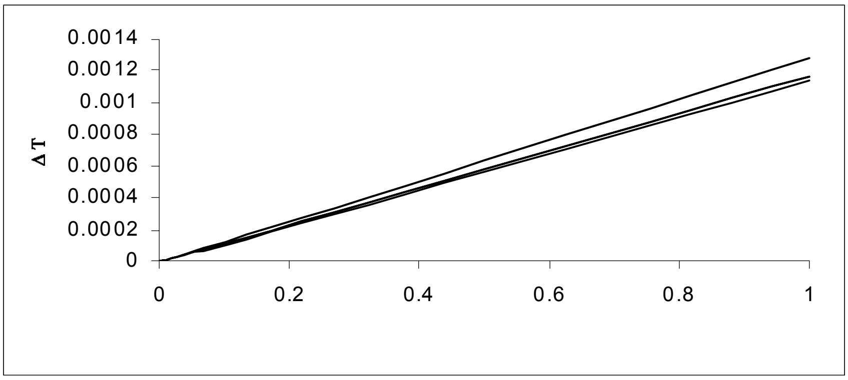

Figure 5: Variation of pressure for conventional lubricant with respect to B

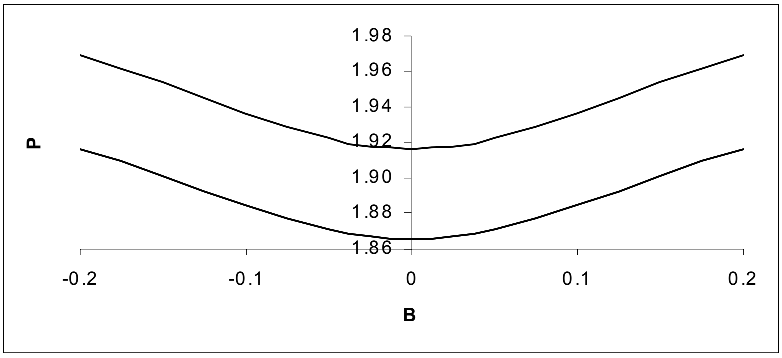

Figure 6: Variation of load carrying capacity for conventional lubricant with respect to B

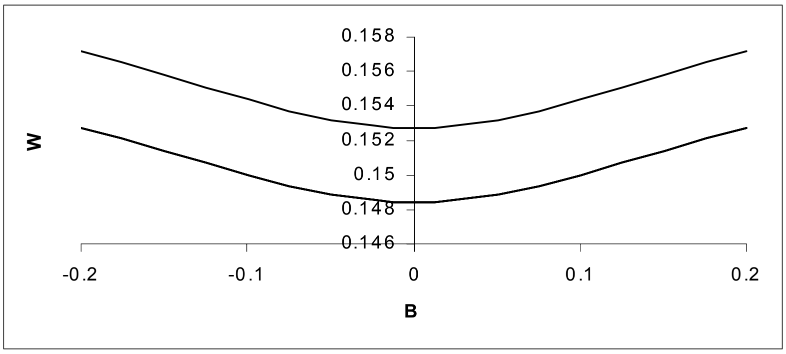

Figure 7: Variation of pressure for conventional lubricant with respect to C

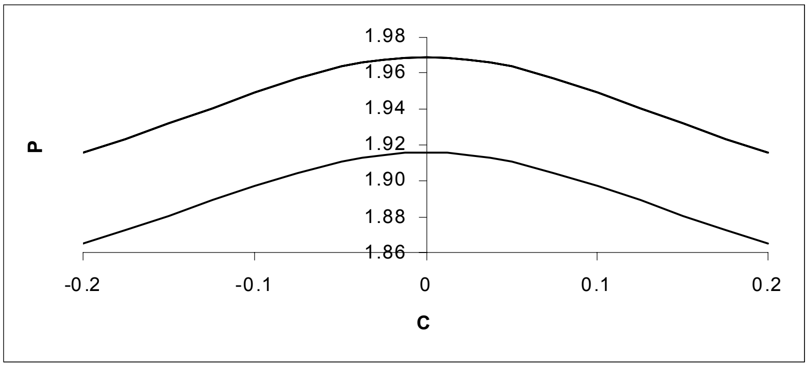

Figure 8: Variation of load carrying capacity for conventional lubricant with respect to C

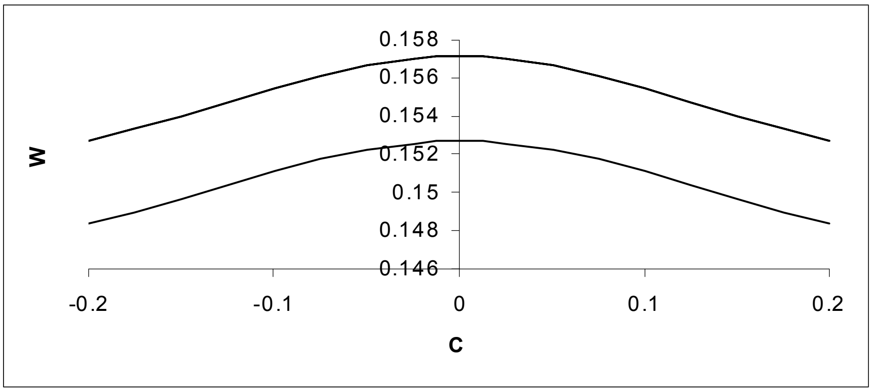

'Prajna' - Journal of Pure & Applied Sciences, 16 (2008) 80-89

AN ANISOTROPIC ANALOGUE OF SCHWARZSCHILD INTERIOR SOLUTION

S.K. Vaidya, V.J. Kaneria and V.H. Kyada
Department of Mathematics, Saurashtra University, Rajkot-360 005

Abstract

We present here an anisotropic version of Schwarzschild interior solution. The solution is matched with the Schwarzschild exterior solution at the boundary. The solution is interpreted as an exact relativistic model for a compact anisotropic star. The numerical estimates of various parameters are given and the physical features of the solution are briefly discussed.

Key words: General Relativity, Anisotropic fluid spheres.

PACS No. 04.20 jb

Introduction

The assumption of local isotropy is very usual in the astrophysical study of massive compact astronomical objects. However, the theoretical investigations of Ruderman (1972) and Canuto (1973) on more realistic stellar models indicate that stellar matter may be anisotropic at least in certain density ranges ($\rho < 10^{15}$ gcm^{-3}) . According to them, the radial pressure may not be equal to the tangential pressure in such massive objects. No celestial body is composed of purely perfect fluid. Therefore it is very interesting to study the anisotropic fluid spheres in the frame work of general relativity. Existence of a solid core, presence of type-p superfluid or any other physical phenomena are responsible for anisotropic behavior. Our aim is not to study the ways of introducing anisotropy in the stellar matter but we are interested in the construction of exact relativistic models for anisotropic fluid spheres with physically reasonable behavior.

Bowers and Liang (1974) have discussed the possible importance of locally anisotropic equations of state for relativistic fluid spheres by generalizing the equations of hydrostatic equilibrium to include the effects of local anisotropy. Their study indicates that anisotropy-if present in the density range expected for relativistic stars (densities upto at least 10^{15} gcm^{-3}) may have non-negligible effect on such parameters as the maximum equilibrium mass and surface red shift. Consenza et al (1981), Bayin (1982), Krori et al (1984), Maharaj and Maartens (1989) and Gokharoo and Mehra (1993) have discussed different exact solutions of Einstein field equations. These solutions discussed various physical aspects of anisotropic fluid spheres. These solutions can be used as models of massive compact objects. Patel and Vaidya (1995) have obtained anisotropic analogue of Finch-Skea (1989) solutions. In the present investigations we give a physically significant exact solution of Einstein field equations for anisotropic fluid sphere using the method developed by Patel and Vaidya (1996). The method is useful to generate static spherically symmetric anisotropic fluid sphere solution from known static perfect fluid solution. Earlier Patel and Vaidya (1996) had obtained anisotropic analogue of Vaidya and Tikekar (1982) solution. In the next section, we will give brief description of the method.

The Method

The spherically symmetric static metric can be cast into the form

$$ds^2 = e^{\nu}dt^2 - e^{\lambda}dr^2 - r^2\left(d\theta^2 + \sin^2\theta d\phi^2\right) \dots \dots \dots \dots \dots \dots \dots \dots \quad (2.1)$$

where ν and λ are the functions of the radial coordinate r. We name the coordinates as x^1=r, $x^2=\theta$, $x^3=\phi$ and $x^4=t$

We shall develop the Einstein field equations for a static anisotropic fluid sphere. The Einstein field equations for non-empty space-times are

$$R_{ik} = -8\pi\left(T_{ik} - \frac{1}{2}Tg_{ik}\right) \dots \dots \dots \dots \dots \dots \dots \dots \dots \dots \dots \quad (2.2)$$

The energy-momentum tensor for anisotropic fluid distribution can be expressed in the form

$$T_{ik} = \rho v_i v_k + p h_{ik} + t_{ik} \quad \dots \dots \dots \dots \dots \dots \dots \dots \dots \dots \dots \dots \dots \dots \quad (2.3)$$

where $v_i = e^{\frac{\nu}{2}}\delta_i^t$ represents the four velocity, ρ is the matter density, is the isotropic fluid pressure and $h_{ik} = v_i v_k - g_{ik}$ is the projection tensor.

The anisotropic pressure tensor t_{ik} is given by

$$t_{ik} = \sqrt{3}S(r)\left(C_i C_k - \frac{1}{3}h_{ik}\right) \dots \dots \dots \dots \dots \dots \dots \dots \dots \dots \dots \dots \dots \quad (2.4)$$

here $C_i = e^{\frac{\lambda}{2}}\delta_i^r$ is a unit radial vector and $S(r)$ is the magnitude of the stress tensor.

It is easy to check that the Einstein field equation (2.2) along with (2.3) and (2.4) for the metric (2.1) reduce to the system of following equations (2.5) to (2.7).

$$8\pi\rho = \frac{1}{r^2} - e^{-\lambda}\left(\frac{1}{r^2} - \frac{\lambda'}{r}\right) \qquad \ldots \qquad \ldots \qquad \ldots \qquad (2.5)$$

$$8\pi \mathrm{p}_r = e^{-\lambda}\left(\frac{\nu'}{r} + \frac{1}{r^2}\right) - \frac{1}{r^2} \qquad \ldots \qquad \ldots \qquad \ldots \qquad (2.6)$$

$$8\pi \mathrm{p}_\perp = \frac{1}{4}e^{-\lambda}\left(2\nu'' + \nu'^2 - \lambda'\nu' + \frac{2}{r}\left(\nu' - \lambda'\right)\right) \qquad \ldots \qquad \ldots \qquad (2.7)$$

where the radial pressure p_r and tangential pressure $\mathrm{p}_\perp$ are given by

$$\mathrm{p}_r = p + \frac{2S}{\sqrt{3}} \quad ,\mathrm{p}_\perp = p - \frac{S}{\sqrt{3}} \quad ,S = \frac{1}{\sqrt{3}}\left(\mathrm{p}_r - \mathrm{p}_\perp\right) \qquad \ldots \qquad \ldots \qquad (2.8)$$

Here follows overhead dash denotes differentiation w.r.t. r.
With the help of (2.6) and (2.7) one can easily check that

$$-16\pi\sqrt{3}Se^{\lambda} = \nu'' + \frac{1}{2}\nu'^2 - \frac{1}{r}\left(\nu' + \lambda'\right) - \frac{1}{2}\lambda'\nu' + \frac{2}{r^2}\left(e^{\lambda} - 1\right) \qquad \ldots \qquad \ldots \qquad (2.9)$$

Substituting $e^{\frac{\nu}{2}} = F \quad ,r^2 = x$ (2.10)

the equation (2.9) can be expressed in the form

$$4xe^{-\lambda}\frac{d^2F}{dx^2} + 2x\frac{d}{dx}\left(e^{-\lambda}\right)\frac{dF}{dx} + \left[\frac{1}{x}\left(1 - e^{-\lambda}\right) + \frac{d}{dx}\left(e^{-\lambda}\right) + 8\pi\sqrt{3}S\right]F = 0 \quad \ldots \qquad (2.11)$$

Let us assume that a solution of (2.11) for the isotropic fluid sphere is known. Let us denote this solution by $\lambda = \lambda_0(r)$ and $\nu = \nu_0(r)$. It is easy to verify that $\lambda = \lambda_0(r)$ and $F = e^{\frac{\nu_0}{2}} + \alpha + \beta x$ satisfy the differential equation (2.11) provided the anisotropy function S is given by

$$-8\pi\sqrt{3}SF = \alpha\left[\frac{1}{x}\left(1 - e^{-\lambda_0}\right) + \frac{d}{dx}\left(e^{-\lambda_0}\right)\right] + \beta\left[\frac{1}{x}\left(1 - e^{-\lambda_0}\right) + 3\frac{d}{dx}\left(e^{-\lambda_0}\right)\right] \ldots \qquad (2.12)$$

where α and β are arbitrary constants. The choice of these constants depends upon the physical requirements of the solution. It is physically required that *S=0* at the centre. i.e. *r=0*. If the function *S* is given by (2.12), then we get an anisotropic fluid sphere solution from an isotropic fluid sphere solution by simply replacing $e^{\frac{\nu_0}{2}}$ by $e^{\frac{\nu_0}{2}} + \alpha + \beta x$. The physical parameters ρ, p_r and $p_\perp$ can be obtained from (2.5), (2.6) and (2.12).

It can be easily proved that a perfect fluid (isotropic) solution with the metric (2.1) is conformally flat if and only if

$$\frac{1}{x}\left(1-e^{-\lambda_0}\right)+\frac{d}{dx}\left(e^{-\lambda_0}\right)=0 \quad \dots \quad \dots \quad \dots \qquad (2.13)$$

In this case, the anisotropic function S is given by

$$-8\pi\sqrt{3}SF = 2\beta x - \frac{d}{dx}\left(e^{-\lambda_0}\right) \quad \dots \quad \dots \quad \dots \qquad (2.14)$$

From (2.14), it is obvious that the anisotropic fluid generalizations of the isotropic conformally flat fluid sphere solutions can be obtained by the above method only if $\beta \neq 0$.

Any physically acceptable anisotropic fluid sphere solution must satisfy the following boundary conditions.

(i) At the surface of the sphere ($r = a$), our interior solution should match with the Schwarzschild exterior solution represented by the metric

$$ds^2 = \left(1-\frac{2m}{r}\right)dt^2 - \left(1-\frac{2m}{r}\right)^{-1}dr^2 - r^2\left(d\theta^2+\sin^2\theta d\phi^2\right) \quad \dots \quad \dots \quad \dots \qquad (2.15)$$

where *m* is the total of the sphere which is constant.

(ii) The radial pressure p_r at the centre should remain finite and it must vanish at the boundary $r = a$ of the sphere.

In the immediate section, we shall apply the above technique to Schwarzschild (1916) interior solution to get corresponding anisotropic analogue.

An Anistropic Analogue of Schwarzschild Interior Solution

The metric for the Schwarzschild (1916) interior solution is given by

$$ds^2 = \left(A - B\sqrt{1-\frac{r^2}{R^2}}\right)^2 dt^2 - \frac{dr^2}{1-\frac{r^2}{R^2}} - r^2\left(d\theta^2 + \sin^2\theta d\phi^2\right)\ldots \qquad \ldots \qquad (3.1)$$

where R , A , B are arbitrary constants. For notations and standard form of this metric, we follow Adler et al (1975). According to technique and notations developed in preceding Section, the metric potentials $\nu_0(r)$ and $\lambda_0(r)$ for the metric (3.1) are given by

$$e^{\lambda_0} = \frac{1}{1-\frac{r^2}{R^2}} \; ; \; e^{\frac{\nu_0}{2}} = \left(A - B\sqrt{1-\frac{r^2}{R^2}}\right)\ldots \quad \ldots \quad \ldots \qquad (3.2)$$

and metric density is given by

$$8\pi\rho_0 = \frac{3}{R^2} \quad \ldots \quad \ldots \quad \ldots \qquad (3.3)$$

It is well known that the space time of Schwarzschild interior solution is conformally flat. So we should take $\beta \neq 0$. For simplicity, we should put $\alpha = 0$. In this case the functions λ, ν and ρ satisfying the equation (2.9) are given by

$$e^{\lambda} = \frac{1}{1-\frac{r^2}{R^2}} \; ; \; e^{\frac{\nu}{2}} = \left(A - B\sqrt{1-\frac{r^2}{R^2}}\right) + \beta r^2 \ldots \quad \ldots \quad \ldots \qquad (3.4)$$

$$-8\pi\sqrt{3}S = \frac{2\beta x}{R^2 F} \quad \ldots \quad \ldots \quad \ldots \qquad (3.5)$$

Here β is an arbitrary constant. It is clear that S vanishes at the centre $r = 0$. The radial pressure p_r and density ρ are given by

$$8\pi\rho = \frac{3}{R^2} \quad \ldots \quad \ldots \quad \ldots \qquad (3.6)$$

$$8\pi p_r = \frac{3B\sqrt{1-\frac{r^2}{R^2}} - A + 4\beta R^2\left[1-\frac{r^2}{R^2}\right] - \beta r^2}{R^2\left[A - B\sqrt{1-\frac{r^2}{R^2}} + \beta r^2\right]} \quad \cdots \quad \cdots \qquad (3.7)$$

The above solution for anisotropic fluid sphere must satisfy the boundary conditions of section-2 at the boundary $r = a$ These boundary conditions specify the constants m, A and B as

$$m = \frac{a^3}{2R^2} \quad \cdots \quad \cdots \quad \cdots \qquad (3.8)$$

$$A = \frac{3}{2}\sqrt{1-\frac{a^2}{R^2}} + 2\beta\left[a^2 - R^2\sqrt{1-\frac{a^2}{R^2}}\right] \quad \cdots \quad \cdots \qquad (3.9)$$

$$B = \frac{1}{2} + \frac{\beta}{\sqrt{1-\frac{a^2}{R^2}}}\left[a^2 - 2R^2\sqrt{1-\frac{a^2}{R^2}}\right] \quad \cdots \quad \cdots \qquad (3.10)$$

When $\beta = 0$, the anisotropy of pressure disappears and we recover the usual Schwarzschild interior solution.

Discussion

We shall now discuss some physical features of the above solution. This solution is with constant density which is given by equation (3.6). The central pressure p_{r_0} for the above solution is given by

$$8\pi p_{r_0} = \frac{3B - A + 4\beta r^2}{R^2(A-B)} \quad \cdots \quad \cdots \quad \cdots \qquad (4.1)$$

OR

$$8\pi p_{r_0} = \frac{3\left[B - \frac{1}{3}A + \frac{4}{3}\beta R^2\right]}{R^2(A-B)} \quad \cdots \quad \cdots \quad \cdots \qquad (4.2)$$

The physical requirements $p_{r_0} \geq 0$ and $\rho > p_{r_0}$ demand

$$f(A,B) \geq 0\,;\, 1 - f(A,B) \geq 0 \quad \ldots \quad \ldots \quad \ldots \qquad (4.3)$$

where $f(A,B)$ is defined by

$$f(A,B) = \frac{3\left[B - \frac{1}{3}A + \frac{4}{3}\beta R^2\right]}{A - B} \quad \ldots \quad \ldots \quad \ldots \qquad (4.4)$$

If $\frac{a}{R}$ and β is given then A and B can be computed from equations (3.9) and (3.10) respectively. For $\beta = 0.1$ and $\beta = 1$ and for various values of a and R satisfying $0 < \frac{a}{R} < 1$, the values of $f(A,B)$ and $1 - f(A,B)$ are abulated in the following two tables.

Table 1: For $\beta = 0.1$

${}^{a}\!/_{R}$	$f(A,B)$	$1-f(A,B)$
0.05	0.000614	0.999386
0.10	0.002302	0.997697
0.15	0.005005	0.994994
0.20	0.008805	0.991194
0.25	0.014077	0.985922
0.30	0.020732	0.979267
0.35	0.029092	0.970907
0.40	0.039503	0.960496
0.45	0.052423	0.947577
0.50	0.068529	0.931470
0.55	0.088810	0.911189
0.60	0.114791	0.885208
0.65	0.148948	0.851051
0.70	0.195614	0.804385
0.75	0.262905	0.737095
0.80	0.369063	0.630937
0.85	0.564062	0.435937
0.90	1.060360	-0.060360

Table 2: For $\beta = 0.1$

a/R	$f(A,B)$	$1 - f(A,B)$
0.05	0.000536	0.999464
0.10	0.002125	0.997875
0.15	0.004813	0.995987
0.20	0.008681	0.991319
0.25	0.013851	0.986149
0.30	0.020494	0.979506
0.35	0.028849	0.971151
0.40	0.039924	0.960754
0.45	0.052154	0.947846
0.50	0.068244	0.931756
0.55	0.088506	0.911494
0.60	0.114465	0.885535
0.65	0.148590	0.851410
0.70	0.195174	0.804826
0.75	0.262437	0.737563
0.80	0.368486	0.631514
0.85	0.563270	0.436730
0.90	1.058870	-0.058870

From the above tables we can see that for $\beta = 0.1$ and $\beta = 1$, the function $f(A,B)$ is an increasing function of a/R. From the tables it is clear that for a/R=0.9, the central density becomes less than the central pressure. This is not desirable. Therefore for $\beta = 0.1$ and $\beta = 1$, the range of validity of our solution is $0 \le a/R \le 0.85$.

Conclusion

Thus, anisotropic version of Schwarzschild interior solution is obtained. Switching of the anisotropy from this solution we can recover the isotropic solution is the salient feature of our solution. Various numerical parameters are also estimated for the discussion of physical significance of the solution.

References

1. Bayin, S.S., Phys. Rev. D. ***26***, 6 (1982)
2. Bowers, R.L. & Liang, E.P.T., Astro. Phys. J. **188**, 657 (1974)
3. Canuto, V., “Neutron Stars General Review” presented at Solvey conference on Astrophysics and Gravitation, Brussels (1973)
4. Consenza, M., Herrera, L., Esculpi, M. and Witten, L., J. Math. Phys., **22**, 118 (1981)
5. Finch, M.R. and Skea, J.E.F., Class. Quantum. Grav., **6**, 467 (1989)
6. Gokaroo, M.K. and Mehra, A.L., Gen. Rel. Grav., **26**, 1 (1993)
7. Krori, K.D., Borgohain, P. and Devi, R., Can. J. of Phys., **62**, 239 (1984)
8. Maharaj, S.D. and Maarten, R.L., Gen. Rel. Grav., **21**, 899 (1989)
9. Patel, L.K. and Vaidya, S.K., Math. Today, **43**, 23 (1995)
10. Patel, L.K. and Vaidya, S.K., APH. N.S., **3**, 177 (1996)
11. R. Adler, M. Bazin, M. Schiffer, Introduction to General Relativity McGraw-Hill-Kogakusha Ltd. (1975)
12. Ruderman, R., Ann. Rev. Astron. Astrophys., **10**, 427 (1972)
13. Vaidya, P.C. and Tikekar R., J. Astrophys. Astron. **3**, 325 (1982)

'Prajna' - Journal of Pure & Applied Sciences, 16 (2008) 90-100

HYPERTENSION-AN OVERVIEW

N.N. Shah, N.P. Chotai and B.G. Patel
A.R. College of Pharmacy and G.H. Patel Institute of Pharmacy
Vallabh Vidyanagar-388 120

Abstract

Hypertension is defined as Systolic Blood Pressure (SBP) of 140mm Hg or greater and/or a Diastolic Blood Pressure (DBP) of 90mm Hg or greater in subjects who are not taking antihypertensive medications.[1,2] Hypertension is an important worldwide public health challenge [3] which accounts for 20 - 50% of all deaths.[4]It carries concomitant increase in risk of heart, vessels, kidney, brain, eye and other organ damage. A meta-analysis showed an increase in the prevalence of hypertension over the years, especially of systolic levels, more in urban than rural areas.[5] It is undetected in 30% of those who have it.[6] Hypertension is often considered as "silent killer" as it as, such doesn't produce symptoms, which may contribute to non-adherence to prescribed therapy and many patients are undertreated. Aim of present article is to create awareness towards causative, pathophysiological and treatment aspects of hypertension, thereby help to improve quality of life.

Hypertension

Hypertension is defined as systolic blood pressure of 140mm Hg or greater and/or a diastolic blood pressure of 90mm Hg or greater in subjects who are not taking antihypertensive medications.[1,2] The classification of BP for Adults Aged 18 years and older[7] has been shown in Table -1.

Table 1: The classification of BP for adults aged 18 years and older

Category	**Systolic Pressure, mm Hg**	**Diastolic Pressure, mm Hg**
Optimal	< 120	< 80
Normal	< 130	< 85
Prehypertension	120 – 139	80 – 89
Hypertension		
Stage 1 (mild)	140 – 159	90 – 99
Stage 2 (moderate)	160 – 179	100 – 109
Stage 3 (severe)	180 –209	110 – 119

EPIDEMIOLOGY AND PREVALENCE OF HIGH BLOOD PRESSURE

High blood pressure as a risk factor

Epidemiological studies have identified an independent link between high BP and various disorders including myocardial infarction (MI), Coronary artery disease (CAD), Peripheral vascular disease, Brain damage (stroke), Congestive Heart Failure (CHF), Eye disorders and impaired kidney function. High risk group includes the elderly, smokers, obese, physically inactive and individuals with dyslipidemia or diabetes mellitus. Prevalence of Hypertension in India among adults is 11%, among teenagers 1% in boys and 0.6% in girls[8]. Hence it is worth making attempt for primary prevention.

RISK FACTORS AND PREDICTORS OF HIGH BLOOD PRESSURE

Heredity

A family history of elevated BP is one of the strongest risk factors for future development of hypertension in individuals.

Genetic factors

The genetic basis of high BP has been well supported by experimental research.

FACTORS INFLUENCING BLOOD PRESSURE

Age

A positive relation is demonstrated between age and BP in most populations with diverse geographical, cultural and socioeconomic characteristics.[9]

Sex

Beginning at adolescence, men tend to display a higher average level. Late in life the difference narrows and the pattern may even be reversed.[9]

Ethnicity

Population studies have consistently revealed higher BP levels in black communities than other ethnic groups.[9]

Socioeconomic status

In countries that are in the post-transitional stage of economic and epidemiological change, consistently higher levels of BP and a higher prevalence of hypertension have been noted in lower socioeconomic groups. This inverse relation has been noted with levels of education, income and occupation. However, in societies that are transitional or pre-transitional, more cases are noted in upper socioeconomic groups.

Early life

It has been recently suggested that an adverse environment during critical periods of development in foetal life and infancy predisposes an individual to risk factors for cardiovascular disease, including high BP. An inverse relationship between BP and birth weight has been demonstrated in longitudinal studies of children as well as adults.[10]

Body weight

In most studies, being overweight is associated with a two fold to six-fold increase in the risk of developing hypertension.[11] For each 10 kg increase in weight, there is a rise of 2-3 mm Hg SBP and 1-3 mm Hg DBP.

Central obesity and the metabolic syndrome

"Central obesity", indicated by an increased waist to hip ratio (WHR), has been positively correlated with high BP in several populations. The co-existence of central obesity, insulin resistance (IR), hyperinsulinaemia (HI), glucose intolerance, dyslipidemia and hypertension has also been highlighted in the recent years.[12, 13, 14]

Nutritional factors

Studies have shown that intake of sodium chloride, in excess of physiological requirements, is associated with high BP and there is an inverse relationship between BP and dietary intake of potassium.[15, 16]

Alcohol

Alcohol consumption is related to high BP. Effects are independent of obesity, smoking, physical activity, sex and age.[17]

Physical activity

Sedentary and unfit normotensive individuals have a 20-50% increased risk of developing hypertension.[18]

Heart rate

When groups of normotensive and untreated hypertensive subjects, are compared, the heart rate of the hypertensive group is invariably higher.

Psychosocial factor

There is evidence that various forms of acute mental stress increase BP.

Environmental factors

Exposure to noise and air pollution has all been implicated as risk factors for high BP. Protecting the public from pollution should be a priority.

ORGAN DAMAGE ASSOCIATED WITH HYPERTENSION

Untreated hypertension increases the risk of vascular damage. These lesions lead to cardiac, renal and cerebrovascular morbidity and mortality, incidence of which is also dependent upon the level of concomitant risk factors.

Heart

Cardiac complications of hypertension are often grouped together and defined as "Hypertensive Heart Disease". Elderly hypertensive patients are prone to angina pectoris, MI and death at a rate 2 to 3 times greater than their normotensive counterparts.

Large and small coronary arteries

Atherosclerotic plaques are frequently found in coronary arteries of hypertensives. The incidence of myocardial infarction and sudden cardiac death is increased in hypertension. It is not known at present how much of this increased incidence is due to atherosclerotic lesions of large coronary arteries, left ventricular hypertrophy, myocardial fibrosis or disease of the coronary arteries.[19]

Congestive heart failure (CHF)

Untreated hypertension may lead to CHF. Meta-analysis of controlled clinical trials, including those of hypertension in the elderly, indicates that antihypertensive therapy can reduce the incidence of CHF by about 50%.[20]

Brain, eye and carotid arteries

Cerebrovascular disease (CVD)

All types of stroke are associated with hypertension. Antihypertensive treatment has been shown to be particularly effective in reducing the incidence of stroke, a 5-6 mm Hg reduction in DBP reducing incidence by about 40%.[21]

Eye

Simple thickening of retinal arteries is related more closely to age than to BP[20] but hypertension can lead to microinfarcts, haemorrhages, retinal detachment, nerve damage and permanent impairment or loss of vision. There is direct relationship between elevation of DBP and a degree of narrowing of optic arterioles. Hypertensive retinopathy can be reversed with effective BP control.

Carotid arteries

Increased prevalence of atherosclerotic complications in hypertensive patients is associated with an increased incidence of atherosclerotic lesions in the carotid arteries.

Kidney

The kidney is an important target of hypertension. Severe and malignant (accelerated) hypertension often leads to renal insufficiency within a few years. Reduction of proteinuria can be achieved by effective BP reduction.[22] Warning signs of renal damage in hypertension are proteinuria or microalbuminuria and CVD.[23] Hypertension remains a leading cause of renal disease accounting for 15-20% of all cases of renal failure in USA.[24]

TREATMENT ASPECTS

It is estimated that a sustained 12 mm Hg reduction in SBP will prevent 1 death for every 11 patients treated.[25] While control rates are improving they are well below goal in Healthy People 2010. Algorithm for treatment of hypertension is shown in figure-1[6] and effect of lifestyle modifications on hypertension is given in table-2.[7]

Fig. 1: Algorithm for treatment of hypertension

Life style modification

↓

Not at goal blood pressure

< 140/90 mm Hg

(<130/80 mm for patients with diabetes of chronic kidney disease*)

↓

Initial drug choices

↓

Without compelling indications		**With compelling indications**
Stage 1 hypertension (SBP 140-159 or DBP 90-99 mm Hg)	Stage 2 hypertension (SBP ≥160 or DBP ≥100 mm Hg)	Drug(s) for compelling indications
Thiazide type diuretics for most; may consider ACE inhibitor, ARB, beta blocker, CCB, or combination	Two drug combination for most (usually thiazide type diuretic+ ACE inhibitor, ARB, beta blocker, or CCB)	Diuretics, ACE inhibitor, ARB, beta blocker, CCB as needed

↓

Not at goal blood pressure

↓

- Optimize dosages or add drugs until goal blood pressure is achieved
- Consider consultation with hypertension specialist

* Lower than previous JNC recommendations.

ACE= angiotensin-converting enzyme; ARB=angiotensin II receptor blocker; CCB=calcium channel blocker.

Table 2: Effect of lifestyle modifications on hypertension

Modification	Recommendation	Approximate SBP reduction (range), mm Hg
Weight reduction	Maintain normal body weight*	5-20 per 10 kg lost
Adopt DASH ** eating plan	Consume a diet rich in fruits, vegetables and low-fat-dairy products with a reduced content of saturated and total fat.	8-14
Dietary sodium reduction	Reduce dietary sodium intake to no more than 100 mmol per day (2.4 g sodium per 6 g sodium chloride)	2-8
Physical activity	Engage in regular aerobic physical activity, e.g. brisk walking (at least 30 min per day, most days of the week)	4-9
Moderation of alcohol consumption	Limit consumption to 2 drinks (1 oz or 30 ml ethanol, 20 oz beer, 10 oz wine, or 2 oz 80-proof whiskey) per day in most men ; ≤ 1 drink in women and lighter weight people	2-4

* Body mass index 18.5-24.9 kg/m^2

** DASH= Dietary Approaches to Stop Hypertension. The effects of implementing these modifications are dose and time dependent and could be dramatic for some individuals.

To reduce morbidity as well as mortality by reducing risk of cardiovascular injury, cerebrovascular events, heart failure, kidney and other organ damage is the primary goal of antihypertensive therapy.

PHARMACOTHERAPY

Depending on other risk factors and coexisting conditions, Joint National Committee-7 (JNC-7) supports the use of following classes of medications for Hypertension:

- Diuretics
- Beta blockers
- Angiotensin converting enzyme (ACE) inhibitors
- Angiotensin-II receptor blockers (ARBs)
- Calcium channel blockers (CCBs)

Currently first line treatment consists of thiazide diuretic, which induces natriuresis, decrease plasma volume and in long term reduce peripheral vascular resistance.[26] Loop diuretics should be reserved for patients who have more significant renal insufficiency.[26] Potassium sparing diuretics can be used for patients who develop significant hypokalemia while taking thiazides.

Beta blockers are commonly used to treat hypertensive patients with tachycardia, anxiety and cardiac arrhythmia. Patients should be monitored for bradycardia, fatigue, CNS adverse effects and symptoms of asthma.[27] They lower BP by following mechanisms.[26]

- Decreasing cardiac contractility and output
- Lowering heart rate
- Diminishing sympathetic reflex (in combination with exercise)
- Reducing central release of adrenergic substances
- Decreasing renin release

ACE-inhibitors lower BP by inhibiting conversion of angiotensin-I to angiotensin-II, reducing vasoconstriction and aldosterone release[26], thereby decreasing sodium and water retention. They impede degradation of bradykinin, promoting vasodilatation. Angiotensin-II receptor blockers (ARBs) bind to their receptors in tissues including adrenal gland and vascular smooth muscles, so prevents effects of angiotensin-II. The addition of a low dose thiazide diuretic to an ARB significantly improves antihypertensive efficacy.[28] ARBs are beneficial in diabetic neuropathy, albuminuria and renal complications.[29, 30]

Aldosterone receptor blockers act via their antimineralocorticoid effect, as aldosterone is having role in pathophysiology of hypertension, heart failure, MI and renal disease. Calcium channel blockers (CCBs) promote vasodilatation by preventing intracellular influx of calcium, which is responsible for increase in tone of arteriolar smooth muscles. If initial monotherapy fails to lower BP to established goal, combination therapy may be successful.[6, 26]

CONCLUSION

Control of hypertension is a complex multidimensional process. Effective management of hypertension depends on detection, patients' compliance to life style modification along with cost effective drug therapy regimens to prevent expensive clinical sequele.[31]

REFERENCES

1. Burt VL, Whelton P, Rocella EJ. Prevalence of hypertension in U.S. adult population: results from Third National Nutrition Examination Survey, 1988-1991. Hypertension 1995; 25: 305-313
2. JNC-6 (Sixth Report of the Joint National Committee on Prevention, Detection, Evaluation and Treatment of High Blood Pressure) Arch Intern Med. 1997; 157: 2413-2444
3. WHO Expert Committee Hypertension Control WHO Technical Series No. 862 Geneva: World Health Organization 1996
4. Report of a WHO expert committee hypertension control. Technical Report series No. 862. World health organization, Geneva 1996, 1
5. Padmavati S. Prevention of Heart Diseases in India 21st Century: Need for Concentrated Effort. Indian Heart Journal 2002; 54:99-102
6. JNC-7 (Seventh Report of the Joint National Committee on Prevention, Detection, Evaluation and Treatment of High Blood Pressure.) JAMA 2003; 289:2560-2572
7. Rao ASC, Yavagal ST, Chinniah D "Blood Pressure in Teenage" JAPI 1980; 28:45
8. Harrison's Principles of Internal Medicine; McGraw Hill, Medical Publishing Division, New York. 15th edition, 2001, Volume 1 p. 212
9. Whelton PK. Epidemiology of hypertension. Lancet 1994; 344:101-106
10. Law CM et al. Initiation of hypertension in utero and its amplification throughout life. British medical journal 1993; 306:24-27
11. MacMahon S et al. Obesity and hypertension : epidemiological and clinical issues. European heart journal 1987; 8:57-70
12. Modan M, Kalkin H. Hyperinsulinemia or increased sympathetic drive as links for obesity and hypertension. Diabetes Care 1991; 14:470-487

13. Reaven GM. Role of insulin resistance in human disease (1988 Banting lecture). Diabetes 1988; 37:1595-1607

14. Sharma AM. Effects of nonpharmacological intervention on insulin sensitivity. Journal of cardiovascular pharmacology 1992; 20:S27-S34

15. INTERSALT Cooperative Research Group. INTERSALT: an international study of electrolyte excretion and blood pressure: results for 24-hour urinary sodium and potassium excretion. British Medical Journal 1988; 297:319-328

16. Yamori Y et al. Gene environment interaction in hypertension, stroke and atherosclerosis in experimental models and supportive findings from a worldwide cross-sectional epidemiological survey: a WHO-CARDIAC Study. Clinical experimental pharmacology, Physiology Supplement. 1992; 20:43-52

17. Pearce KA, Furberg CD. The primary prevention of hypertension. Cardiovascular risk factors 1994; 4:147-153

18. Paffenbarger RS et al. Physical activity and incidence of hypertension in college alumni. American Journal of Epidemiology 1983; Vol. 117, No. 3: 245-257

19. Wilson PW, Kannel WB.Hypertension, other risk factors, and the risk of cardiovascular disease. In: Laragh HJ, Brenner BM (eds). Hypertension: Pathophysiology, Diagnosis, and Management. New York: Raven Press. 1995:127-144

20. Zanchetti A, Sleight P, Brikenhager WH. Evaluation of organ damage in hypertension. Journal of Hypertension 1993; 11:875-882

21. Yussuf S, Thom T, Abbott RD. Changes in hypertension treatment and in congestive heart failure mortality in the United States. Hypertension 1989; 13 (Suppl.1): 174-179

22. Collins R et al. Blood pressure, stroke and coronary heart diseases. Part 2. Short-term reductions in blood pressure: overview of randomized drug trials in their epidemiological context. Lancet 1990; 335:827-838

23. Ruilope LM. Proteinuria and renal function. Blood pressure, 1993; 2 (Suppl.1): 55-58

24. Rosansky SJ et al. The association of blood pressure levels and change in renal functions in hypertensive and non-hypertensive subjects. Archives on internal medicine 1990; 150:2073-2074

25. Ogden LG, He J, Lydick E,Whelton PK. Long-term absolute benefit of lowering blood pressure in hypertensive patients according to the JNC-6 risk stratification. Hypertension. 2000; 35:539-543

26. Saseen JJ, Carter BL. Essential Hypertension. In: Applied Therapeutics: The Clinical Use of Drugs, 7th ed. Koda-Kimble MA,Young LY, Kradjan WA, Guglielmo BJ, eds. Baltimore: Lippincott Williams & Wilkins. 2001
27. Carter BL. Management of Essential Hypertension In: Pharmacotherapy: Self-Assessment Program, 4th ed. Kansas City, Mo: American College of Clinical Pharmacy. 2001
28. Carter BL, Saseen JJ.Hypertension. In: Pharmacotherapy: A Pathophysiologic Approach, 5th ed. DiPiro JT, Talbert RL, Yee GC, et al., eds. New York: McGraw-Hill. 2002
29. Brenner BM, Cooper ME, deZeeuw D, et al. Effects of losartan on renal and cardiovascular outcomes in patients with type 2 diabetes and nephropathy. N Engl J Med. 2001; 345: 861-869
30. Lewis EJ, Hunsicker LG, Clarke WR, et al. Retrospective effect of the angiotensin receptor antagonist irbesartan in patients with nephropathy due to type 2 diabetes. N Engl J Med. 2001; 345:851-860
31. Paramore LC, Halpern MT, Lapuerta P, Impact of poorly controlled hypertension on health care resource utilization and cost. Am J Manag Care 2001; 7:389-398

'Prajna' - Journal of Pure & Applied Sciences, 16 (2008) 101-109

LOW TEPMERATURE TRANSPORT PROPERTIES OF n-WSe$_2$ SINGLE CRYSTALS

K.D. Patel, C.K. Sumesh, Achamma John Mathai, V.M. Pathak and R. Srivastava
Department of Physics, Sardar Patel University, Vallabh Vidyanagar-388 120

Abstract

Hall effect measurements on semiconducting materials provide important information about transport properties which are essential to know if the material grown is suitable for device fabrication. Further if these measurements are done at different temperatures, particularly at low temperatures then additional information about the conduction mechanisms involved and the role of defects in the process of conduction can be obtained. In light of this, present paper discusses the precise measurements of low temperature resistivity, Hall coefficient, carrier density and mobility on WSe$_2$ single crystals grown by direct vapour transport technique over temperature range of 100-300 K. It has been observed from the $\ln \sigma$ vs 1000/T curve that there are two regions of conduction in which activation energy obtained are 0.13eV and 0.23eV in the temperature range of 300-150K and 150-100K respectively.

Introduction

Considerable literature exists on the electrical properties of the semiconducting transition metal dichalcogenide layer crystals of MX$_2$ type, where M is transition metal e.g. molybdenum or tungsten and X is chalcogen e.g. selenium or tellurium. These semiconductors have attracted wide research interest due to their unusual structural properties [1-3]. As a result these materials possess flexible nature along with good carrier mobility to prove them potential candidates for fabricating flexible high mobility electronic devices such as SBDs, FETs, solar cells etc [4]. However, the difficulty in the fabrication of low resistance ohmic contacts to the MX$_2$ layers is still a major obstacle yet to be overcome, for formation of devices.

Theory and Background

When a uniform electrically conducting medium is placed in a magnetic field so that the current density flow is perpendicular to the applied magnetic field, a Lorentz force deflects moving charge carriers to generate an electric field perpendicular to both current density and magnetic field. However, to make this simple Hall effect observable for analysis of charge transport properties, particularly of semiconducting solid samples, following conditions must be satisfied.

(i) Sample must be homogenous in all respect i.e. thickness, doping concentration, surface and bulk structure etc.

(ii) Sample must be connected via ohmic contacts that occupy negligible surface area.

(iii) There must be a stable source of current and magnetic field.

There are varieties of ohmic contact geometries, amongst which van der Pauw geometry [5] is the most favored one by researchers to study irregularly shaped semiconducting crystals or slabs. This is because it provides flexibility in choosing four contacts at four sites on the periphery of the sample surface. It is preferable to fabricate samples from thin plates/sheets of the semiconductor material and to adopt a suitable geometry, as shown in figure 1 a. Four leads are connected to the four ohmic contacts on the sample. These are labeled 1, 2, 3, and 4 counterclockwise as shown in figure 1a. It is important to use the same wire content and geometry for all four leads in order to minimize thermoelectric effects. Similarly, all four ohmic contacts should consist of the same material.

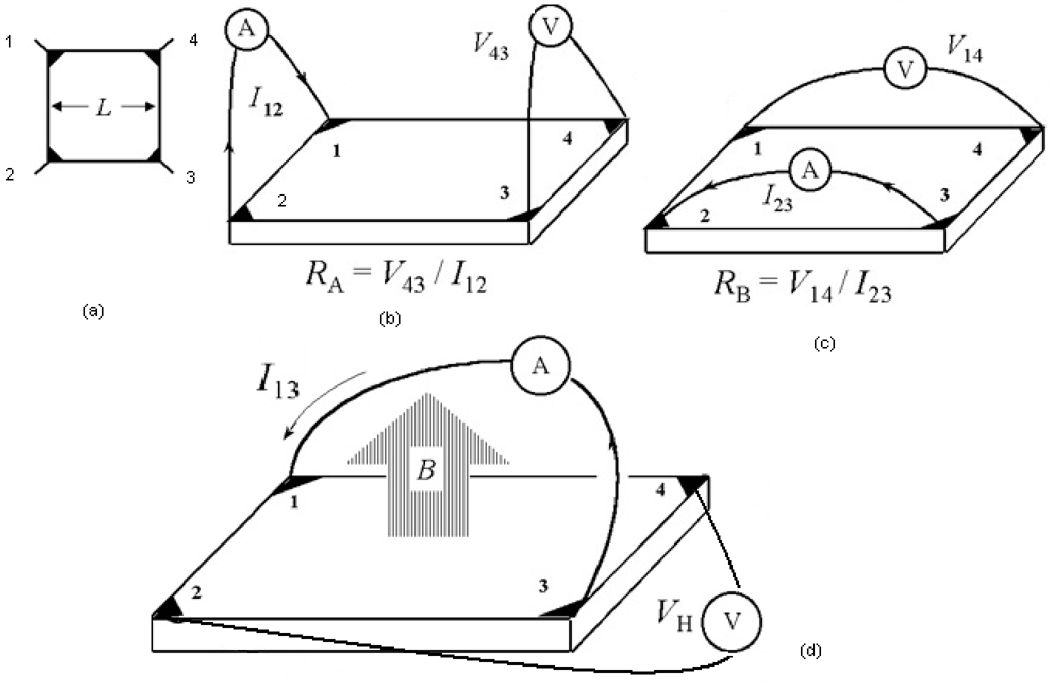

Fig. 1: (a) Sample geometry for van der Pauw resistivity and Hall effect measurements, (b) & (c) Schematic of a van der Pauw configuration used in the determination of the two characteristic resistances R_A and R_B and (d) Schematic of a van der Pauw configuration used in the determination of the Hall voltage V_H

For each measurement point in a Hall experiment, up to 32 individual resistance measurements are required to be made for both A and B type of geometries. Here geometry A corresponds to R12,43 and R23,14 and geometry B corresponds to R41,32 and R34,21. Each van der Pauw resistivity requires 8 measurements (terminal interchange and current reversal for both figure 1b and c) and the Hall resistance requires 4 measurements (terminal interchange and current reversal for figure 1d). The sequence of the measurements is as follows.

(i) Zero field resistance measurements (8 measurements).
(ii) Hall resistance measurements for +ve magnetic field, +B (4 measurements).
(iii) Resistivity measurements for +ve magnetic field ,+B (8 measurements).
(iv) Hall resistance for -ve magnetic field, –B (4 measurements).
(v) Resistivity measurements for -ve magnetic field, –B (8 measurements).

By knowing the thickness 't' of the sample and measurement of voltage and current with polarity reversal across the contacts, the resistivities can be calculated from the following equations [6,7].

$$\rho_A = \frac{\pi f_A t\left[m, cm\right]}{\ln(2)}\left(\frac{V^{+}_{12,43} - V^{-}_{12,43} + V^{+}_{23,14} - V^{-}_{23,14}}{I^{+}_{12} - I^{-}_{12} + I^{+}_{23} - I^{-}_{23}}\right)\left[\Omega.m, \Omega.cm\right] \quad \ldots\ldots\ldots\ldots\ldots\ldots\ldots (1)$$

and

$$\rho_B = \frac{\pi f_B t\left[m, cm\right]}{\ln(2)}\left(\frac{V^{+}_{34,21} - V^{-}_{34,21} + V^{+}_{41,23} - V^{-}_{41,23}}{I^{+}_{34} - I^{-}_{34} + I^{+}_{41} - I^{-}_{41}}\right)\left[\Omega.m, \Omega.cm\right] \quad \ldots\ldots\ldots\ldots\ldots\ldots\ldots (2)$$

Here $V^{+}_{12,43}$ means voltage measured between contact 4 and 3 when positive forced current is allowed to pass between contact 1and 2. Similarly I^{+}_{12} denotes +ve forward current measured between contacts 1 and 2. The geometrical factors f_A and f_B are functions of Q_A and Q_B, respectively, given by:

$$Q_A = \left(\frac{R^{+}_{12,43} - R^{-}_{12,43}}{R^{+}_{23,14} - R^{-}_{23,14}}\right) = \left(\frac{V^{+}_{12,43} - V^{-}_{12,43}}{I^{+}_{12} - I^{-}_{12}}\right)\left(\frac{I^{+}_{23} - I^{-}_{23}}{V^{+}_{23,14} - V^{-}_{23,14}}\right) \quad \ldots\ldots\ldots\ldots\ldots\ldots\ldots (3)$$

$$Q_B = \left(\frac{R^{+}_{34,21} - R^{-}_{34,21}}{R^{+}_{41,23} - R^{-}_{41,23}}\right) = \left(\frac{V^{+}_{34,21} - V^{-}_{34,21}}{I^{+}_{34} - I^{-}_{34}}\right)\left(\frac{I^{+}_{41} - I^{-}_{41}}{V^{+}_{41,23} - V^{-}_{41,23}}\right) \quad \ldots\ldots\ldots\ldots\ldots\ldots\ldots (4)$$

The relationship between f and Q is expressed by the transcendental equation,

$$\frac{Q-1}{Q+1}=\frac{f}{\ln 2}\cosh^{-1}\left(\frac{1}{2}\exp\left[\frac{\ln 2}{f}\right]\right) \qquad \text{......................} \ (5)$$

The two resistivities must agree to within ±10%. If they do not, then the sample is too inhomogeneous, or anisotropic, or has some other problem. If they agree, the average resistivity is given by,

$$\rho_{av}=\frac{\rho_A+\rho_B}{2}\left[\Omega.m,\Omega.cm\right] \qquad \text{......................} \ (6)$$

Similarly with the help of same measurements of voltage and current along with the magnetic field reversal the two Hall coefficients are calculated by the following equations.

$$R_{HC}=\frac{t(m)}{B(T)}\left[\frac{V_{31,42}^{+}(+B)-V_{31,42}^{-}(+B)+V_{31,42}^{-}(-B)-V_{31,42}^{+}(-B)}{I_{31}^{+}(+B)-I_{31}^{-}(+B)+I_{31}^{-}(-B)-I_{31}^{+}(-B)}\right]\left[m^{3}.C^{-1}\right] \qquad \text{..........} \ (7)$$

and

$$R_{HD}=\frac{t(m)}{B(T)}\left[\frac{V_{42,13}^{+}(+B)-V_{42,13}^{-}(+B)+V_{42,13}^{-}(-B)-V_{42,13}^{+}(-B)}{I_{42}^{+}(+B)-I_{42}^{-}(+B)+I_{42}^{-}(-B)-I_{42}^{+}(-B)}\right]\left[m^{3}.C^{-1}\right] \qquad \text{...........} \ (8)$$

where R_{HC} and R_{HD} are the Hall coefficients for configuration shown in figure 1d and its terminal interchange respectively. These two should also agree to within ±10%. If they do not agree, it indicates that the sample is too inhomogeneous, or anisotropic, or has some other problem. If they agree, then the average Hall coefficient can be calculated by,

$$R_{Hav}=\frac{R_{HC}+R_{HD}}{2}\left[m^{3}.C^{-1}\right] \qquad \text{......................} \ (9)$$

From the average value of resistivity and Hall coefficient the Hall mobility can be calculated by,

$$\mu_H=\frac{\left|R_{HAv}\right|}{\rho_{Av}}\left[m^{2}.V^{-1}.S^{-1}\right] \qquad \text{......................} \ (10)$$

Where ρ_{Av} is the zero field resistivity.

Experimental

Crystals of WSe_2 were grown by direct vapour transport (DVT) method inside a dual zone horizontal furnace [8-10]. The microstructural examinations of as-grown surfaces of the crystals were done with the help of Axiotech 100 reflected light microscope, (Carl Zeiss Jena, Germany). The crystals with flat shining surfaces were chosen for further study. The crystals were then washed in acetone to remove contaminations and to make the surface clean. It was kept in the oven for a couple of minutes at 60^0C to dry out the crystals completely. Ohmic contacts on these crystals were made along the basal plane by fusing of indium and attaching low strain Ag alloy wires to them at 275^0C.

The Hall effect measurements have been carried out by the Hall effect measurement system model 7504, supplied by Lakeshore Cryotronics, Inc., USA for the determination of the Hall parameters at different temperatures under magnetic field of ±5 kG. For the conformity of the van der Pauw geometry, samples were mounted on a PCB sample holder onto which six contacts are provided. Each of these contacts were provided with shielding by passing them between grounded tracks, which helps in eliminating measurement errors. Central space between the six probes is provided for sample mounting. The sample is required to be fixed with the help of adhesives like quick fix etc.

The software provided for operating Lakeshore set up was first run in variable current mode to check the ohmic nature of current transport through different sets of any two probes amongst all the four probes and by varying the combination of probes for passage of current and consequent measurement of voltage drop across them. e.g. (12,12), (23,23), (34,34) and (41,41) etc. After that, the instrument is programmed in variable magnetic field mode where all the necessary selections like field reversal, current reversal, maximum field, field steps, van der Pauw geometry etc. are to be made as per the requirement and then the programme is allowed to run for final measurements and calculations of all required parameters namely; resistivity, Hall coefficient, Hall mobility, carrier concentration etc. Simultaneously, the nature of variation of these parameters can also be observed on the setup's display by selecting the particular variable. The Hall effect measurements over a range of temperatures is made possible with the help of Lakeshore temperature controller (Model 340), which balances the cooling power provided by a Closed Cycle Refrigerator model CCR 75014 against two heater circuits using GaAs and Si diodes as low temperature sensors.

The sample is located near the top of the copper sample well and is at a significant distance from the cold end. A temperature sensor mounted directly to the sample provides a much more accurate measure of the actual sample temperature. The temperature sensor on the sample insert is used to monitor the sample temperature. The whole set up was carefully placed between the magnet pole pieces. A Hall probe was also placed near the cryostat between the pole gape for magnetic field measurement and control. When the variables were set correctly, temperature was also set constant at the desired value. After stabilizing the set temperature, measurements were done using the program mentioned above and the obtained data were stored as spreadsheet in the computer memory. The experiments were repeated from room temperature to 100 K in the step of 25 K.

Results and Conclusion

The ohmic nature of contacts prepared for van der Pauw geometry for various pairs of contacts at 300 K is shown in the figure 2. The resistance between pair of contacts is in the range 100-130kΩ. The average van der Pauw factor between the pair of contacts is found to be 0.7. This deviation from ideal requirement of unity probably originates from the anisotropic nature of WSe_2 sample taken for present investigation and not from other conditions mentioned earlier. Such a conclusion seems to be supported by the good linear nature of I-V characteristics as shown in figure 2.

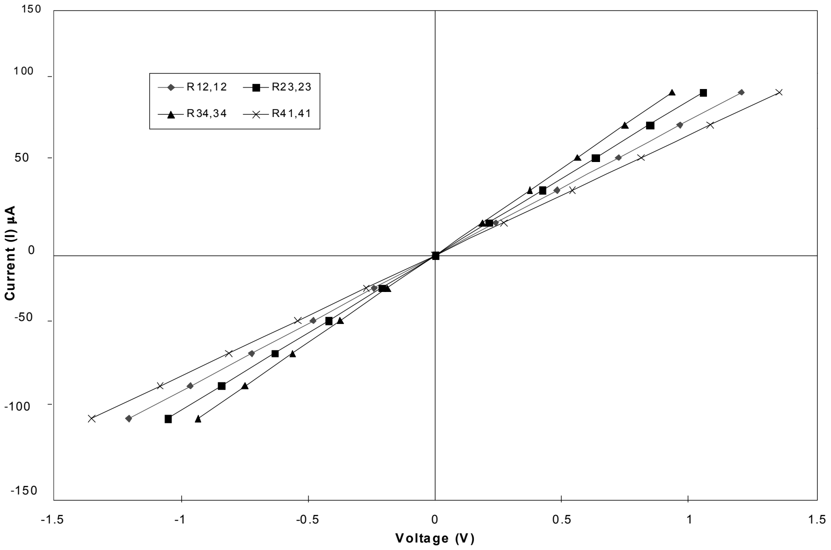

Fig. 2: I - V Characteristics of the Pair of contacts (12,12), (23,23), (34,34) and (41,41)

The resistivity, Hall coefficient, density and mobility of WSe_2 single crystals were measured over the temperature range of 300K to 100K and are tabulated in table 1.

Table 1: Hall parameters of WSe_2 crystals

Temperature (K)	Resistivity (ohm·cm)	Hall Coefficient 'Rh' (cm^3/C)	Density ($/cm^3$) X10^{14}	Mobility ($cm^2/(V\ s)$)
299	20.45	-136	459	6.55
275	26.86	-144	432	5.388
250	36.90	-143	436	3.92
225	57.01	-9.53	654	1.684
200	94.41	-23.69	270	2.47
175	155.17	-34.63	180	2.251
150	262.87	-3270	27.2	8.696
125	283.32	-11130	5.6	37.62
100	4064	-68220	0.9	14500

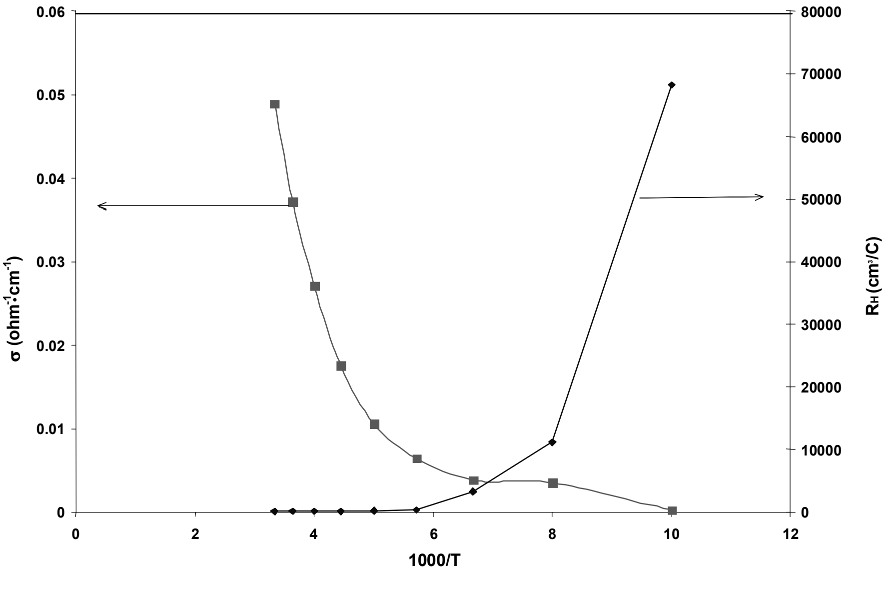

Fig. 3: R_H and σ of n - WSe_2 Crystals as a function of 1000/T

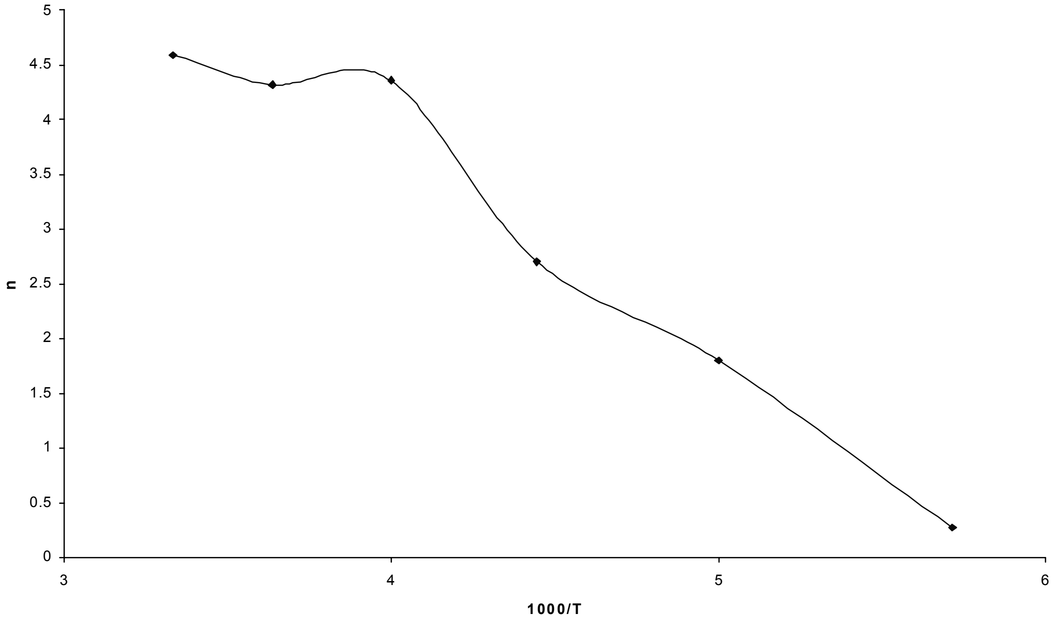

Fig. 4: Carrier concentration vs. 1000/T for n-WSe_2 Crystals

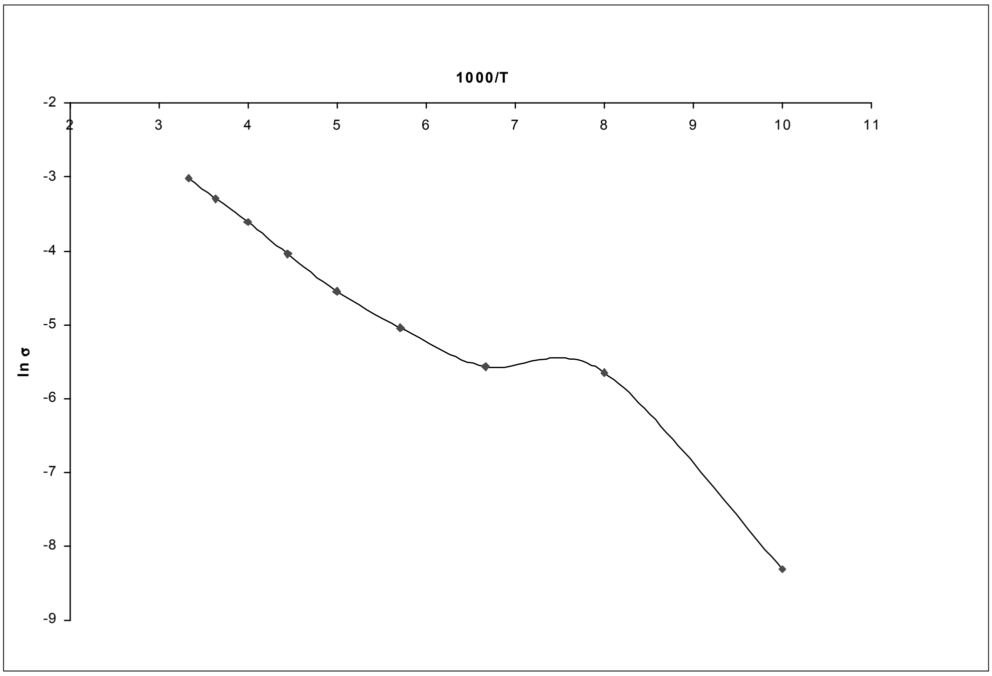

Fig. 5: Conductivity vs. 1000/T for n-WSe_2 Crystals

The sign of Hall coefficient remains negative all throughout the range of measurement temperature, indicating the conductivity type of the crystals is n-type. This again shows that the quality of ohmic contacts made for present investigations is good and stable through out the range of reported measurements. The conductivity of the sample decreases with the temperature and thus again confirms the semiconducting nature of the grown WSe_2 crystals. Fig. 5 shows the variation of ln σ vs. 1000/T with two different straight line regions corresponding to the temperature range of 150-100K and 300-150K. Activation energy in these two regions is 0.23eV and 0.13eV respectively. The measured carrier concentration at room temperature is $4.6x10^{16}cm^{-3}$. This is in agreement with the reported [1] value of $3.5x10^{16}$ cm^{-3}.

References

1. Kulyuk L., Nonlinear optics. **29**, 501 (2002)
2. Wilson A. and Yoffe A.D., Adv. Phys., **18**, 193 (1969)
3. Grant A.J., Griffiths T.M., J. Phy. C: Solid State Phys., **8** (1974)
4. Podzorov V., Appl. Phy. lett., **84** (2004)
5. van der Pauw L.J., Philips Res. Rep.13, **1** (1958)
6. Lake Shore 7500/9500 Series Hall System User's Manual
7. Dieter K. Schroder, *Semiconductor Material and Device Characterization,* (John Wiley & Sons, Inc. Publications) p. 95 (1990)
8. Fivaz R., Phys. Rev. **163**,743 (1967)
9. Pouizet J., J. Phys. III, 1697 (1996)
10. Upadhyayula L.C., J. Appl. Phy. **39**, 4736 (1968)
11. Levy F., Phys. Rev. **B46**, 15, 404 (1992)

'Prajna' - Journal of Pure & Applied Sciences, 16 (2008) 110-120

ELECTORN IMPACT TOTAL IONIZATION CROSS SECTIONS FOR BORON CHLORIDES (BCl_X, X=1–3); THRESHOLD - 2keV

Kirti M. Korot*, Bobby Antony and Minaxi Vinodkumar***
*V.P. & R.P.T.P. Science College, Vallabh Vidyanagar - 388 120
**Department of Applied Physics, ISM University, Dhanbad - 826 004, Jharkhand

Abstract

In this article we report calculations of total ionization cross sections (Q_{ion}), for the boron chlorides, BCl_x (x=1–3) upon electron impact at energies from circa threshold to 2000 eV. Spherical Complex Optical Potential (SCOP) formalism is employed to evaluate total inelastic cross section, Q_{inel}. The Q_{ion} are derived from the Q_{inel}, using our Complex Spherical Potential - ionization contribution (CSP-ic) method. Mutual comparison of ionization cross sections for all boron chlorides is carried out to get a general picture of contribution of individual ionization cross sections. Present calculations also provide information, hitherto sparse, on the excitation processes of these targets. The results are compared with available experimental and other theoretical data and overall good agreement is observed.

Introduction

Absolute electron impact ionization cross sections are measured and calculated since 1930s. The ionization of a molecule on electron impact is a very fundamental and important collision process. These cross sections find practical applications in many branches of science viz. fusion edge plasmas, gas discharge plasmas, planetary, stellar and cometary atmosphere, radiation chemistry, mass spectrometry and chemical analysis [1].

Boron Trichloride (BCl_3) is a nonpolar, plane symmetric (D_{3h} symmetry) molecule. It is a major source of reactive radicals generated by electron impact dissociative processes, including electron attachment. For this reason it is extensively used in plasmas for the commercial etching of various semiconductors, metal surfaces [2-4] and in deposition and doping of boron [5]. Boron trichloride has been used for reactive sputter etching of aluminum in the semiconductor industry, for boron doping of optical waveguide fibers and for the removal of water from the vacuum chambers. The modeling of such plasmas is a challenging task, made even more difficult due to the scarcity of data on basic atomic and molecular processes involving BCl_3 and its fragments. Due to the highly reactive nature of BCl_3, it is very attractive as an etchant but at the same time it is very difficult to handle this radical in the scattering experiments, especially those with the crossed beam techniques and the results obtained have serious uncertainties [6].

Despite the technological interest in BCl_3 radical and the research on its chemistry in plasmas, there is paucity of information about the other major fragment species BCl_2 or its cations. The most detailed study of electron impact partial and total ionization of BCl_3 was conducted by Jiao *et al* [7] using Fourier transform mass spectrometry. Probst *et al* [8] have calculated ionization cross sections for BCl_3 using modified additivity rule employing Deustch and Märk (DM) formalism and Kim *et al* [9] have calculated ionization cross sections for BCl_3 using Binary encounter Bethe (BEB) formalism. Huo [10] have reported calculations for ionization cross sections for many radicals including BCl_x (X=1-3). There is probably no experimental data noticed in the literature for the total ionization cross sections for BCl and BCl_2 on electron impact, while the theoretical data for these two radicals are due to [8 - 10].

Theoretical Methodology

We have briefly described here the theoretical formalism employed to determine various total cross sections (TCS) for the impact of electrons on the targets studied. A more detailed description can be found in our earlier papers [11-15]. Our aim in this paper is to calculate Q_{ion} for all boron chlorides. Towards this goal, we have employed the well-known spherical complex optical potential (SCOP) formalism, through which the total elastic cross sections Q_{el} and its inelastic counterpart, Q_{inel} are obtained such that,

$$Q_T(E_i) = Q_{el}(E_i) + Q_{inel}(E_i) \tag{1}$$

In the present range of electron energy (threshold to 2 keV), many scattering channels that lead to discrete as well as continuum transitions in the target are open. Therefore we represent the electron-molecule system by a complex potential,

$$V(r, E_i) = V_R(r, E_i) + i\, V_I(r, E_i), \tag{2}$$

such that

$$V_R(r, E_i) = V_{st}(r) + V_{ex}(r, E_i) + V_{pol}(r, E_i) \tag{3}$$

The three terms on the RHS of the eq. (3) represent various real potentials arising from the electron target interaction namely, static, exchange and the polarization potentials respectively. The most important basic input for evaluating all these potentials is the charge density of the target. This is obtained from the spherically averaged molecular charge-density $\rho(r)$, which is determined from the constituent atomic charge densities derived from the wave functions of Bunge *et al* [16]. The charge density of the target is made single centre by expanding the charge density of the atomic constituents at the center of mass of the system.

The molecular charge density $\rho(r)$, so obtained is renormalized to incorporate the covalent bonding as in our earlier papers [12]. For the exchange potential, we have employed Hara's 'free electron gas exchange model' [17] and for the polarization potential V_p, we have used parameter free model of correlation - polarization potential given by Zhang *et al* [18] which contains some multipole non-adiabatic corrections in the intermediate region and it smoothly approaches the correct asymptotic form at large '*r*'. The target properties used here are the best available from the literature and are given in table 1.

Table 1: Target properties

Target	IP eV [9]	Bond length Å [19,20]	Bond angle [19,20]
BCl	10.2	1.716	180°
BCl_2	8.75	1.731	125°
BCl_3	11.73	1.742	120°

Finally, the imaginary part V_I of the complex potential is the absorption potential which represents appropriately the combined effects of all inelastic channels. Here, we have employed a well-known non-empirical quasi-free model form given by Staszeweska *et al* [21]. Thus,

$$V_{abs}(r, E_i) = -\rho(r)\sqrt{\frac{T_{loc}}{2}} \cdot \left(\frac{8\pi}{10k_F^3 E_i}\right)\theta(p^2 - k_F^2 - 2\Delta)\cdot(A_1 + A_2 + A_3) \quad (4)$$

The local kinetic energy of the incident electron is

$$T_{loc} = E_i - (V_{st} + V_{ex}) \quad (5)$$

The absorption potential is not sensitive to long range potentials like V_{pol}. In eq.(4), $p^2 = 2E_i$, $k_F = [3\pi^2\rho(r)]^{1/3}$ is the Fermi wave vector and Δ is an energy parameter. Further $\theta(x)$ is the Heaviside unit step-function, such that $\theta(x) = 1$ for $x \geq 0$, and is zero otherwise. The dynamic functions A_1, A_2 and A_3 occurring in the eq. (4) depend differently on $\rho(r)$, I, Δ and E_i. The energy parameter Δ determines a threshold below which $V_{abs}=0$, and the ionization or excitation is prevented energetically. We have modified the original model, by considering Δ as a slowly varying function of E_i around I. The modification introduced in our paper has been to assign a reasonable minimum value $0.8I$ to Δ and expressing this parameter as a function of E_i around I as follows.

$$\Delta(E_i) = 0.8I + \beta(E_i - I) \quad (6)$$

Suppose that E_p is the value of E_i at which our Q_{inel} attains maximum. In eq. (6) β is then obtained by requiring that $\Delta = I + 1$ (eV) at $E_i = E_p$, beyond which Δ is held constant equal to *I*. The expression for $\Delta\ (E_i)$ eq. (6), is meaningful since Δ fixed at *I* would not allow excitation at incident energy $E_i \leq I$. On the other hand, if parameter Δ is much less than the ionization threshold, then V_{abs} becomes substantially high near the peak position. After generating the full complex potential given in Eq. (2), we solve the Schrödinger equation numerically and employ partial wave analysis to get complex phase shifts that are used to find cross sections given in eq. (1).

The Q_{inel}, cannot be measured directly. The measurable quantity which is of more practical importance is the Q_{ion}. Q_{inel} can be partitioned into two main contributions viz.

$$Q_{inel}(E_i) = \sum Q_{exc}(E_i) + Q_{ion}(E_i) \tag{7}$$

Where, the first term is the sum over total excitation cross sections for all accessible electronic transitions. The second term is the total cross section of all allowed ionization processes induced by the incident electrons. The first term arises mainly from the low-lying dipole allowed transitions for which the cross section decreases at higher energies. Now, the second term in eq. (7), electron impact ionization corresponds to infinitely many open channels, as against the electronic excitation, which comes from a small number of discrete scattering channels. Therefore, ionization contribution in Q_{inel} increases as the incident energy increases, thereby making Q_{ion} to dominate in Q_{inel}. Thus from eq. (7),

$$Q_{inel}(E_i) \geq Q_{ion}(E_i) \tag{8}$$

There is no rigorous way to extract out Q_{ion} from Q_{inel}. But in order to achieve this, a reasonable approximation can be evolved by starting with a ratio function,

$$R(E_i) = \frac{Q_{ion}(E_i)}{Q_{inel}(E_i)} \tag{9}$$

such that, $0 < R \lesssim 1$

We require $R = 0$ when $E_i \leq I$ For a number of stable atoms and molecules like Ne, O_2, H_2O, CH_4, SiH_4 etc., for which the experimental cross sections Q_{ion} [22-24] are known accurately the ratio *R* rises steadily as the energy increases above the threshold, and approaches unity at high energies. Thus,

$$\begin{aligned} R(E_i) &= 0 \quad && for \quad E_i \le I \\ &= R_P && at \quad E_i = E_P \\ &\cong 1 && for \quad E_i >> E_P \end{aligned} \qquad (10)$$

In eq. (10) R_p is the value of R at $E_i = E_p$. The general observation is that, at energies close to peak of ionization, the contribution of Q_{ion} is about 70–80% of the total inelastic cross sections Q_{inel}. As the ionization threshold for these targets are less than 12 eV (table 1) we choose $R_p = 0.7$. For calculating the Q_{ion} from Q_{inel} we need R as a continuous function of energy for $E_i \ge I$ hence we represent the ratio R in the following manner,

$$R(E_i) = 1 - f(U) \qquad (11)$$

Presently the above ratio has been determined using the following analytical form [11-15].

$$R(E_i) = 1 - C_1\left(\frac{C_2}{U+a} + \frac{\ln(U)}{U}\right) \qquad (12)$$

Where, U is the dimensionless variable defined by, $U = \frac{E_i}{I}$.

The reason for adopting a particular functional form of $f(U)$ in eq. (12) can be understood as follows. As E_i increases above I, the ratio R increases and approaches 1, since the ionization contribution rises and the discrete excitation term in eq. (7) decreases. The discrete excitation cross sections, dominated by dipole transitions, fall off as $\ln(U)/U$ at high energies. Accordingly the decrease of the function $f(U)$ must also be proportional to $\ln(U)/U$ in the high range of energy. However, the two-term representation of $f(U)$ given in eq. (12) is more appropriate since the first term in the brackets ensures a better energy dependence at low and intermediate E_i. The dimensionless parameters C_1, C_2, and *'a'*, involved in eq. (12) reflect the properties of the target under investigation. The three conditions stated in eq. (10) are used to determine these three parameters and hence the ratio R. This method is called the Complex Scattering Potential –ionization contribution, (CSP-ic). Having obtained Q_{ion} through CSP-ic, the summed excitations cross sections $\sum Q_{exc}$ can be easily calculated vide eq. (7).

Results and Discussion

The theoretical approach of SCOP along with our CSP-ic method discussed above offers the determination of the total inelastic cross sections $Q_{inel,}$ total ionization cross sections Q_{ion} along with a useful estimate on electronic excitations in terms of the summed cross section $\sum Q_{exc}$. Present data of total ionization cross sections for all BCl_x, X=1-3 are given in Table 2 and are plotted in figs 1-4. Total ionization cross sections for all these targets are calculated using the CSP-ic method.

Table 2: Total ionization cross sections Q_{ion} for BCl_x, (X=1-3) in Å^2

E_i (eV)	BCl	BCl_2	BCl_3
10	---	0.02	---
20	2.76	3.94	2.56
30	4.52	7.16	7.09
40	5.35	8.86	9.70
50	5.74	9.71	11.01
60	5.81	10.03	11.53
70	5.79	10.13	11.80
80	5.68	10.07	11.89
90	5.56	9.98	11.86
100	5.41	9.83	11.78
200	4.23	7.78	9.89
300	3.44	6.42	8.18
400	2.94	5.44	6.94
500	2.56	4.67	6.02
600	2.28	4.13	5.42
700	2.03	3.72	4.85
800	1.87	3.38	4.42
900	1.71	3.12	4.08
1000	1.60	2.91	3.75
2000	0.96	1.78	2.20

Figure 1 shows the plot of Q_{ion} for e – BCl scattering with available comparison. There is probably no experimental data available in the literature for this radical. The present results are in excellent accord with the theoretical values of Huo [10] throughout the energy range. The theoretical data of Kim *et al* [9] are slightly lower than the present values below 100 eV and in better agreement at higher energies. The peak of the ionization threshold is around 60 eV, which is same for all the theories including present results.

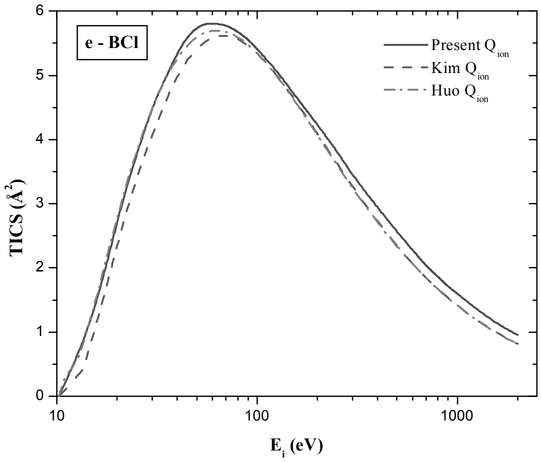

Fig. 1: Total ionization cross sections for e – BCl scattering in Å^2

There are no experimental data reported in the literature for the Q_{ion} of e – BCl_2 scattering. The present results are compared with the theoretical values of Kim *et al* [9] and Huo [10] in figure 2. Present Q_{ion} at low energies are in good agreement with other theoretical values [9,10]. However, at higher energies our values are higher than the compared data [9,10]. Also, it is worth noting that the peak of the ionization cross section is identical for all the three data and the nature of the curve is also similar.

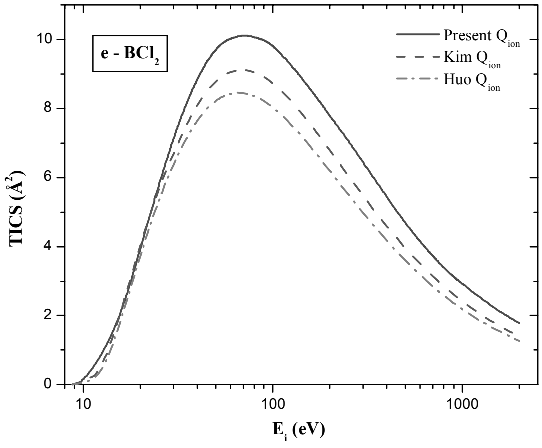

Fig. 2: Total ionization cross sections for e – BCl_2 scattering in Å^2

BCl_3 radical is more widely studied theoretically than experimentally. The theoretical results are due to Probst *et al* [8], Kim *et al* [9] and Huo [10], while the experimental results are reported by Jiao *et al* [7]. Probst *et al* [8] have calculated the total ionization cross sections using Deustch and Märk (DM) formalism and using Modified additivity rule (MAR). The present results are in excellent accord with the DM results of Probst *et al* [8] throughout their reported energy range, while the MAR results are in good agreement at low energies. Beyond 30 eV they seem to underestimate the present result, which is a regular feature of DM formalism [16]. However the MAR results of Probst *et al* [8] are only up to 200 eV and better results of MAR are expected at high energies. The theoretical data of Kim *et al* [9] are slightly lower than the present results throughout the energy range. Jiao *et al* [7] have measured Q_{ion} for e – BCl_3 only up to 60 eV. Their results are higher than present results up to 20 eV and seem to cross over to lower values later. The theoretical results of Huo [10] are lower than all the reported theoretical and experimental data above 30 eV. For radical targets, the experimental uncertainties are likely to be large.

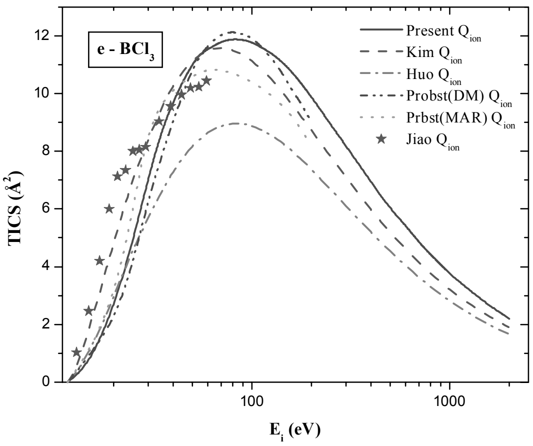

Fig. 3: Total ionization cross sections for e – BCl_3 scattering in $Å^2$

Finally, in fig 4 relative comparison of Q_{ion} for all the three boron chlorides are shown. In the present study the basic inputs are the target charge density, ionization threshold etc. of the target (Table 1). The size of the molecule is determined by the total number of electrons and their configuration. There is a large difference in the peak value of the ionization cross section for all three targets which is attributed to the difference in their ionization threshold and total number of electrons in the target. Q_{ion} increases with the increase in geometrical size of the target. This is well reflected in these curves. However, it should be noted that at sufficient high energies Q_{ion} for all the targets merge irrespective to the size of the target.

This is because, at high energies the interaction time of the incident electrons with the target is significantly reduced, lowering the corresponding cross sections.

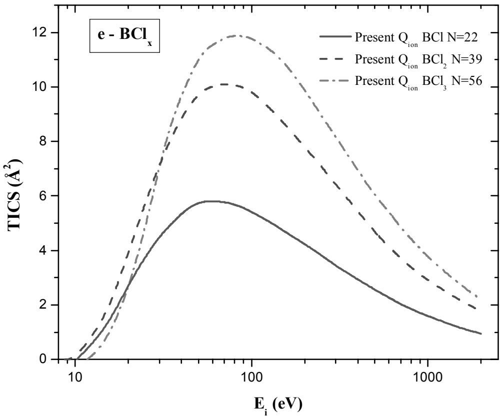

Fig. 4: Comparison for Total Ionization cross sections of e - BCl_x scattering in $Å^2$

Conclusion

Electron impact total ionization sections for the boron chlorides, BCl_x (X=1-3) are calculated using the well known spherical complex optical potential method and reported in Table 2. The complex scattering potential - ionization contribution (CSP-ic) formalism developed by the authors [11-15] was used to derive the total ionization cross section for these targets. This method has been tested successfully for a large number of atomic and molecular targets. The derived theoretical inelastic cross section serves as the upper bound and gives a useful estimation of the total ionization cross sections. We note that in view of the approximations made here, no definitive values are claimed, but by and large our results fall well within the experimental error limits for the available data. Present theoretical results for the total ionization cross sections show a good agreement with most of other theoretical investigations. Moreover, mutual comparison of total cross sections for all the boron chlorides is carried out and it reflects the fact that the total cross sections increases appropriately. Also, the present method employed here provides an estimate of electronic excitations in relation to ionization cross sections in a particular target. We have not provided the data of total excitation cross sections but are available with the authors. Lastly we hope this work may inspire the experimentalists as there is paucity of experimental data for all the boron chlorides.

Acknowledgement

Minaxi Vinodkumar is thankful to University Grants Commission, New Delhi for Major Research Project under which part of this work is carried out.

References

1. Märk T. D. and Dunn G. H. (Eds.), Electron Impact Ionization, Springer, Wein, (1985)
2. Flamm D. L. and Donnelly V. M., Plasma Chem. Plasma Proc. **1**, 317 (1981)
3. Coburn J. W., Plasma Chem. Plasma Proc. **2**, 1 (1982)
4. Greenberg K. E., Hebner G. A.and Verdeyen J. T., Appl. Phys. Lett. **44**, 299 (1984)
5. Slaovi A., Foulan F., Fuchs L., Foganassy E. and Siffert P., Appl. Phys. A **50**, 317 (1990)
6. Domaracka A., Denga E. P., and Szmytkowski Cz., Phys. Rev. A **71**, 052711 (2005)
7. Jiao C. Q., Nagpal R. and Haaland P., Chem. Phys. Lett. **265**, 239 (1997)
8. Probst M., Deutsch H., Becker K. and Märk T. D., Int. J. Mass Spectrom. **206**, 13 (2001)
9. Kim et al, http://physics.nist.gov/PhysRefData/Ionization/molTable.html
10. Huo W., http://www.ipt.arc.nasa.gov/databasemenu.html
11. Vinodkumar M., Joshipura K. N., Limbachiya C. and Mason N., Phys Rev. A **74**, 022721 (2006)
12. Vinodkumar M., Joshipura K. N. and Mason N. J., Acta Physica Slovaka **56(4)**, 521 (2006)
13. Vinodkumar M., Joshipura K. N., Limbachiya C. G. and Antony B. K., Eur. Phys. J. D. **37**, 67 (2006)
14. Vinodkumar M., Limbachiya C., Antony B. and Joshipura K. N., J. Phys. B: At. Mol. Opt. Phys. **40**, 3259 (2007)
15. Joshipura K. N., Vinodkumar M., Limbachiya C. G. and Antony B. K., Phys. Rev. A **69**, 022705 (2004); Joshipura K. N., Vinodkumar M., Antony B. K. and Mason N. J., Eur. Phys. J. D. **23**, 81 (2003)

16. Bunge C. F., Barrientos J. A. and Bunge A. V., At. Data Nucl. Data Tables **53**, 113 (1993)
17. Hara S., J. Phys. Soc. Jpn. **22**, 710 (1967)
18. Zhang X., Sun J. and Liu Y., J Phys. B **25**, 1893 (1992)
19. Lide D. R., CRC Handbook of Physics and Chemistry, 74th edition (Chemical Rubber Company, Boca Raton, FL), (1993-94)
20. Please see the website: http://srdata.nist.gov/cccbdb/
21. Staszewska G., Schewenke D. W., Thirumalai D. and Truhlar D. G., Phys. Rev. A **28**, 2740 (1983)
22. Krishnakumar E. and Srivastava S. K., J. Phys. B **21**, 1055 (1988)
23. Karwasz G. P., Brusa R. S. and Zecca A., Riv. Nuovo Cimento **24(1)**, 1 (2001)
24. Basner R., Schmidt M., Tarnovsky V., Becker K. and Deustch H., Int. J. Mass Spectrom. Ion Process. **171**, 83 (1997)

'Prajna' - Journal of Pure & Applied Sciences, 16 (2008) 121-126

BINDING ENERGY AND MASSES OF QQq BARYONS IN ANALOGY WITH H_2^+ MOLECULE

Ajay Majethiya, Bhavin Patel and P.C. Vinodkumar
Department of Physics, Sardar Patel University, Vallabh Vidyanagar - 388 120

Abstract

Heavy flavor baryons containing two charm (beauty) quarks with light flavour combinations are studied in analogy with H_2^+ molecule using the Born-Oppenheimer approximation. The ground state masses of heavy flavour baryons are computed for different heavy interquark distances. The predicted masses of doubly heavy baryons are found to be in accordance with other model predictions as well as with the existing experimental states.

Introduction

In recent times, there is a renewed interest in the field of hadron spectroscopy particularly at the heavy flavour sector due to many new discoveries reported at various experiments. In the heavy flavour spectroscopy, doubly heavy hadrons (hadrons containing two heavy quarks) become important as some of these states are observed experimentally [1-4]. Many new states are being detected in recent experiments by various experimental groups like CDF, SELEX, BaBar, CLEO, etc [1-4]. Many of these states are also predicted by different theoretical models [5-13]. For the study of the properties of doubly heavy hadrons, their mass spectra and wave functions are important parameters. However due to the discrepancies among the theoretical model predictions of these parameters, there is a demand to review them in view of the new experimental observations. From theoretical viewpoint, not only the heavy flavour mesons are important in the hadron spectroscopy but heavy baryons (QQq) are also of special interest as they can test the strong interaction from those of three body forces relevant to the fundamental degrees of freedom provided by QCD. It is observed that ideal QQq baryon bears strikingly similar with the simplest molecular-ion (H_2^+), in the sense that both the systems are three body bound states held together by coulomb like force and containing two heavy particles and one lighter particle. Motivated by this similarity, we adopt the well known method of Born-Oppenheimer approximation to study the QQq systems. Even though the H_2^+ and QQq are similar systems, there exists fundamental difference between them, that is the inter-nuclear interaction at short distances in the case of ion is repulsive, whereas the color coulomb interaction between the two Q-Q is attractive. However at very short distances, the Q-Q interaction (due to the asymptotic freedom of the color interaction) becomes much weaker than the

Q-q interaction, thus justifying the employment of Born-Oppenheimer approximation for the study of QQq systems [6]. For the present study, we consider the case of a QQq system similar to the well known H_2^+ molecular ion, and predict masses of doubly heavy baryons with various quark compositions. A schematic representation of the co-ordinates to describe QQq system is shown below.

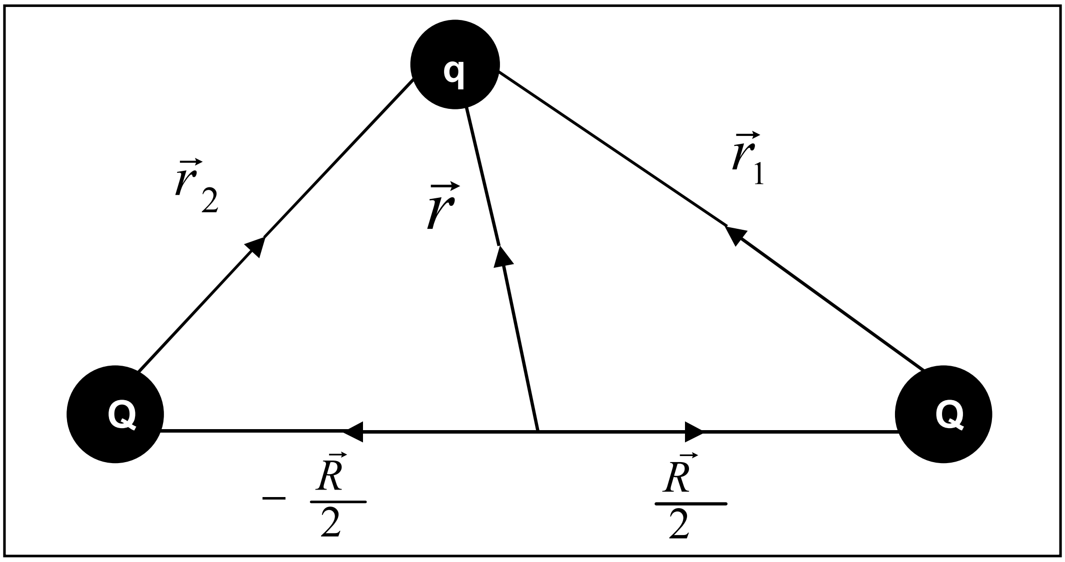

Fig. 1 Co-ordinate system of QQq system

Theoritical Methodology

We define the following coordinates,

$$\vec{X} = \frac{M\left(\vec{x}_1 + \vec{x}_2\right) + m\,\vec{x}_3}{2M + m} \tag{1}$$

as the 3-body center of mass co-ordinate and the two relative co-ordinates as

$$\vec{R} = \vec{x}_1 - \vec{x}_2 \quad and \quad \vec{r} = \vec{x}_3 - \frac{\vec{x}_1 + \vec{x}_2}{2} \tag{2}$$

Here $\vec{x}_1$, $\vec{x}_2$ and $\vec{x}_3$ are the position vectors of the two heavy quarks and the light quark respectively from an arbitrary origin. M and m are the masses of the heavy quark and light quark respectively. Following Born-Oppenheimer approximation adopted for H_2^+ molecule, we represent the full wave function ψ as

$$\psi(R,r)=\phi(R)\varphi(R,r) \tag{3}$$

Here, φ represents the light quark ground state for a static configuration of the heavy quarks (Q), and ϕ stands for the amplitude to find Q in this configuration when q is in the state φ [6]. Accordingly, the Hamiltonian can be separated into the CM part and the part governing the relative motion. By assuming two body color coulomb interactions among the quarks, the Hamiltonian governing the relative motion is given by [6]

$$h=-\frac{\nabla_R^2}{2M_{red}}-\frac{2\alpha_s}{3R}-\frac{\nabla_r^2}{2m_{red}}-\frac{2\alpha_s}{3}\left(\frac{1}{r_1}+\frac{1}{r_2}\right) \tag{4}$$

Where, $M_{red}=\frac{M}{2}$, $m_{red}=\frac{2\,m\,M}{2M+m}$; $\vec{r}_1=\left|\vec{r}-\frac{\vec{R}}{2}\right|, \vec{r}_2=\left|\vec{r}+\frac{\vec{R}}{2}\right|$. (5)

Since the positions of heavy quark explicitly enter in the potential, the energy eigenvalue depends on the co-ordinate R also. Taking the trial wave function in the form

$$\varphi(R,r)=\frac{f(r_1)+f(r_2)}{\sqrt{2(1+S(\lambda,R))}}\ ;\ f(r)=\frac{\lambda^{\frac{3}{2}}}{\sqrt{\pi}}e^{-\lambda r} \tag{6}$$

We get the light quark energy as

$$E(R)=-\frac{\lambda^2}{2}+\frac{\lambda(\lambda-1)-C(\lambda,R)+(\lambda-2)\varepsilon(\lambda,R)}{1+S(\lambda,R)} \tag{7}$$

Where, $\varepsilon(\lambda,R)=\frac{\lambda^3}{\pi}\int d^3r\frac{\mathrm{e}^{-\lambda(r_1+r_2)}}{r_2}$; $S(\lambda,R)=\frac{\lambda^3}{\pi}\int d^3r\ \mathrm{e}^{-\lambda(r_1+r_2)}$; and

$$C(\lambda,R)=\frac{\lambda^3}{\pi}\int d^3r\frac{\mathrm{e}^{-2\lambda r_1}}{r_2}\ .$$

The parameter λ is determined by minimizing the energy expression given by (7). The mass of the baryonic system (QQq) is given by

$$M_{QQq}=\sum_{i=1}^{3}m_i+E(R) \tag{8}$$

here, $m_{i=1,2,3}$ represent the constituent quark mass parameters of the model. At different inter heavy quark separations, the binding energies are computed for the different choices of the quark compositions. The model parameters employed here are listed in Table 1.

Table 1: The model parameters employed in the present study

m_u = 338 MeV ,	m_d = 350 MeV ,	m_s = 500 MeV
m_c = 1578 MeV,	m_b = 4940 MeV ,	$\alpha_s(\mu_0 = 1\ GeV)$ = 0.7

The strong running coupling constant is computed using

$$\alpha_s(\mu) = \frac{\alpha_s(\mu_0)}{1 + \frac{33 - 2n_f}{12\pi}\alpha_s(\mu_0)\ln\left(\frac{\mu_0}{\mu}\right)^2} . \tag{9}$$

Here, $\alpha_s(\mu_0)$ is the strong coupling constant at the threshold production of mesons in the (uds) sector with a threshold energy around 1 GeV and n_f is the flavor number. For the present calculations we have taken the value of $\alpha_s(\mu_0 = 1\ GeV)$ at the nucleonic scale as 0.7 and the $\alpha_s\ (\mu = 2m_Q)$ for heavy systems are calculated using equation (9).

Results and Discussions

The computed binding energies and masses of the doubly charmed and doubly beauty baryons at different QQ separations are listed in Table 2. It is seen that as distance between two heavy quarks increases from a typical radius (1/ 2m$_Q$) in Fermi, the binding energy reaches to a saturated value which do not further change appreciably by increasing the distance even by an order of magnitude. We consider this saturated value of the binding energy for the present study. Our predictions are compared with other theoretical and known experimental results and are found to be in accordance with the available experimental values as well as in accordance with the predictions of other theoretical models. Our results for ccu, ccd and ccs states are closer to the predictions of [7]. The predicted ccd state is in good agreement with the experimental observations of SELEX Collaboration [2]. This method thus, appears to be very effective to calculate the ground state masses of doubly charmed and doubly beauty baryons. In the case of doubly beauty baryons (bbq, bbs) our results are nearer to the predicted results of [5] & [8], while the predicted bbc state is found to be off by 220 MeV with the recent theoretical result [6]. We hope to resolve these discrepancies by incorporating the spin dependent interactions among the quarks within the baryon. Detail experimental investigations of the mass spectroscopy of these doubly heavy baryons and their excited states are expected to resolve the discrepancies seen among the theoretical predictions [5-6]. Other properties including the excited states, transitions and decays of heavy baryons based on the present model are being pursued.

Table 2 : Predicted masses of the doubly heavy baryons and their binding energies at different Q-Q separation distances

Baryonic System (QQq)	Q-Q Separation R in (fm)	Binding energy E in (MeV)	Mass of QQq Baryons (M_{QQq} in MeV)	
			Present	Others
ccu	0.059	-23.32	3470.68	3673[5] 3545[7] 3659[8] 3544[10]
	0.197	-23.29	3470.71	
	0.394	-23.21	3470.79	
	0.590	-23.07	3470.93	
ccd	0.059	-24.06	3481.93	*3481[2] 3673[5] 3545[7] 3544[10] 3645[12]
	0.197	-24.03	3481.96	
	0.394	-23.95	3482.04	
	0.590	-23.81	3482.19	
ccs	0.059	-32.97	3623.03	3825[5] 3640[7] 3742[8] 3640[10] 3733[12]
	0.197	-32.92	3623.07	
	0.394	-32.81	3623.18	
	0.590	-32.61	3623.38	
bbu	0.0197	-12.19	10205.8	10219[5] 10110[7] 10216[8]
	0.197	-12.00	10206.0	
	0.394	-11.74	10206.5	
	0.986	-9.980	10208.0	
bbd	0.0197	-12.61	10217.4	10219[5] 10110[7] 10216[8] 11480[13]
	0.197	-12.52	10217.6	
	0.394	-12.10	10217.9	
	0.986	-10.33	10219.7	
bbs	0.0197	-17.70	10362.2	10374[5] 10278[8] 10360[9] 10374[11]
	0.197	-17.67	10362.5	
	0.394	-17.61	10362.9	
	0.986	-14.50	10365.5	
bbc	0.0197	-46.69	11411.3	11190[6] 11480[13]
	0.197	-46.07	11411.9	
	0.394	-44.94	11413.1	
	0.986	-38.20	11419.8	

[* - Experimental Value]

Acknowledgement: This work is part of a major research project (F. 32-31/ 2006(SR)) financed by UGC.

References

1. I.V. Gorelov (CDF Collaboration), arXiv:hep-ex/0701056 (2007)
2. M. Mattson *et al*. (SELEX collaboration), Phys. Rev. Lett. **89**, 112001 (2002)
3. Aubert B. et al. (BABAR Collaboration), Phys. Rev. Lett. **98**, 122011 (2007)
4. S.B. Athar et al., (CLEO Collaboration), Phys. Rev. **D71**, 051101(2005)
5. D. Ebert, et al., Phys. Rev. **D54**, 3619 (1996)
6. Yu.Jia/jhep10200607 (2006)
7. V.V. Kiselev and A.K. Likhoded, Phys. Usp. 45, 455 (2002)
8. C. Albertus et al., arXiv:hep-ph/0610131v1(2006), arXiv:hep-ph/0610030v2 (2007)
9. S.P. Tong et al., Phys. Rev. **D62**, 054024 (2000)
10. S.S. Gershtein et al., Phys. Rev. **D62**, 054021 (2000)
11. A. Ali Khan et al., Phys. Rev. **D62**, 054505 (2000)
12. R. Lewis et al., Phys. Rev. **D64**, 094509 (2001)
13. J.D. Bjorken, Proceedings of the ICHS, MD, 1985 FERMILAB-CONF-85-069

'Prajna' - Journal of Pure & Applied Sciences, 16 (2008) 127-149

PHYSICS OF CARBON NANOTUBES

S.L. Kakani, Subhra Kakani* and Anuj Nuwal
Institute of Technology & Management, Bhilwara - 311 001 (Raj.)
*University College of Science, ML Sukhadia University, Udaipur (Raj.)

Abstract

Carbon Nanotubes (CNTs) are amongst the most explored one-dimensional nanostructures and have attracted tremendous interest from fundamental science and technological perspectives . These are currently being studied in an effort to understand their novel structural, electronic and mechanical properties and to explore their immense potential for many applications in nanoelectronics , and as actuators and sensors. This paper presents the Physics of CNTs.

Keywords: Carbon nanotubes, Single walled nanotubes, Multiwalled nanotubes, Tunnelling spectra, Density of states, Luttinger Liquid, Superconductivity, Nanotube composites

Introduction

Carbon nanotubes (CNTs), discovered by Iijima [1] in 1991 are among the most exciting new materials and are currently being studied in an effort to understand their novel structural, electronic and mechanical properties [2-8]. They are hollow cylinders of graphite sheets. They can be looked at as single molecules, regarding their small size (~ nm in diameter and ~ μm ength), or as quasi-one dimensional crystals with translational periodicity along the tube axis . There are infinitely many ways to roll a sheet into a cylinder, resulting in different diameters and microscopic structure of tubes. These are defined by the **chiral angle**, the angle of hexagon helix around the tube axis. One can explain some properties of carbon nanotubes within a macroscopic model of an homogeneous cylinder; whereas other depend crucially on the microscopic structure of the tubes. The latter include , for e.g. the electronic band structure, in particular , their metallic or semiconducting nature. The fairly complex microscopic structure with tens to hundreds of atoms in the unit cell can be understood in a very general way with the help of the nanotube symmetry. This greatly simplifies calculating and understanding physical properties like optical absorption, phonon eigenvectors, and electron – phonon coupling.

The single- walled tubes generally have smaller diameters than the multiwalled nanotubes (typically of the order of 1-2 nm). Di et al [9] have shown that single – walled nanotubes, like multiwalled nanotubes can be produced catalytically.

Review and present finding

Carbon nanotubes are amongst the stiffest and strongest fibres known, with Young's moduli as high as 1T Pa and tensile strengths of up to 63 G pa. Qian et al [10] have shown that an addition of just 1 wt% CNTs results in a 25% increase in the tensile strength of polystyrene – based composite film. With the rapid progress towards the synthesis of large quantity and high quality CNTs in recent years carbon nanotubes have been used as nanofillers to enhance the mechanical strength of polymeric materials [11-14]. Among the mechanical properties of nanotubes, the axial Young's modulus (Y) shows an extraordinary feature in that its value is exceptionally high. Direct measurement on individual nanotubes using atomic force microscopy have shown that carbon nanotubes can accommodate extreme deformations without fracturing [15]; they also have the extraordinary capability of returning to their original, straight , structure following deformation. In addition, carbon nanotubes are excellent electrical conductors [16], with current densities up to 10^{11} A m^{-2}, and have very high thermal conductivities [17].

Carbon nanotubes also have remarkable electronic properties and can be metallic or semiconducting depending or their structure and diameter. There is currently great interest in exploiting these properties by incorporating carbon nanotubes into some form of matrix. A wide range of polymer matrices have been employed, and there is growing interest in nanotubes/ceramic and nanotubes/metal composites [18-19]. In many cases these composites have employed polymer matrices, but there is also interest in other matrix materials, such as ceramics and metals.

Carbon nanotubes as one-dimensional (1D) molecular conductors are also among the best candidates for investigating the possibility of **1D superconductivity** [20]. Experiments show superconductivity correlations in SWNTs at low temperature ($T_c \sim 15\,k$) and entirely end – bonded MWNTS at $T_c \sim 12\,k$ [20].

The aim of this paper is to review recent work on carbon nanotubes and to assess how successful this work has been in exploiting the full potential of nanotubes.

The carbon nanotubes have structures closely related to those of fullerences [1]. Figure 1 shows **armchair nanotube**; **zigzag nanotube** and **chiral nanotube**. The terms 'zigzag' and 'armchair' refer to the arrangement of hexagons around the circumference. In 'chiral' structure, the hexagons are arranged helically around the tube axis. Experimentally, the tubes are generally less perfect than the idealised versions shown in Fig. 1, and as already noted, may be either multiwalled nanotubes (MWNT) or single walled nanotubes (SWNT). Nanotubes are most commonly made of carbon, but they have also been produced from materials such as boron nitride and gallium nitride [21]. A tube made of a single graphite layer rolled up into a hollow cylinder is called SWNT, whereas a tube comprising several, concentrically arranged cylinders is referred to as MWNT. SWNTs are produced by ablation, high pressure CO conversion (Hi PCO), or the arc discharge technique and typically have diameter ranging from 0.7 nm (the diameter of C_{60} molecule) to ~ 3 nm, they can be several microns in length [22]. SWNTs form hexagonal- packed bundles during the growth process [7]. The wall to wall distance between two tubes is in the same range as the interlayer distance in graphite ($3.41A^0$). MWNTs have similar lengths to SWNTs, but much larger diameters. Their inner and outer diameters are around 5 and 100 nm, respectively, corresponding to ≈ 30coaxial tubes. Confinement effects are expected to be less dominant than in SWNTs, because of the large circumference. Many of the properties of MWNTs are already quite close to graphite. While the MWNTs have a wide range of application, they are less well defined from their structural and hence electronic properties due to the many possible number of layers.

To understand the atomic structure of CNTs, one can imagine taking structure of graphite (Fig. 2), and removing one of the two-dimensional planes, which is called a graphene sheet. Fig. 3(a) shows a single graphene sheet. One can view a CNT as a rolled – up graphene strip which forms a closed cylinder (Fig. 3). The basis vectors $a_1 = a\left(\sqrt{3}\,,0\right)$ and $a_2 = a\left(\frac{\sqrt{3}}{2},\frac{3}{2}\right)$ generate the graphene lattice, where a = 0.142 nm is the carbon-carbon bond length. A and B are the two atoms in the unit cell of graphene. In cutting the rectangular strip, one defines a circumferential or chiral (or wrapping) vector,

$$C = na_1 + ma_2 \quad .... (1)$$

Where m and n are integers (Fig. 4) . The chiral vector spans the circumference of the tube formed by joining the dotted lines shown in Fig. 4. Those tubes with chiral vectors of the form (n,0) are termed Zigzag tube (Fig. 1 (a)) whereas when n = ma so-called 'armchair' tube results (Fig. 1 (b)). All other values of n and m produce a chiral tube (Fig. 1 (c)).

From Eq. (1) the CNT radius can be obtained:

$$R = \frac{C}{2\pi} = \left(\frac{\sqrt{3}}{2\pi}\right) a\sqrt{n^2 + m^2 + nm} \quad .... (2)$$

The direction of the chiral vector is measured by the **chiral angle** θ, which is defined as the angle between $\vec{a}_1$ and c. The chiral angle θ can be calculated from

$$Cos\theta = \frac{a_1.c}{|a_1|.|c|} = \frac{n + {}^{m}\!/_{2}}{n^2 + nm + m^2} \quad .... (3)$$

A key theoretical result is that the armchair nanotubes are metallic, whereas for all other SWNTs, when n = m = 3 l (l is an integral) the tubes are metallic; otherwise they are semiconducting. CNTs show superconducting or metallic properties depending on the helicity of the carbon rings around the tube.

Electronic Properties of CNTs

The excellent and striking electronic properties of CNTs can be understood within a tight-binding frame work [22-25]. In the direction along c (i.e. along the circumference of the tube) , periodic boundary conditions constrain the values of electron wave vector to those given by,

$$c.k \quad = 2\pi q \qquad\qquad (q = 1, 2, ------ n) \quad .... (4)$$

Considering the particular example of an armchair case, Eq. (4) can be reduced to

$$k_x n \sqrt{3}\, a_0 \quad = 2\pi q \quad .... (5)$$

where $a_0 = \left(\sqrt{3}\right) 0.142\ nm$ is the graphite lattice constant and n defines the chiral vector for the armchair tube tube (here c = n $[a_1 + a_2]$)

The well- known tight – binding dispersion relation for a 2D graphite sheet [26, 27] is

$$E_{2D}(k_x, k_y) = \pm \gamma_0 \left\{ 1 + 4\cos\left(\frac{\sqrt{3}k_x a_0}{2}\right)\cos\left(\frac{k_y a_0}{2}\right) + 4\cos^2\left(\frac{k_y a_0}{2}\right) \right\}^{1/2} \quad ---(6)$$

Substituting the allowed values of k_x from (5) in (6), one obtains

$$E^{A}{}_{1D}\left(k_y\right) = \pm \gamma_0 \left\{ 1 \pm 4\cos\left(\frac{q\pi}{n}\right)\cos\left(\frac{k_y a_o}{2}\right) + 4\cos^2\left(\frac{k_y a_0}{2}\right) \right\}^{1/2}$$

$$(-\pi < k_y a_0 < \pi) \; .... (7)$$

where the superscript A denotes that (7) is valid for armchair CNTs. It is assumed that the value of the overlap integral for graphite and nanotube are identical. The 1D dispersion relations given by (7) are shown graphically in Fig. (5) for the case of a (5,5) armchair SWNT. Obviously, there are six dispersion curves for both the valence and conduction bands. In each case, four bands are double degenerate (bold continuous lines) and two bands are non degenerate (thin, dashed lines). Clearly, ten electron levels comprise the valence bands and ten comprise the conduction bands, as expected from the fact that there are ten hexagons around the circumference of a (5, 5) nanotubes. We may note two particularly noteworthy features of the dispersion relations shown in Fig. 5. First, there is a very high degree of degeneracy at the Brillouin Zone boundary. This can be easily understood from the fact that at $k_y\, a_0 = \pi$, Eq. (7) reduces to

$$E^{A}{}_{1D} = \pm \gamma_0 \quad \text{............} \ (8)$$

The second, and most important feature of Fig. 5 in terms of the electronic properties of armchair nanotubes is that the highest valence band and lowest conduction band are degenerate at $k_y = \pm {}^{2\pi}\!/_{3a_0}$ and each cross the Fermi energy (E = 0) at that point. This is true of all armchair nanotubes. Thus, all armchair nanotubes should be metallic.

Although a number of groups carried out conductance on multi- walled tubes using both scanning tunnelling spectroscopy [25, 28-29] and two– and four – probe geometries [30, 31] , conclusive experimental verification of the theoretical predictions outlined above appeared only in 1998 [32, 33]. Fig. 6 shows atomically resolved STM images of a range of nanotubes: armchair, zigzag and chiral tubes with different degrees of chirality. By acquiring scanning tunnelling spectra for each of these types of tube it was possible to correlate their structural and electronic properties.

Fig. 7(a) shows the tunnelling spectra acquired at 4K, for various tubes. Fig. 7(b) shows their derivatives $\left({}^{dI}\!/_{dV}\right)$. These apart from the contribution of a bias-dependent transmission term [34] provide a good measure of the local density of states of the tubes. The density of states can be expressed as

$$D(E) = \frac{\sqrt{3}\,a^2}{2\pi R} \sum_i \int dk\ \delta\left(k - k_i\right) \left|\frac{\partial \varepsilon}{\partial k}\right|^{-1} \quad \text{...........} \ (9)$$

where $\varepsilon\left(k_i\right) = E$ and $d = 2R$ is the diameter of the tube. Eq. (9) can be reduced to

$$D(E) = \frac{a\sqrt{3}}{\pi^2 R\gamma} \sum_{m=1}^{N} \frac{|E|}{\sqrt{E^2 - E_m{}^2}} \quad \text{...........} \ (10)$$

where $\varepsilon_m = |3m+1|\left({}^{a\gamma}\!/_{2R}\right)$ for semiconducting tubes and $\varepsilon_m = |3m|\left({}^{a\gamma}\!/_{2R}\right)$ for metallic tubes. In the case of metallic tubes, the m = 0 band gives a non-zero density of states at the Fermi level, with $D(E) = \frac{a\sqrt{3}}{\pi^2 R\gamma}$. The expression for the density of states shows van Hove singularities when $E = \pm\varepsilon_m$, which is indicative of quasi – one dimensional materials (Fig. 8).

Wildoer et al. [32] observed two distinct 'families' of ${dI}/{dV}$ spectra for chiral tubes: Those with a gap of ~ 0.5 – 0.6 V (spectra 1- 4 in Fig. 7 (a)) and those with a much larger apparent gap, 1.7 - 2.0 V (spectra 5 – 7). The gap values for the first family of curves are plotted versus the tube diameter in Fig. 7 (c). The solid line is a fit to band gap, $E_g = {2\gamma_0 a}/{d}$, where a is a carbon- carbon spacing (0.142 nm) and d the tube diameter. Fig. (9) shows that the band gap of semiconducting nanotubes decreases inversely with an increase in diameter.

We may note that there are some deviations in the electronic properties of the nanotubes from the simple π - orbital graphene picture describe above due to curvature. As a result of curvature: (i) the hopping integrals describing the three bonds between nearest neighbours are not identical and (ii). $\sigma - \pi$ hybridization and charge self – consistency become important. Since curvature becomes larger with a decrease in the nanotube diameter, deviations from the simple π - orbital graphene picture become more important in small diameter nanotubes and require a more careful treatment beyond the simple tight- binding graphene model.

Metallic CNTs

Metallic CNTs have attracted significant attention because their current carrying ability is unparallel in the family of emerging nanowires. Ballistic transport has been observed and values for the conductance that approaches the theoretical limit have been measured at small biases. They hold promise as interconnects in both silicon nanoelectronics and molecular electronics because of their low resistance and strong mechanical properties. The unique band structure of metallic CNTs, which is partly responsible for their superb current carrying capacity deviates significantly from the parabolic bandstructure of a free electron in a nanowire (within the effective mass approximation). From a basic physics perspective , metallic nanotubes have been of immense interest to condense matter researchers studying electron- electron interactions because they exhibit the novel physics of **Luttinger Liquid behaviour**.

The electron-electron interaction are also known to modify significantly the transport of the nanotubes [35], leading to the breakdown of the conventional **Fermi Liquid Picture**. In fact the 1D character of the system leads to a strong correlation among electrons, inducing of the so-called Luttinger liquid [35, 36]. This effect was studied more in general, taking into account in the presence of long – range Coulomb interaction, even for systems with a range between 1 and 2 dimensions [37-39]. The Luttinger liquid behaviour is characterized by a power-law suppression of physical observables, such as tunnelling conductance, over a wide range of temperature, indeed the tunnelling conductance G reflects the power law dependence of the tunnelling density of states (DOS), in a small bias experiment [40].

$$G = \left(dI \middle/ dV \right) \propto T^{\alpha} \qquad \text{.............} (11)$$

for $eV \langle\langle k_B T$, where V is the bias voltage, T is the temperature, and k_B is Boltzmann constant. Evidence of Luttinger liquid behaviour in SWNTs has been reported in many experiments [35, 41, 42], where the temperature dependence of the resistance above a crossover temperature T_c was measured [43]. The critical exponent α assumes different values for an electrode – bulk junction (α_{bulk}) and for an electrode –end junction (α_{end}) for MWNTs [44-47].

Experiments clearly provides evidence of **superconductivity** in nanotubes suspended between superconducting contacts, showing the so called proximity superconductivity transitions below 1 K have been observed in thick ropes of nanotubes between normal and highly transparent electrodes [48, 49].

A few years ago, ultrasmall- diameter single wall nanotubes (USCN), with a diameter of ~ 0.4 nm, have been produced inside the channels of a Zeolite matrix. Possible metallic geometries compatible armchair (3,3) and Zigzag (5,0) ones. The ultrasmall diameter of these tubes induces many unusual properties, such as a superconducting transition temperature $T_c = 15\,K$ [50], much larger than that observed in bundles of larger diameter tubes [51].

Quite recently [52] a similar superconducting transition temperature was reported in entirely end – bonded MWNTs. It was found that the emergence of superconductivity $(T_c = 12\,K)$ is highly sensitive to the junction structures of the Au electrode / MWNTs [52].

Nanotubes are excellent wires, with near- perfect experimentally measured conductances. At first sight this is surprising because surface scattering disorder, defects and phonon scattering , which lead to decrease in conductance, seem ineffective [6].

At high biases, the current carrying capacity of CNTs is significantly affected by electron-phonon scattering. The conductance is largest at zero bias and decreases with an increase in bias. The current that flows in long nanotube (many mean free paths) at large biases will be approximately

$$I = \frac{4e^2}{h} 160\, MeV = 30 \mu A \quad \text{.............} (12)$$

A number of experiments have now reported currents comparable to $30 \mu A$ in long nanotubes [53-54].

In contrast to small diameter nanotubes, large diameter nanotubes show an increase in differential conductance with applied bias [55, 56].

For a metallic CNT, the density of states per unit length at the Fermi energy is $D(E) = {}^{4}\!/_{\pi\, v_F}$ **quantum capacitance** per unit length [57] as

$$C_Q = \frac{4e^2}{\pi \hbar v_F} \sim 0.4\, a F\, n m^{-1} \quad \text{.................} (13)$$

where v_F is the Fermi velocity. C_Q is comparable with the electrostatic capacitance, $C_E \sim 0.1\, a F\, n m^{-1}$. Obviously, both the classical and quantum capacitance need to be taken into account when analysing the electrical properties of CNTs.

The kinetic inductance of metallic CNTs is given by

$$L_k = \frac{\pi}{4e^2\, v_F} \quad \text{................} (14)$$

for Fermi velocity $v_F = 8 \times 10^5\ m/s, \quad L_k \sim 4 pH\, n m^{-1}$.

The **magnetic inductance** of a nanotube over a ground plane is given by

$$L_m = \frac{\mu}{2\pi}\cosh^{-1}\left(\frac{2h}{d}\right) \quad \text{.....................} \; (15)$$

for d = h = 1.5 nm, one obtains $L_m \sim 5.5 \times 10^{-4}\ pHnm^{-1}$. Obviously, the kinetic inductance is about ten thousand times larger than the magnetic inductance and hence cannot be neglected in the modeling of CNT interconnects. It would take over 10000 nanotubes arranged in parallel for the magnetic inductance to become equal to the kinetic inductance.

The large value of kinetic inductance has an important effect on the speed at which signals are propagated in a transmission line consisting of a single nanotube. The wave velocity for signal transmission in the nanotubes transmission line is

$$\text{Wave velocity} = \frac{1}{\sqrt{LC}} \sim \sqrt{\frac{1}{L_K}\left(\frac{1}{C_E}+\frac{1}{C_Q}\right)} \quad \text{...................} \; (16)$$

When $C_Q << C_E$, the wave velocity for propagation of an electromagnetic signal is

$$\text{Wave velocity} \sim \frac{1}{\sqrt{L_K\, C_Q}} = v_F \quad \text{......................} \; (17)$$

If there are N nanotubes in parallel then the expression for the velocity of signal propagation is

$$\text{Wave velocity} = \sqrt{\frac{1}{L_K + NL_M}\left(\frac{N}{C_E}+\frac{1}{C_Q}\right)}$$

which reduces to the classical expression $\sqrt{1/L_M\, C_E}$, when the magnetic inductance and electrostatic capacitance dominate.

Metal Contacts

Contacts play a crucial role in electronic devices. In traditional contacts between metals and semiconductors, the Fermi level pinning usually dominates, leading to a Schottky barrier at the contact. The presence of the Schottky barrier implies that electronic transport across the contact is dominated by thermionic emission over the Schottky barrier, significantly increasing the contact resistance. Now, the question arises, how is the physics modified for nanotubes / metal for electron transport.

The key difference between nanotube / metal contacts and traditional contacts is that the former are essentially planar whereas nanotube contacts can show various structures. The different contact geometries and the reduced dimensionality of nanotubes can have a strong effect on the contact behaviour. The type of metal used to contact the CNT has a strong influence on the properties of the contacts. The evidence of Schottky barriers at contacts is intimately related to the behaviour of CNT transistors with such contacts. For a typical CNT with a bandgap of 0.6 eV, and for the CNT midgap 4.5 below the vaccum level [58, 59] metal workfuncitons larger than 4.8 eV (or less than 4.2 eV) would thus lead to a negative Schottky barrier, i.e. the metal contacts the CNT in the valence (conduction) band, giving an Ohmic contact. Thus, one may expect that Au (5.5 eV) and Pd (5.1 eV) would give Ohmic contacts. While most of the research on the properties of the nanotubes / metal contacts has focused on fabricating the Ohmic contacts to contact the lowest possible contact resistance, for electrical insulation and tunnelling applications, it is important to develop contact that have high resistance.

Applications of Nanotubes

Most applications of the CNTs are based on the unique electronic structure, mechanical strength, flexibility, and dimensions of nanotubes. CNTs are potential building blocks for nanoscale electronic devices [61-63]. The remarkable properties of CNTs could enable diverse applications in nanoelectronics as nanoscale circuits, transistors, diodes, future sensing or computing [1, 63-65]. A field effect transistor (FET), which is the basic component of computer circuitry, has been demonstrated based on individual SWCNTs [64, 66]. Very recently Sakurai et al. [67] demonstrated CNT – FETs integrating ferroelectric thin films as gate insulators (ferroelectric – gate CNT- FETs). This offer potential as non-volatile memory elements and high sensitivity sensors. For low voltage, digital applications, the CNT – FETs with a planar gate geometry provides an on current that is comparable to that expected for a ballistic MOSFET [68]. Rueckes et al. [69] suggested that a memory cell can be created on the basis of two crossing nanotubes. Akita et al. [70] demonstrated the functioning of nanotweezers composed of two multiwall nanotubes with their spacing controlled by an applied voltage.

A key obstactle to the commercial application of CNTs in nanoelectronics is that, through diverse techniques such as arc discharge [1, 60], thermal decomposition of hydrocarbons over catalysts [71] and laser vaporization of graphite [72] have been developed to produce

CNTs, none of these synthetic methods can be used for reliable preparation of only semiconducting or metallic naontubes. To solve this problem, **heteronanotubes** whose properties are chemistry dependent are highly desired. Up to now, a large number of tubular structures, e.g., B N, WS_2, MoS_2, BC_2 N, V_2O_5 etc. [73] have been proposed.

These inorganic fullerence – like structures have attracted considerable basic and applied interest because of their unusual geometry, uniform physical properties and significant advantages for applications.

There is currently great interest in exploiting the remarkable properties of CNTs by incorporating CNTs into some form of matrix. A wide range of **polymer matrices** have been employed [5], and there is growing interest in nanotube / ceramic and nanotube / metal composites. A commonly used method for preparing nanotubes / polymer composites has involved mixing nanotube dispersions with solutions of the polymer and then evaporating the solvents in a controlled way. However, the solution mixing approach is limited to polymers that freely dissolve in common solvents. An alternative is to use thermoplastic polymers (i.e., polymers that soften and melt when heated), and then apply melt processing techniques. Composite fibres with a high degree of nanotube orientation were produced by melt spinning.

Polycarbonate is another thermoplastic polymer that has been used as a matrix for nanotube composites [74, 75]. Nanotube / epoxy composites have also been prepared by a number of groups [76 - 80]. An alternative method for preparing nanotube / polymer composites is to use the monomer rather than the polymer as a starting material, and then carry out in Situ polymerisation [81 - 85]. The nanotubes in these composites are distributed evenly throughout the polymer (either randomly oriented or aligned). For some applications, however, a layered arrangement is advantageous. Photovoltaic devices containing layers of nanotubes or nanotube / polymer composites have been prepared [1, 86]. The subject of carbon nanotubes has grown rapidly over the past 8 years or so into a vibrant and exciting area of research. However, this is still a new subject and the research work carried out so far may have hardly scratched the surface of what is possible.

Future Aspect

This brief review has covered only a subset – albeit a broad and, we hope, representive subset – of the rapidly expanding body of literature on carbon nanotubes. There are many features that make CNTs different from traditional materials, including chirality – dependent electronic properties, the one – dimensional nature of electrostatic screening and presence of several direct bandgaps. Understanding these novel properties and their impact on devices is quite crucial in the development and evolution of CNT applications.

References

1. S. Iijima, Nature **354**, 56 (1991)
2. S.L. Kakani and Amit Kakani, in Material Science, Chapter 20, New Age International Publishers, New Delhi -2 (2004)
3. C.N.R. Rao, J. Mater. Chem. **9**, 1-14 (1999)
4. C.N.R. Rao, G.U. Kulkarni, A. Govindarraj, B.C. Satishkumar, and P. John Thomas, Pure Appl. Chem. **72**, 21 (2000)
5. P.J.F. Harris, Int. Mats. Rev. **49**, 31 (2004)
6. M.P. Anantram and F. Leonard Rep. Prog. Phys. **69**, 507 (2006)
7. S. Reich, C. Thomsen and J. Maultzsch, Carbon Nanotubes, Wiley- VCH Verlag GmbH and Co. K GaA (2004)
8. P.M. Ajayan, in 'Handbook of Nanostructured Materials and Nanotechnology', Vol. 5 H.S. Nalwa (ed.), Academic Press (2000)
9. H. Dai, A.G. Rinzler, P. Nikolaev, A. Thess, D.T. Colbert and R.E. Smalley, Chem. Phys. Lett. **260**, 471 (1996)
10. D. Qian, E.C. Dickey, R. Andrews, T. Rantell, Appl. Phys. Lett. **76**, 2868 (2000)
11. A.M. Cassell, N.R. Franklin, T.W. Tombler, E.M. Chan, J. Han, H. Dai, J. Am. Chem. Soc. **121**, 7975 (1999)
12. S. Fan, M.G. Chapline, N.R. Franklin, T.W. Tombler, A.M. Cassell, H. Dai, Science **283**, 512 (1999)
13. H.J. Dai, Surf. Sci **500**, 218 (2002)
14. B.Q. Wei, R. Vagtai, Y. Jung, J. Ward, R.Z. Hang, G. Ramanath, P.M. Ajayan, Chem. Mater. **15**, 1598 (2003)
15. M.R. Falvo, G.J. Clary, R.M. Jaylor, V. Chi, F.P. Brooks, S. Washburn and R. Superfine, Nature **389**, 582 (1997)
16. K. Anazauva, K. Shimotani, C. Manabe, H. Watanabe, and M. Shimizu, Appl. Phys. Lett. **81**, 739 (2002)
17. P. Kim, L. Shi, A. Majumdar, and P.L. McEuen, Phys. Rev. Lett. **87**, 215502 (2001)
18. E.T. Thostenson, Z.F. Ren and J.W. Chou, Compos. Sci Technol. **61**, 1899 (2001)
19. K.T. Lau and D. Hui, Composites Part B, Engineering **33**, 263 (2002)

20. S. Bellucci, M. Cini, P. Onorato, and E. Perfetto, Phys. Rev. **B 75**, 014523 (2007)
21. G. Rannie, S and T R, January / February, 2006 Pages 4-10
22. (a) P. Moriarty, Rep. Prog. Phys. **64**, 297 (2001)
22. (b) N. Hamada, S - I Savada and A. Oshiyama, Phys. Rev. Lett. **68**, 1579 (1992)
23. R.Saito, M.Fujita, G.Dresselhaus, and M.S.Dresselhaus, Appl. Phys. Lett.**60**, 204 (1992)
24. J.W. Mintmire, B. I. Dunlap, and C.T. White, Phys. Rev. Lett. **68**, 631 (1992)
25. M.S. Dresselhaus, G. Dresselhaus, and P.C. Eklund, 'Science of Fullerence and carbon nanotubes' (Academic 1996)
26. N.W. Ashcroft and N.D. Mermin, Solid State Physics (Saunders College Publishing, 1976)
27. S.L. Kakani, and C. Hemrajani, Solid State Physics (Sultan Chand, New Delhi, 4th ed. 2007)
28. Z. Zhang and C.M. Lieber, Appl. Phys. Lett. **62**, 2792 (1993)
29. K. Sattler, Carbon 33, **915** (1995)
30. T.W. Ebbesen, H.J. Lezec, H. Hiura, J.W. Bennet, H.F. Ghaemi, and T. Thio, Nature 382, **54** (1996)
31. L. Langer, V. Bayot, E. Grivei, J.P. Issi, J.P. Heremans, C.H. Olk, L. Stockman, C. Vanhaesendonck and Y. Bruynseraede, Phys. Rev. Lett. **76**, 479 (1996)
32. JWG Wildoer, L.C. Venema, A.G. Rinzler, R.E. Smalley and C. Dekker, Nature **391**, 59 (1998)
33. T.W. Odom, J- L, P. Kim, and C.M. Lieber, Nature **391**, 62 (1998)
34. R.M. Feenstra, Scanning Tunneling Microscopy, J.A. Stroscio and W. Kaiser (eds.) (Academic 1993)
35. Z. Yao, H.W. Ch Post ma, L. Balentaz and C. Dekker, Nature **402**, 273 (1999)
36. R. Egger and A.O. Gogolin, Phys. Rev. Lett. **79**, 5082 (1997); Eur. Phys. J. B3, 281 (1998)
37. S. Bellucci and P. Onorato, Ann. Phys. **321**, 934 (2006), Phys. Rev. B71, 075418 (2005)
38. S. Bellucci and J. Gonzalez, Eur. Phys. J. B. **18**, 3 (2000)

39. S. Bellucci and J. Gonzalez, and P. Onorato Phys. Rev. Lett. **95**, 186403 (2005)
40. C.L. Kane and M.P.A. Fisher, Phys. Rev. **B46**, 15233 (1992); Phys. Rev. Lett.68, 1220 (1992)
41. C.L. Kane, L. Balentz and M.P.A. Fisher, Phys. Rev. Lett .**79**, 5086 (1997)
42. M. Bockrath, D.H. Cobden, J. Lu, A.G. Rinzler, R.E. Smalley, L. Balentz and P.L. McEuen, Nature **397**, 598 (1999)
43. J.E. Fischer, H. Dai, A. Thess, R. Lee, N.M. Hanyani, D.L. Dehaas and R.E. Smalley, Phys. Rev. **B55**, E 4921 (1997)
44. A. Bachtold, M. de Jonge, K. Grove - Rasmusse, C. Schoneberger, Phys. Rev. Lett. **87**, 166801 (2001)
45. A. Yu Kasumov et al., Science **284**, 1508 (1999)
46. A.F. Morpurgo et al., Science **286**, 263 (1999)
47. S.L. Kakani and Subhra Kakani, Superconductivity, New Age Internaitonal Publihsers, New Delhi (2007)
48. M. Kociak, A.V. Kasumov, S. Gueron, B. Reulet, I.I. Khodos, Y.B. Gorbatov, V.T. Volkov, L. Vaccarini, and H. Bouchiat, Phys. Rev. Lett. **86**, 2416 (2001)
49. A. Kasumov, M. Kociac, M. Ferrier, R. Deblock, S. Gueron, B. Reulet, I. Khodas, O. Stephan, and H. Bouchiat, Phys. Rev. **B68**, 214521 (2003)
50. Z. Tang et al., Science **292**, 2462 (2001)
51. M. Kociak, A.Y. Kasumov, S. Gueron, B. Reulet, I.I. Gorbatov, V.T. Volkov, L. Vaccarinik and H. Bouchiat, Phys. Rev. Lett. **86**, 2416 (2001)
52. I. Takesue, J. Haruyama, N. Kobayashi, S. Chiashi, S. Maruyama, N. Kobayashi, S. Chiashi, S. Maruyama, T. Sugai and H. Shinohara, Phys. Rev. Lett. **96**, 057001 (2006)
53. Z. Yao, C.L. Kane and C. Dekker, Phys. Rev. Lett. **84**, 2941 (2000)
54. P.G. Collins, M. Herbam, M. Arnold, R. Martel and Ph Avouris, Phys. Rev. Lett. **86**, 3128 (2001).
55. S. Frank, P. Poncharral, Z.L. Wang, and W.A. de Heer, Science **280**, 1744 (1998)
56. Y. X. Liang, Q.H. Li and T.H. Wang, Appl. Phys. Lett. **84**, 3379 (2004)
57. P.J. Burke, IEEE Trans., Nanotechnol. **1**, 129 (2002)
58. N. Ago et al., J. Phys. Chem. **B103**, 8116 (1999)

59. S. Suzuki, C. Bower and Y. Watanabe, Appl. Phys. Lett. **76**, 4007 (2000)
60. P.M. Ajayan and T.W. Ebbersen, Rep. Prog. Phys. **60**, 1025 (1997)
61. C. Dekker, Phys. Today **52**, 22 (1999)
62. J.T. Hu, T.W. Odom and C.M. Lieber, Acc. Chem. Res. **32**, 435 (1999)
63. P.G. Collins and A. Avouris, Sci. Am. **283**, 62 (2000)
64. S.J. Tans, A.R.M. Verschueren and C. Dekker, Nature **393**, 49 (1998)
65. A. Javey, J. Guo, Q. Wang, M. Lundstroom and H. Dai, Nature **424**, 654 (2003)
66. R. Martel, I. Schmidt, H.R. Shea, T. Hertel, P. Avouris, Appl. Phys. Lett. **73**, 2447 (1998)
67. T. Sakurai, T. Yoshimura, S. Akita, N. Fujimura and Y. Nakayama, Jpn. J. Appl. Phys. **45**, L 1036 (2006)
68. P.A. Alvi, K.M. Lal, M.J. Siddiqui and S. Alim H. Naqvi, Indian J. Pure and Appl. Phys. **43**, 899 (2005)
69. T. Rueckes, K. Kim, E. Joselevich, et. al., Science **298**, 94 (2000)
70. S. Akita, Y. Nakayama, S. Mizooka, et. al. Appl. Phys. Lett. **79**, 1691 (2001)
71. S. Amelinckx, X.B. Zhang, D. Bernaertz, X.F. Zhang, V. Ivanov and J.B. Nagy, Science **265**, 635 (1994)
72. A. Thess, R. Lee, P. Nikolaev, H.J. Dai, P. Petit, J. Robert, C.H. Xu, Y.H. Lee, S.G. Kim, A.G. Rinzler, D.T. Colbert, G.E. Scuseria, D. Tomanek, J.E. Fischer, and R.E. Smalley, Science **273**, 483 (1996)
73. L.M. Cao, X.Y. Zhang, C.X. Gao, W.K. Wang, Z.L. Zhang and Z. Zhang, Nanotechnology **14**, 931 (2003)
74. P. Potschke, T.D. Fornes and D.R. Paul; Polymer **43**, 3247 (2000)
75. M. Sennett, E. Welsh, J.B. Wright, W.Z. Li, J.G. Wen and Z.F. Ren, Appl. Phys. **A76**, 111 (2003)
76. P.M. Ajayan, O. Stephan, C. Colliex and D. Trauth; Science 265, 1212 (1994)
77. J. Sandler, M.S.P. Shafffer, T. Prasse, W. Bauhofer, K. Schulte and H. Windle, Polymer **40**, 5967 (1999)
78. A. Allaoui, S. Bai, H.M. Cheng and J.B. Bai, Compos. Sci Technol. **62**, 1993 (2002)
79. X. Xu, M.M. Thwe, C. Shearwood and K. Liao, Appl. Phys. Lett. **81**, 2833 (2002)

80. D. Puglia, L. Valentini, and J.M. Kenny, J. Appl. Polymer Sci., **88**, 452 (2003)

81. M. Cocher, W.K. Maser, A.M. Benito, M.A. Callegas, M.T. Martinez, J.M. Benojt, J. Schreiber and O. Chauvet, Chem. Commun. 1450 – 1451 (2001)

82. M.S.P. Shaffer and K. Koziol, Chem. Commun. 2074 – 2075 (2002)

83. C. Park, Z. Ounaies, K.A. Watson, R.E. Crooks, J. Smith, S.E. Lowther, J.W. Connell, E.J. Siochi, J.S. Harrison and T.L. St. Claix, Chem. Phys. Lett. **364**, 303 (2002)

84. K. Jurewicz, S. Delpeux, V. Bertagna, F. Beguin and E. Frackowiak, Chem. Phys. Lett. **347**, 36 (2001)

85. M. Hughes, G.Z. Chen, M.P. Shaffer, D.J. Fray and A.H. Windle, Chem. Mater. **14**, 1610 (2002)

86. A. Mamedov, N.A. Kotov, M. Prato, D.M. Guldi, J.P. Wicksted and A. Hirsch, Nature Mater **1**, 190 (2002)

FIGURE CAPTIONS

Figure 1. (a) armchair (n, m) = (5, 5); (b) Zigzag (n, m) = (9, 0); Ciral (n, m) = (10, 5)

Figure 2. Illustration of the graphite structure , showing the parallel stacking of two dimensional planes called graphene sheets.

Figure 3. (a) a_1 *and* a_2 are the lattice vectors of graphene $|\vec{a}_1| = |\vec{a}_2| = \sqrt{3}a$, where a is the carbon- carbon bond length. There are two atoms per unit cell shown by A and B. SWNTs are equivalent to cutting a strip in the graphene sheet and rolling them up such that each carbon atoms is bonded to its three nearest neighbours. The creation of a (n, 0) zigzag nanotube is shown in (b) creation of a (n, n) armchair nanotube (c). A (n, m) chiral nanotube (d) The bonding between a nanotube. The n =2 quantum number of carbon has 4 electrons. Three of these electrons are bonded to its three nearest neighbours by Sp^2 bonding in a manner similar to graphene. The fourth electron is a orbital perpendicular to the cylindrical surface.

Figure 4. The relationship between the graphene lattice basis vectors a_1, a_2 and the chiral vector $c = na_1 + ma_2$ used to characterize CNTs. Two limiting cases are shown: (n, 0) indices are associated with zigzag tubes whereas (n, n) indices are associated with armchair tubes. All other tubes are chiral.

Figure 5. The one-dimensional dispersion relation for an armchair (5, 5) nanotubes.

Figure 6. Atomically resolved STM images of single –walled carbon nanotubes. Dashed arrows represents the tube axis T and solid arrows indicate the direction of the hexagons comprising the graphene lattice (H). The angle between T and H is the chiral angle. Tubes Nos 10,11 and 1 are chiral whereas tubes No.s 7 and 8 are Zigzag and armchair type respectively.

Figure 7. (a) Scanning tunnelling spectra of various CNTs. Tubes 1-6 are chiral whereas 7 and 8 are Zigzag and armchair respectively. (b) ${}^{dI}\!/_{dV}$ plots which provide a measure of the tube density of states (c). Energy gap versus diameter for semiconducting chiral tubes (d). Normalized differential conductance $\left(\left({}^{dI}\!/_{dV}\right)/\left({}^{I}\!/_{V}\right)\right)$ spectra nanotube 9. Sharp peaks are observed which closely match the shape of the theoretical density of curve

shown in the inset to the right (The peaks arise from the ${1}/{\sqrt{E}}$ dependence of the 1D density of states). The left inset shows the raw ${dI}/{dV}$ data.

Figure 8. Density of states for $(11, 0)$ and $(12, 0)$ CNTs computed from tight binding shown Van Hove Singularities.

Figure 9. Bandgap versus radius for zigzag CNTs. The bandgap decreases inversely with increase in diameter. The points with zero bandgap correspond to metallic nanotubes which satisfy $n - m = 3 * I$, where I is an integer. Note that when curvature induced effects are introduced all metallic nanotubes (except armchair) develop a small bandgap.

Figure 1

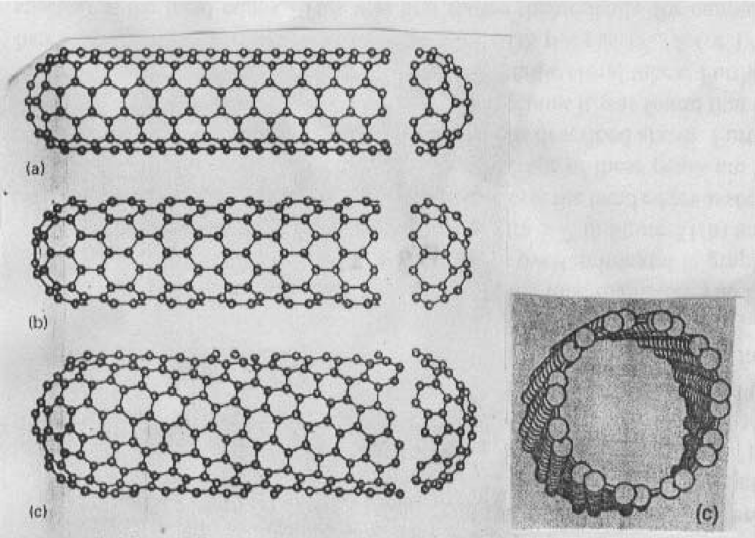

a armchair $(n, m)=(5, 5)$; *b* zigzag $(n, m)=(9, 0)$; *c* chiral $(n, m)=(10, 5)$

Figure 2

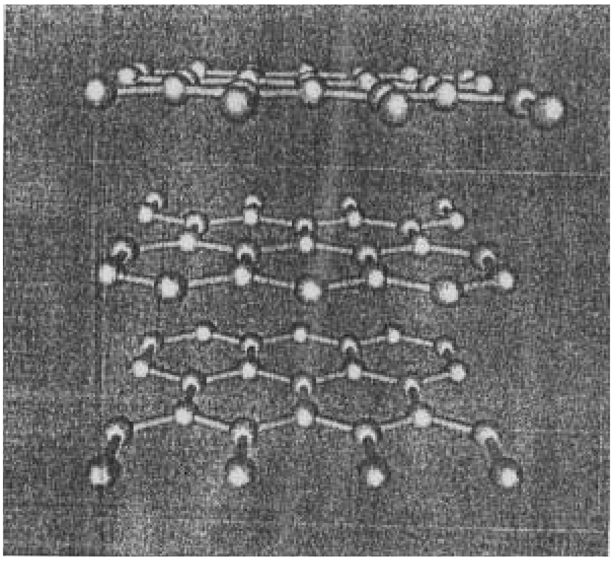

Figure 3

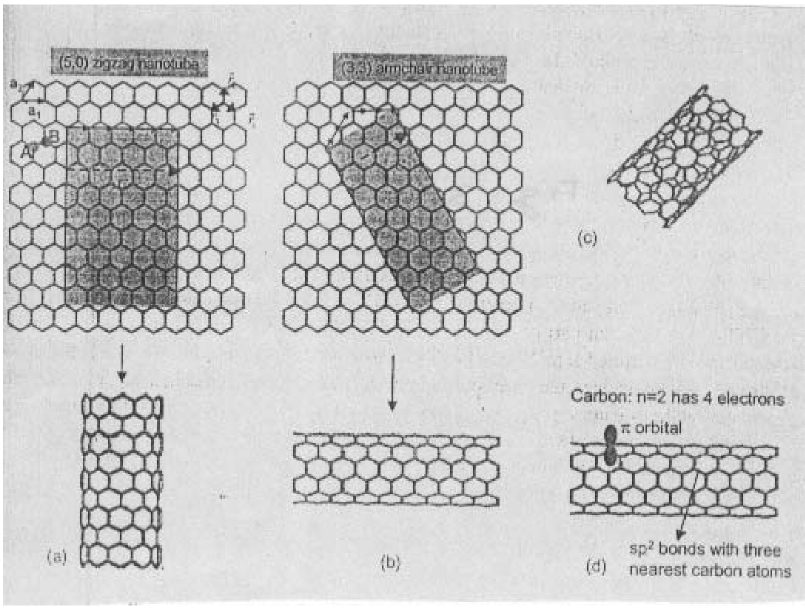

Figure 4

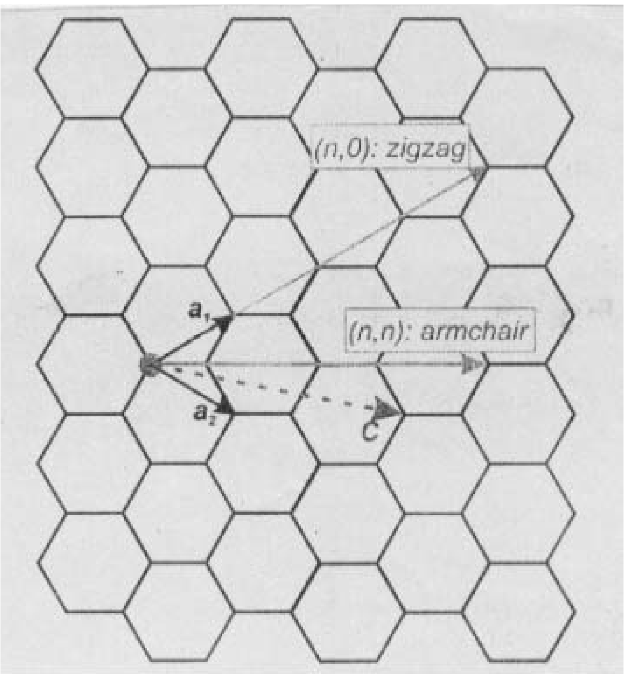

Figure 5

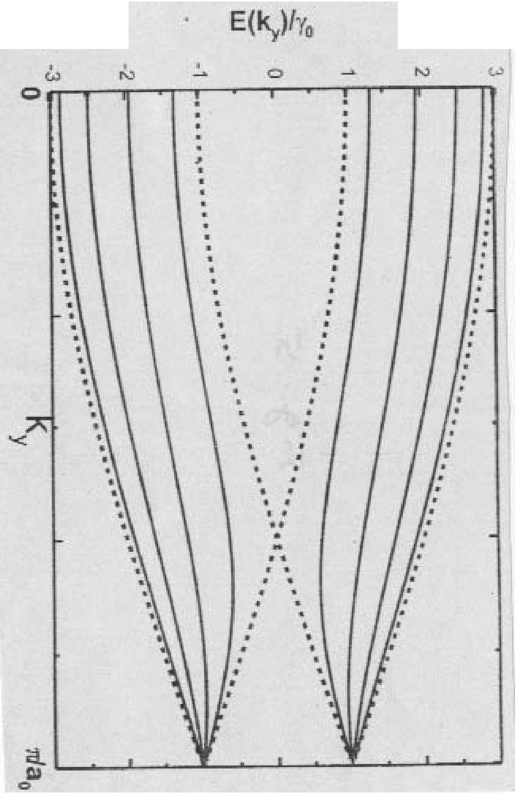

Figure 6

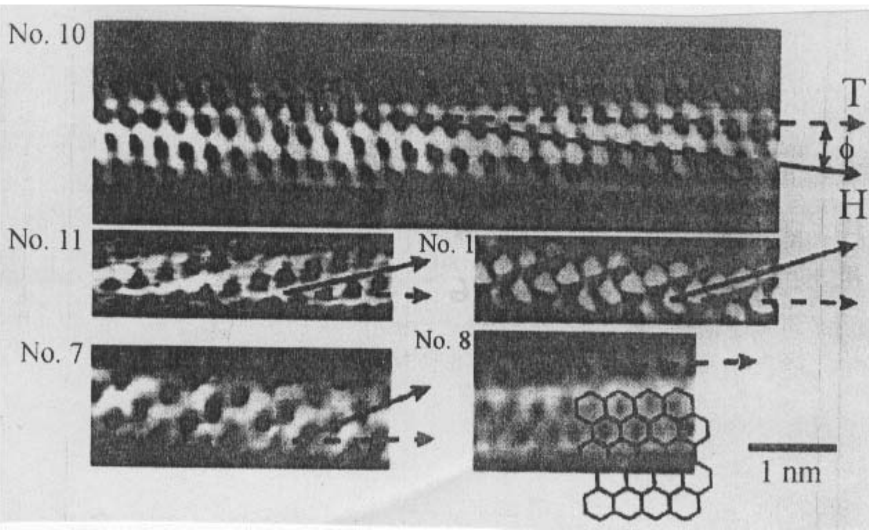

Figure 7

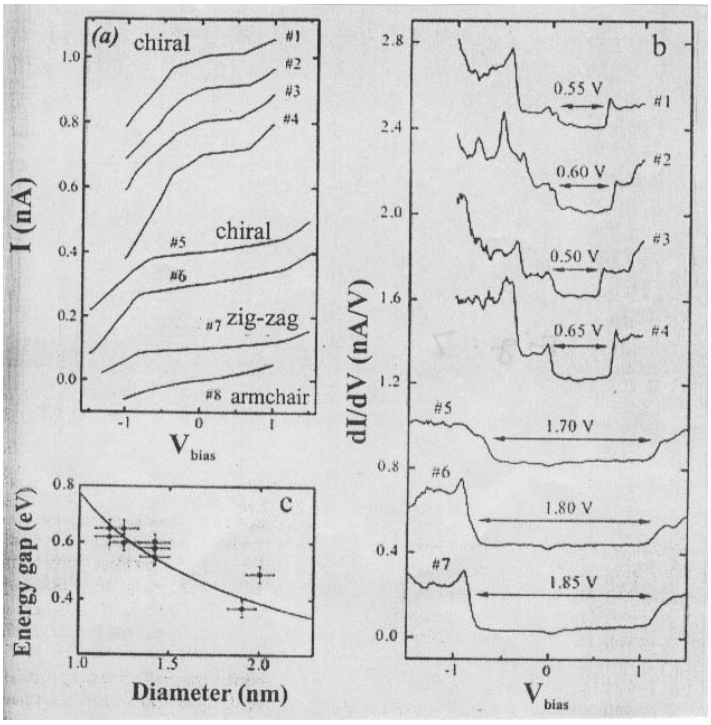

Figure 8

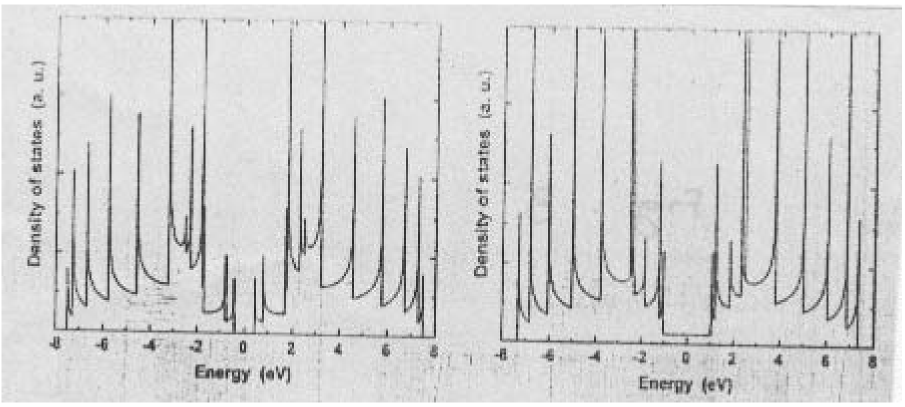

Figure 9

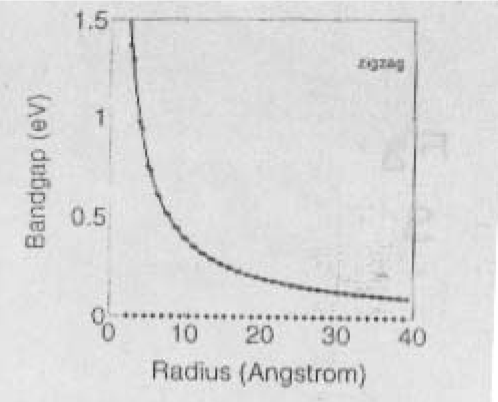

'Prajna' - Journal of Pure & Applied Sciences, 16 (2008) 150-164

INFRARED SPECTROSCOPY OF DONOR-ACCEPTOR COMPLEXES OF INDOLE (BENZOPYRROLE)

G.K. Solanki, Mukesh Patel and A.T. Oza
Department of Physics, Sardar Patel University, Vallabh Vidyanagar-388 120

Abstract

In this paper we report the preparation and spectroscopic studies of six 1:1 complexes of indole - namely indole-TCNQ, indole-DDQ, indole -TCNE, indole -chloranil, indole-TNF and indole-iodine. We have carried out the infrared spectra in the range 400 cm^{-1} -4000cm^{-1} and their analysis are described. All the complexes shows $ah\nu=B(h\nu\text{-}Eg)^{3/2}$ behaviour, where a is absorbance, ν is frequency and Eg is the band gap. The optical absorption edges of this forbidden direct transition are about 0.225 eV, which is the Peierls gap. Indole-chloranil and indole-TCNE shows three Gaussian envelopes of electronic absorption and other complexes reveal one Gaussian curves and two of three Lorentzian envelopes. Here for the first time in organic semiconductors, mixed Lorentzian and Gaussian envelopes are found even though the donor (indole) is kept same.

Key words: Infrared spectroscopy, charge transfer complesxes, indole (benzopyrrole), band assignments

Introduction

There is a still a lot of interest in the studies of organic semiconductors and quasi-one dimensional conductors. The disordered and ordered thin films of α-sexithiophene have been characterized with optical properties (Lane et al. [1]). Conducting complex salts N-CH^{2N+1} iso Qn(TCNQ)$_2$ have been synthesized (Stardup et al. [2]). Porphyrin films are studied using impedance spectroscopy (Savenge et al. [3]). Bis- pyrrolotetrathiafulvalene is used as a donor with acceptors like TCNQ, DDQ and TCNQF$_4$ to form an isotropic conductors (Tachibara et al. [4]) (BEDT-TTF)$_2$I$_3$ was studied for superconductivity in the form of thin films (Wojerechowski et al. [5]. High field electrical conduction and Seeback coefficient were studied on the derivatives of aspartic acid and on some more organic semiconductors (Rasu et al. [6]). Here we have prepared some new donor-acceptor complexes of a simple donor like indole (benzopyrrole) and we report the infrared spectra in 400 cm^{-1} – 4000 cm^{-1} and their analysis.

Experimental

Indole is a white dielectric material and it is an insulator. It is actually benzopyrrole. Indole (0.5 gm) was taken and grinded with TNF (2,4,5,7-tetranitro-9-flourenone) (0.163 gm) to form blue 1:1 complex. Similarly black coloured indole-TCNQ

(TCNQ=7,7,8,8-Tetracyano-p-quinodimetane) was prepared by grinding 0.5 gm indole with 0.287 gm TCNQ. Indole-chloranil (1:1) complex was a blue material obtained by grinding 1.0 gm indole with 0.476 gm chloranil. Black indole-TCNE (TCNE=Tetracyanoethylene) was prepared in a mortar by grinding 0.5 gm of indole with 0.431 gm of TCNE. Indole-I_2 a tar-like black complex was obtained by mixing 1.0 gm of indole with 0.465 gm of molecular iodine. Ir was partially liquid like a paste and when grinding was continued for a long time, it was becoming liquid. Liquid dries after 4-5 days only to form flakes of the black complex. The samples for infrared measurements were compactions (pellets) after compressing a grinded mixture with KBr in a die under high pressure. The Nicolet 400 D spectrophotometer was used for recording the infrared spectra in the range 400 cm^{-1} -4000 cm^{-1}.

Results and Discussion

Molecular structures of indole and organic acceptors are shown (Figure 1). The infrared spectrum of only indole is shown (Figure 2) for comparison with those of its charge transfer complexes. The spectra in the range between 400 cm^{-1} and 4000 cm^{-1} of indole-I_2 and indole–TNF are shown here (Figure 3). The spectrum of indole-TCNQ is shown separately (Figure 4). The spectra of indole – chloranil and indole-TCNE are shown together (Figure 5).

Indole – I_2 (1:1) complex shows two Lorentzian envelopes and one Gaussian envelope in the whole infrared range (Figure 3). A Lorentzian at 3402 cm^{-1}, which can be ascribed to N-H stretching vibration. One Gaussian envelope containing a large number (about 13) of molecular vibrations is located 1428 cm^{-1} and it is very strong with 93.5% absorption. There is one more Lorentzian envelope around 749 cm^{-1} containing about 6 to 7 vibrations. The Lorentzian line shape shows strong electron-phonon coupling and Gaussian shows free electron scattering. Band assignment is carried out (Table 1).

Indole – TNF shows almost similar spectrum to that of indole-I_2 and is therefore, taken on the same figure i.e. figure 3. Two Lorentzian envelopes are situated around 3420 cm^{-1} and 763 cm^{-1}. One Gaussian is found located around 1354 cm^{-1} and shows about 98% absorption and contain 11-12 molecular vibrations. Band assignments are summarized (Table 1).

Indole-TCNQ spectrum is somewhat different (Figure 4) and shows all three pronounced Lorentzian situated at 3402 cm^{-1}, 1428 cm^{-1} and 749 cm^{-1}. Moreover, there are many gap modes within the region of featureless absorption, i.e. between 3400 cm^{-1} and 1600 cm^{-1}. These are donor levels stabilized between the valence and conduction bands within the forbidden gap region. Absence of any Gaussian shows that electron-phonon resonance is very pronounced and the electrons are strongly localized by phonon drag. There are resonance-anti-resonance spikes in the frequency interval between 1200 $cm^{-1}$and 900 cm^{-1}. This shows contribution of the real part of dielectric constant, which was dispersion shape, and the sample is almost transmitting in this range. It also reveals the formation of electron-hole pairs across a small band gap. Band assignment is carried out (Table 1).

Next is indole-DDQ (Figure 4b). It shows two Gaussians around 3207 cm^{-1} and 1455 cm^{-1}. The high frequency Gaussian is sharp and low frequency Gaussian is broad. The featureless absorption is found in the range between 3200 cm^{-1} and 2000 cm^{-1} having a strong donor level at 2267 cm^{-1}. Band assignments have been carried out (Table 2).

Indole-TCNE shows all three Gaussian envelopes showing delocalization of charge carriers (Figure 4). There are two strong local phonon modes one at 3275 cm^{-1} and the other at 2234 cm^{-1} within the region of featureless absorption. These are nothing but stabilizations of donor levels. The three Gaussians are centered around 3500 cm^{-1}, 1428 cm^{-1} and 763 cm^{-1}. It is recently found that the large damping coefficients leads to energy transfer from molecular vibrations to electronic motions and thus, electrons gain kinetic energy to be free and give rise to free electronic Gaussian (A.T. Oza [7]). Here also there are resonance-anti-resonance spikes between 1200 cm^{-1} and 900 cm^{-1} as in indole-TCNQ and interpretation is the same. Band assignments are carried out (Table 2).

Indole-chloranil also shows all the three Gaussian envelopes as in indole-TCNE and the spectrum is take in the same figure i.e. figure 5. Here N-H group of indole interacts strongly with C-Cl group of chloranil and there is possibility of hetero-polymerization proceeding through the charge transfer interaction. The spectrum seems to be that of a heteropolymer or a substituted compound. Featureless absorption can be extended from about 1850 cm^{-1} to 500 cm^{-1} along background absorption. This reveals that it is true that the formation of a Gaussian is the first step towards suppression of a Peierls transition and free charge density wave from a potential barrier to face only a small pinning gap due to commensurability with the lattice. Band assignments are carried out (Table 2).

The full width at half maximum of either a Lorentzian or a Gaussian are related with the electron-phonon coupling constant and are summarized here (Table 3). All the five iodole complexes studied here obey $a h\nu = B(h\nu - E_g)^{3/2}$ relation for forbidden direct transition across the Peierls gap in the featureless absorption region (Figures 6 and 7). The featureless Gaussian at 3500 cm^{-1} for indole-chloranil and indole-TCNE are fitted here revealing straight lines in Ln A vs $(K-K_0)^2$ plot (Figure 8). Other indole complexes show the Lorentzian line-shape at about this wave number. Ln σ vs n is the optical conductivity and n is of coupled vibrations is plotted (Figure 9).

Conclusion

Here for the first time in organic semiconductors mixed Lorentzian and Gaussian envelopes are found even when the donor (indole) is kept same. Gaussian is the first step towards suppression of Peierls transition. Indole-chloranil is extreme in which two Gaussian bands ride over a featureless background, which is the extension of a forbidden direct transition down to 500 cm^{-1}(0.0625 eV).

References

1. P.A. Lane, M. Liess, X. We, J. Portee, J. Shinar, A.J. Franta and Z.V. Vardony, Chem. Phys. (Netherlands) **227,** 57 (1968)
2. Y.A. Stardup, E.M. Hinzman, Vu. A. Khaftanera and J. Olejniczak, Theor. Exp. Chem., (USA) **33**, 95 (1997)
3. T.J. Savenge, E. Moons, G.K. Boschloo, A. Croseus and J.J. Schoolam, Phys. Rev. **B55**, 9685 (1997)
4. H. Tachibara, T. Kawai, G.K. Mertger, Zong Kyukuon and M.P. Caver, Synth. Metals **84**, 420 (1997)
5. R. Wojerechowski, J. Ulansf, M. Krydjewski, A. Tracz and J.K. Jeszka, Synth. Metals **94**, 27 (1998)
6. M. Rasu and G.J. Rasu, Appl. Surface Sci. (Netherlands) **12E**, 246 (1998)
7. A.T. Oza, Canad. J. Phys. **80**, 1175 (2002)

Table - 1: Band assignments in the IR spectra of indole complexes

Indole –I_2		**Indole –TNF**		**Indole –TCNQ**	
Wave No. (cm^{-1})	**Band assign**	**Wave No. (cm^{-1})**	**Band assign**	**Wave No. (cm^{-1})**	**Band assign**
3402.24	ν_{N-H} stretching	3449.25	ν_{N-H} stretching	3402.24	ν_{N-H} stretching
1696.27	δ_{N-H} stretching	3382.09	δ_{C-H} bending symmetric	3140.30	$\nu_{C=H}$ stretching
1636.82	$\nu_{C=N}$ stretching	3106.72	δ_{C-H} bending asymmetric	3052.99	$\nu_{C=H}$ stretching
1575.37	$\nu_{c=c}$ stretching	1743.28	$\nu_{c=O}$ stretching	28.78.36	New Band
1541.79	δ_{N-H} bending	1622.39	ν_{C-C} ring	2173.13	$\nu_{C=N}$ stretching
1461.19	δ_{C-H} bending asymmetric	1535.07	$\nu_{C=N}$ stretching	2126.12	$\nu_{C=C}$ ring
1427.61	δ_{C-H} bending symmetric	1401.19	$\nu_{c=O}$ stretching	1635.82	$\nu_{C=C}$ ring
1320.15	$\nu_{c=c}$ stretching	1353.73	$\nu_{C=C}$ ring	1508.21	δ_{N-H} bending
1219.40	$\nu_{C=N}$ 1158.96stretching	1246.27	$\nu_{C=N}$ stretching out plane	1461.19	δ_{C-H} bending asymmetric
1158.96	ν_{C-C} ring	1205.97	$\nu_{C=N}$ stretching in plane	1427.61	δ_{C-H} bending symmetric
1111.94	$\nu_{C=N}$ stretching	1085.07	π_{C-H} Wagging	1347.01	$\nu_{C=N}$ stretching
923.88	π_{C-H} Wagging	923.88	π_{C-H} Wagging	1246.27	$\nu_{C=C}$ ring
897.01	π_{C-H} Wagging	762.29	π_{C-H} Rocking	111.94	$\nu_{C=C}$ ring

Table - 2: Band assignments in IR spectra of indole-complexes

Indole –DDQ		**Indole –TCNE**		**Indole –Chloranil**	
Wave No. (cm^{-1})	**Band assign**	**Wave No. (cm^{-1})**	**Band assign**	**Wave No. (cm^{-1})**	**Band assign**
3207.46	ν_{C-H} stretching	3274.63	ν_{N-H} stretching	3476.12	ν_{N-H} stretching
2267.16	$\nu_{C=N}$ stretching	2233.58	$\nu_{C=N}$ stretching	1682.74	$\nu_{C=O}$ stretching
1682.84	$\nu_{C=C}$ ring	1608.96	$\nu_{C=C}$ ring	1635.82	δ_{C-N} bending out plane
1561.94	δ_{N-H} bending	1595.52	$\nu_{C=C}$ ring	1575.37	δ_{C-N} bending in plane
1273.13	δ_{C-H} bending symmetric	1608.96	$\nu_{C=C}$ ring	1454.48	ν_{C-H} bending
1192.54	$\nu_{c=O}$ stretching	1521.64	δ_{N-H} bending	1219.40	$\nu_{C=C}$ ring
897.01	π_{C-H} Wagging	1488.06	$\delta_{C=H}$ bending	1152.24	$\nu_{C=C}$ ring
742.54	π_{C-H} Rocking	1427.61	δ_{C-H} bending asymmetric	850.00	$\nu_{C=Cl}$ stretching
614.93	π_{C-H} Rocking	1353.73	ν_{C-C} stretching	762.69	$\nu_{C=Cl}$ stretching
		1246.27	ν_{C-C} stretching	688.81	π_{C-H} Rocking
		1132.09	ν_{C-C} stretching	614.93	π_{C-H} Rocking
		1031.34	ν_{C-C} stretching		
		856.72	π_{C-H} Rocking		
		762.69	π_{C-H} Rocking		

Table - 3: Electronic absorption envelope for the five charge transfer complexes of indole

Name	**Full-width at half maximum (Δk) cm^{-1}**	**Full-width at half maximum (Δk) cm^{-1}**	**Full-width at half maximum (Δk) cm^{-1}**
Indole-I_2	230 (L)	600(G)	400 (L)
Indole-TNF	130 (L)	650 (G)	400 (L)
Indole-TCNQ	190 (L)	530 (L)	200 (L)
Indole-TCNE	120 (G)	530 (G)	660 (G)
Indole-chloranil	300 (G)	520 (G)	480 (G)
Indole-DDQ	500 (G)	600 (G)	600 (G)

G means Gaussian and L means Lorentzian

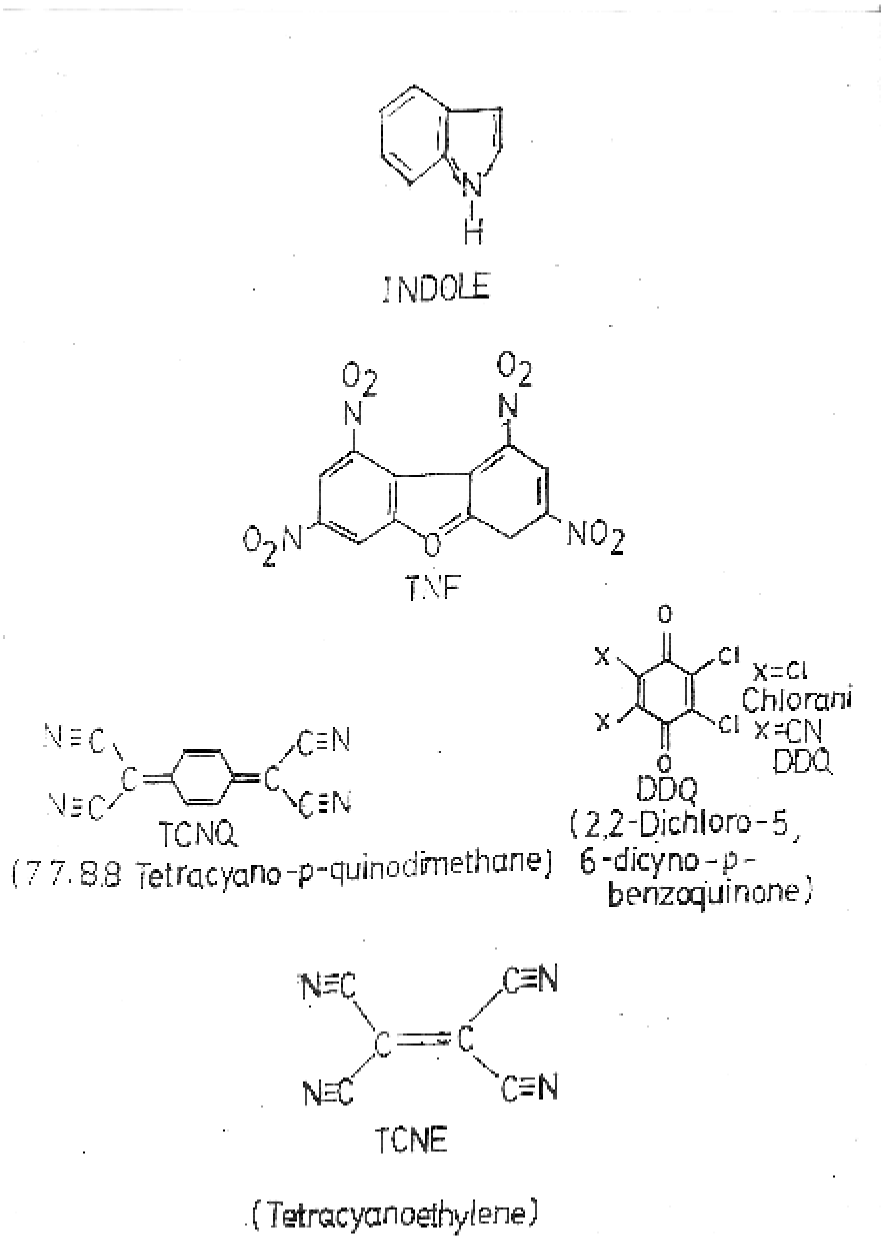

Figure-1: Moleculer structures of indole and organic acceptors

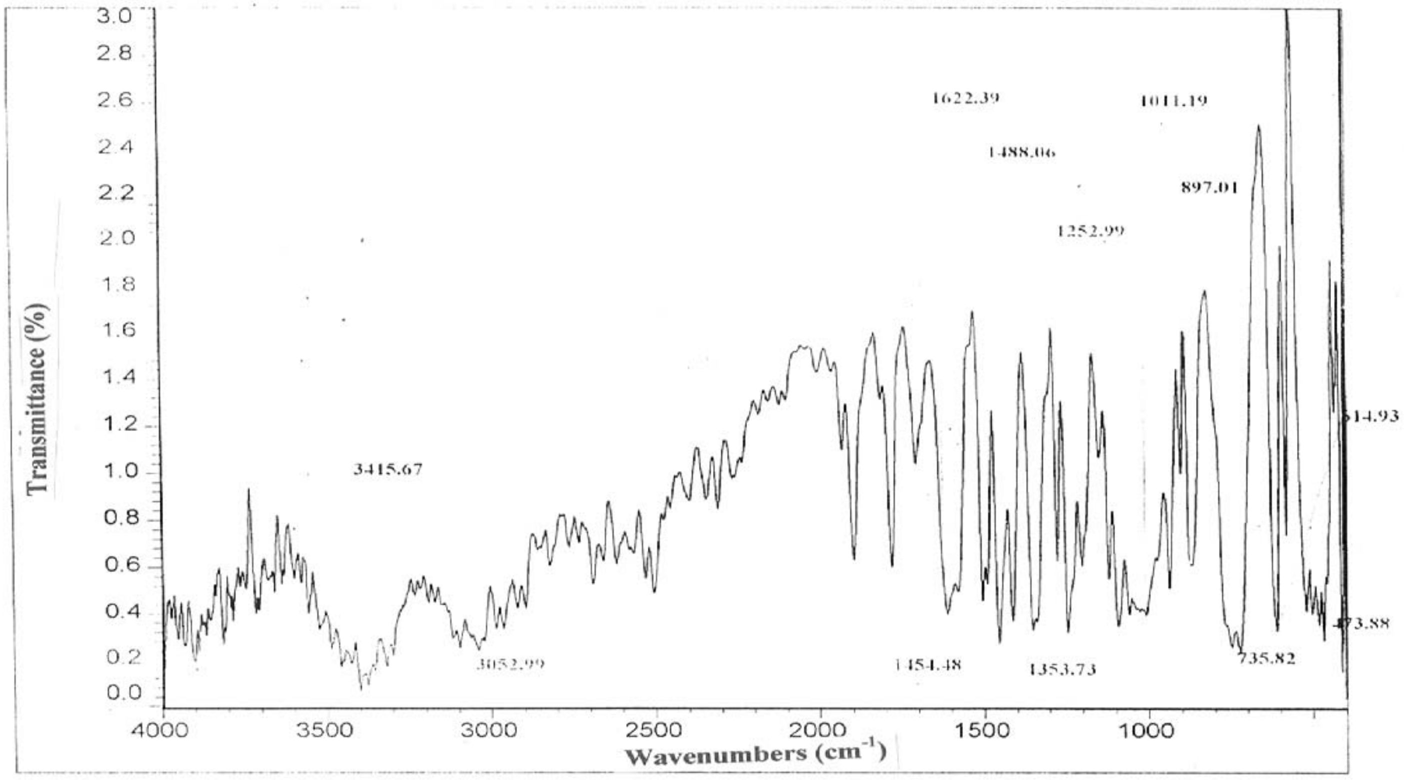

Figure 2 Infrared spectrum of indole

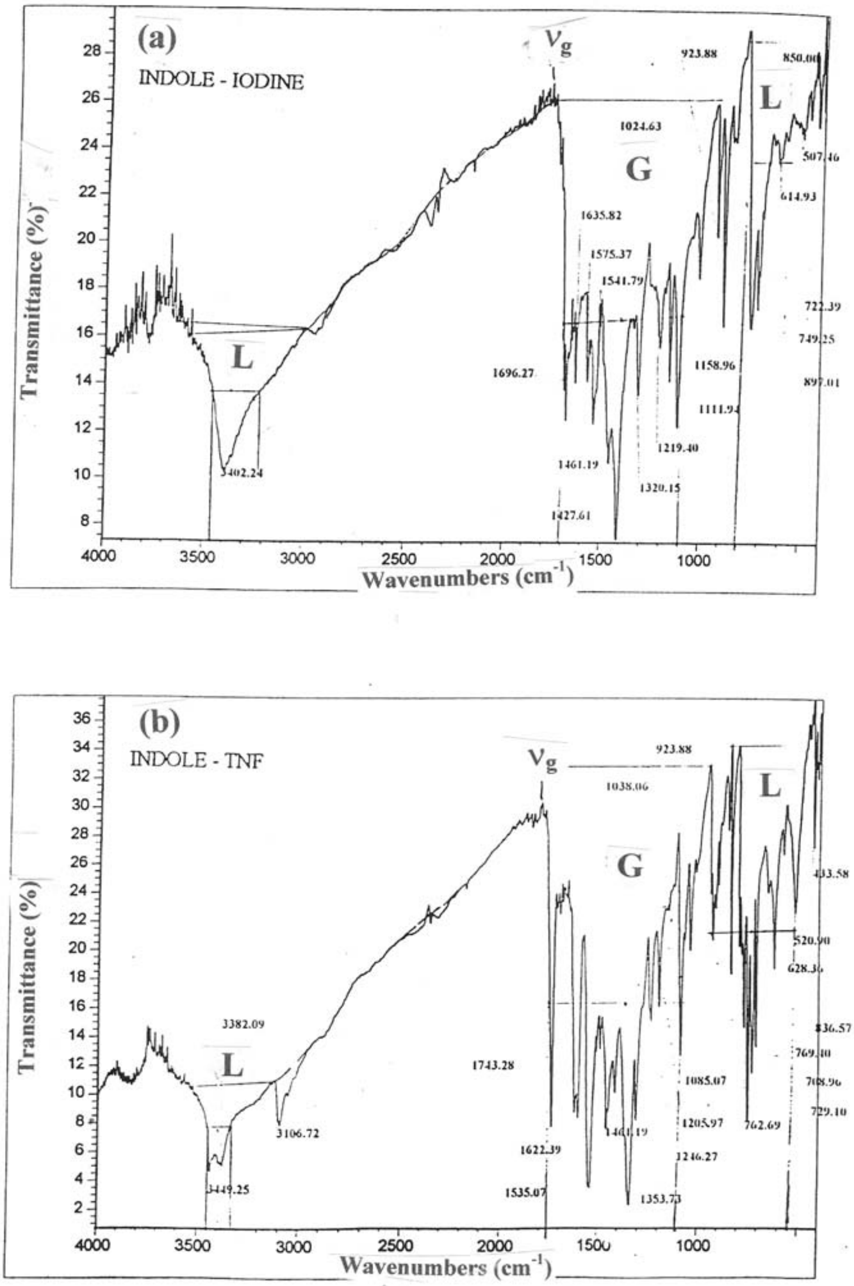

Figure 3 Infrared spectra of
(a) Indole-I$_2$
(b) Indole-TNF

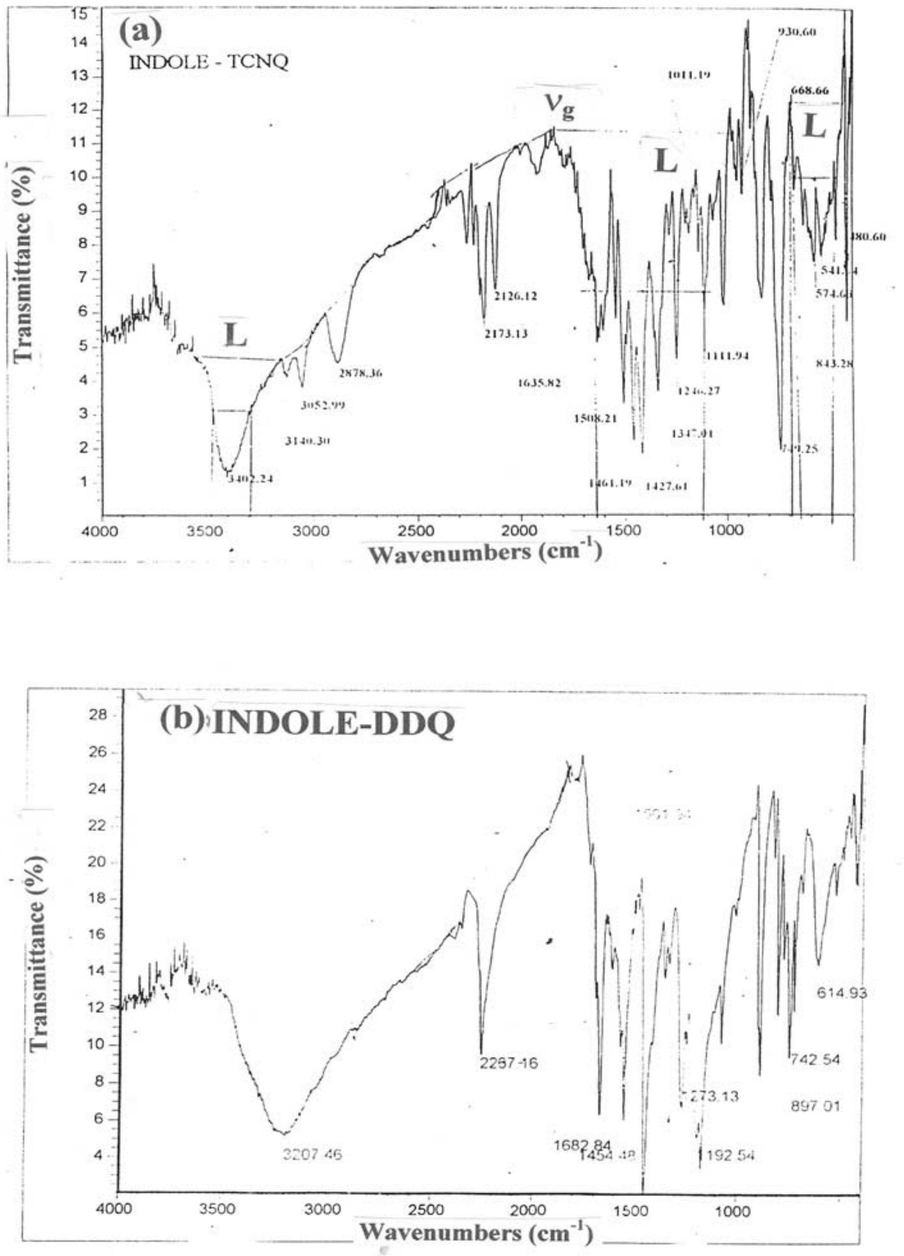

Figure 4 Infrared spectra of
(a) Indole-TCNQ
(b) Indole-DDQ

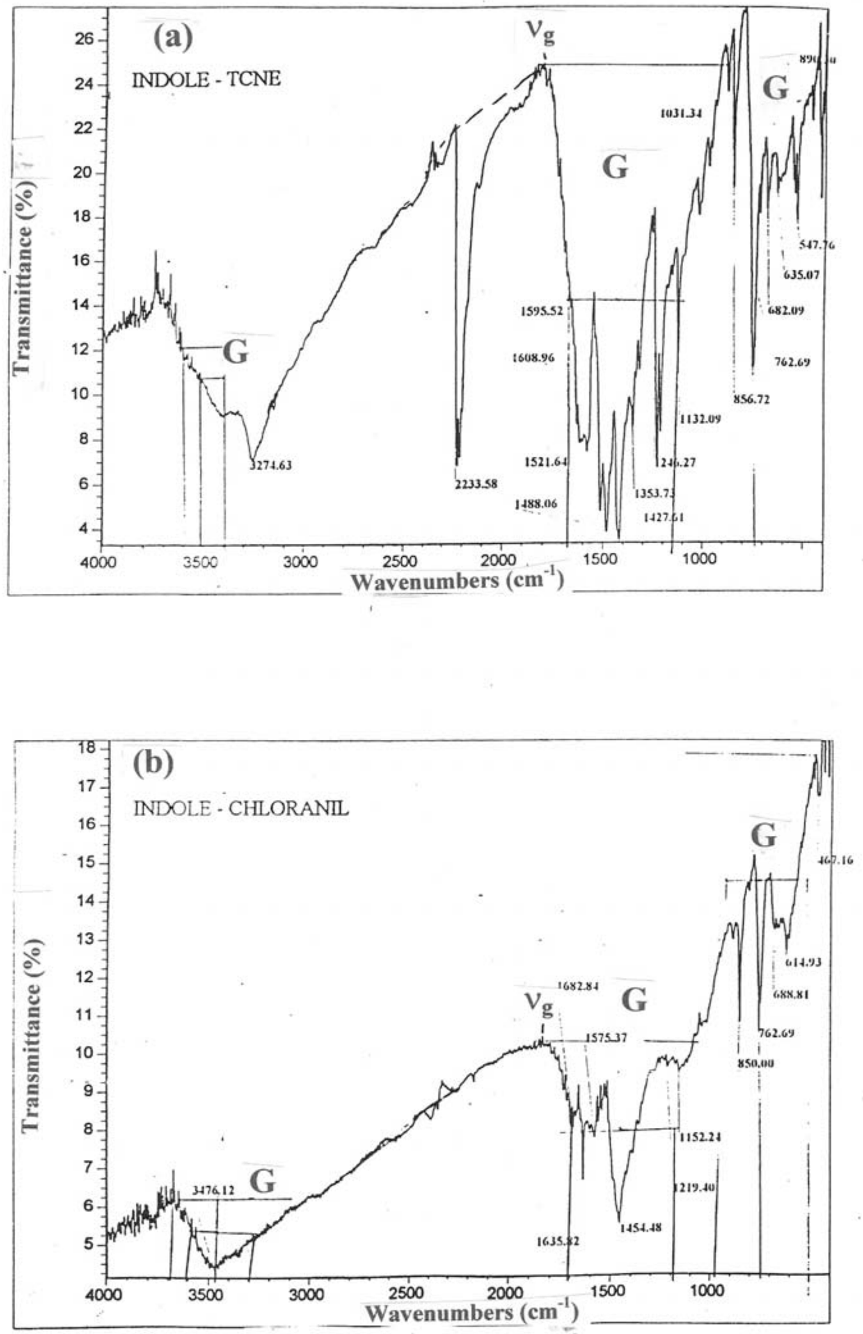

Figure 5 Infreared spectra of
(a) Indole-TCNF
(b) Indole-chloranil

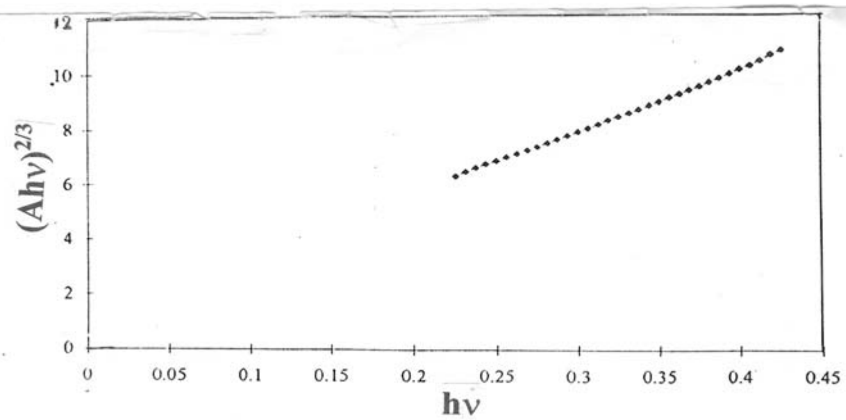

$(Ah\nu)^{2/3}$ vs hν plot for Indole-I_2

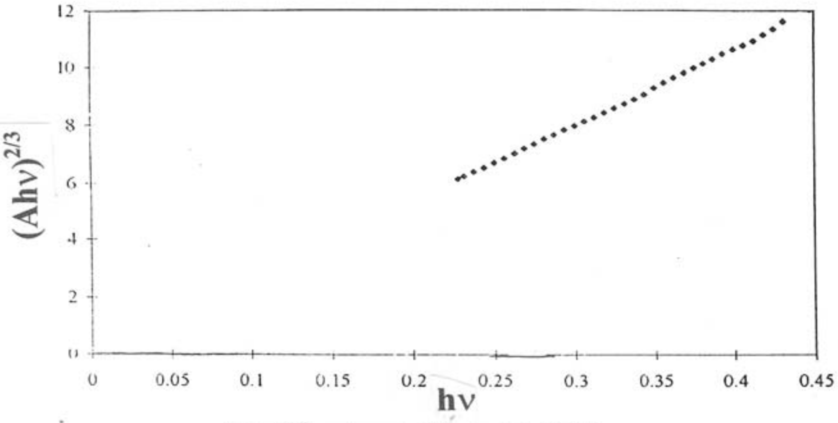

$(Ah\nu)^{2/3}$ vs hν plot for Indole-TNF

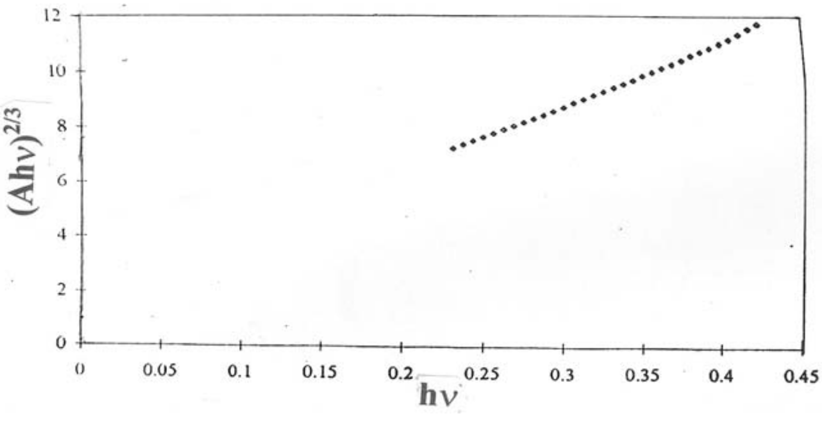

$(Ah\nu)^{2/3}$ vs hν plot for Indole-TCNQ

Figure - 6: $(Ah\nu)^{2/3}$ vs hν plot for indole – I_2, Indole-TNF and Indole-TCNQ

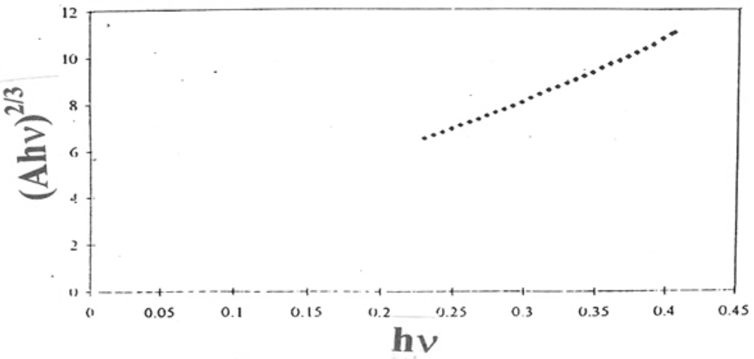

$(Ah\nu)^{2/3}$ vs hν plot for Indole-Chloranil

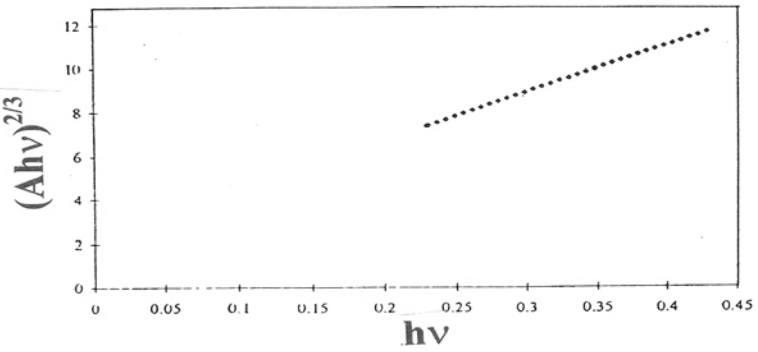

$(Ah\nu)^{2/3}$ vs hν plot for Indole-TCNE

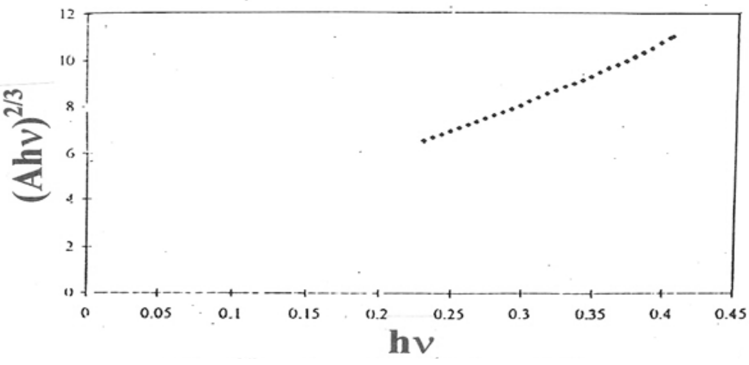

$(Ah\nu)^{2/3}$ vs hν plot for Indole-DDQ

Figure - 7: $(Ah\nu)^{2/3}$ vs hν plot for Indole–chloranil, Indole-TCNE and Indole-DDQ

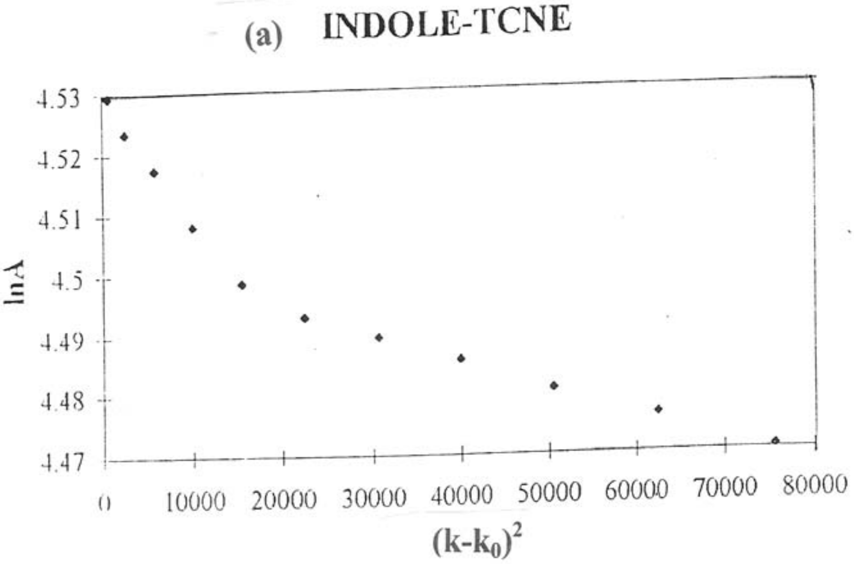
(a) INDOLE-TCNE

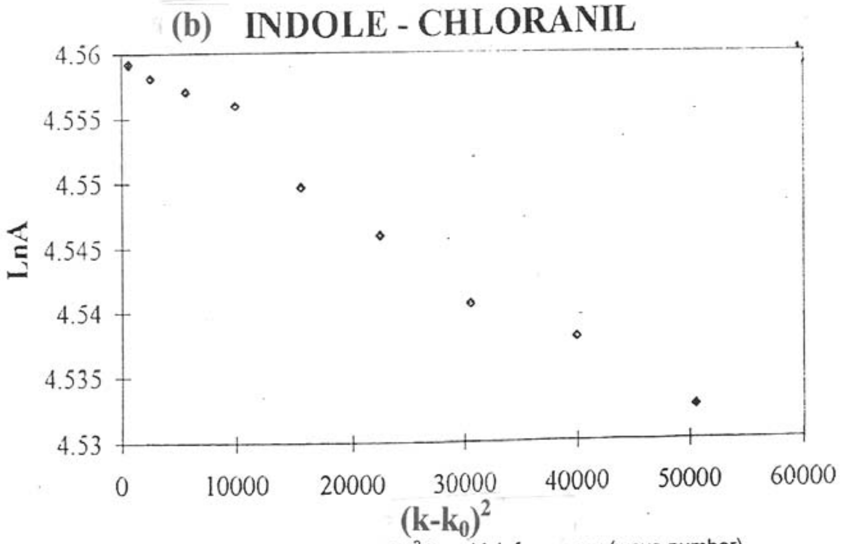
(b) INDOLE - CHLORANIL

Figure 8 Ln A vs $(K - K_o)^2$ for a high frequency (wave number) Gaussian for
(a) indole-TCNE
(b) indole-chloranil

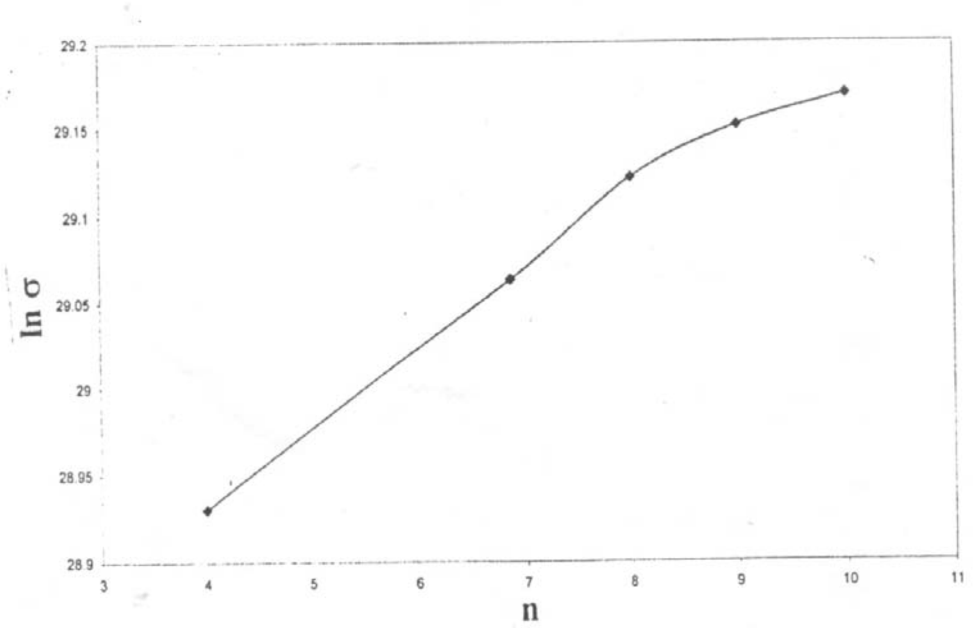

Figure - 9: Ln σ vs 'n' for central peaks in absorption in the infrared spectra

'Prajna' - Journal of Pure & Applied Sciences, 16 (2008) 165-171

GROWTH AND X-RAY DIFFRACTION STUDIES OF ZnTe CRYSTALS GROWN BY PHYSICAL VAPOR TRANSPORT TECHNIQUE

K.D. Patel, J.R. Gandhi, G.K. Solanki and S.G. Patel
Department of Physics, Sardar Patel University, Vallabh Vidyanagar - 388 120

Abstract

ZnTe is a wide band gap compound semiconductor and has attracted many researchers due to its interesting luminescence properties. In this paper authors present their investigations on growth of ZnTe crystals by Physical Vapor Transport technique. The structural characterization was accomplished by X-Ray diffraction (XRD) studies and it was found to be cubic. Lattice parameters, volume and X-ray density have been measured for the grown crystals. The particle sizes for number of reflections have been calculated using Scherrer's formula.

Keywords: ZnTe crystal, physical vapor transport, XRD, EDAX

Introduction

The wide band gap II-VI compounds are the promising materials for their use in many optoelectronic applications. ZnTe having a direct band gap of 2.26 eV at room temperature is one of the most important among them. Due to its wide band gap, it can effectively emit light of 540 nm. This is the promising material for its application in pure Light Emitting Diode and Laser Diode (Wu-Yih Uen et al. [1], Nishito et al. [2]). It also has a potential application as an IR optics, crystal pieces for vacuum deposition and window material for CdTe based solar cells (Ishizaki et al. [3], Meyers [4]). Because of its large electro-optic coefficient among most of the compound semiconductors it can be used as a terahertz detector (T. Asahai et al. [5], Hewitt & Zhang [6], M. Herrmann et al. [7], Takahashi et al. [8]). ZnTe crystals are non-toxic, moisture resistant, and they conserve working parameters after gamma irradiation up to 107 Rad and continuous heating up to 400 K, therefore, they are widely used for multipurpose ionizing radiation detectors of Scintillator-sillicon photodiode type to be used for radiation monitoring, medical and technical tomography, X-ray medical devices, non destructive testing systems and custom inspection, spectrometry of alpha and beta radiation as well as soft X-rays ([9], [10]). Crystallization from the vapor phase has an advantage over a melt growth, particularly for II-VI compounds as they have high melting temperature which can make the melt growth process difficult to be handled. Physical vapor transport acts as a purification process because of difference in vapor pressure of native elements and impurities (Su et al. [11], Muller et al. [12]). Though to increase the transport rate and to reduce the growth temperature, the transporting agent (I_2) can be employed in case of Chemical Vapor Transport technique (Hartmann [13]), but the disadvantage is the high level of unintentional doping of transporting agent (I_2) (Catano et al. [14], Koyama et al. [15], Mimoto et al. [16]).

To increase the life time and to improve the performance of the electro optical-devices based on ZnTe compound it is necessary to improve the basic properties of the grown compound. Here the authors present their work on growth and structural characterization of ZnTe crystals grown by PVT technique.

Experimental

ZnTe crystals have been grown by a Physical Vapor Transport Technique (PVT). A 10 gram of mixture of Zn (Purity: 99.99%, Make: Fluka Chemi) and Te (Purity: 99.99%, Make: Aldrich, USA) were taken in stoichiometric proportion in a quartz ampoule for a charge preparation. This ampoule was evacuated at the pressure of 10^{-5} Torr and than sealed. This sealed ampoule was placed in a dual zone furnace of constant reaction temperature to obtain a charge of the material. During the synthesis of the charge, temperature was slowly increased up to 1023 K at the rate of 10 K/hr. The ampoule was kept at this final temperature for 4 days. Then the furnace was slowly cooled at the rate of 20 K/hr and brought to room temperature. The resulting orange yellowish charge was obtained in the ampoule. This charge was crushed and transferred to other quartz ampoule. This ampoule was also evacuated at a pressure of 10^{-5} Torr and placed in a two zone horizontal furnace for 10 days with a temperature gradient of 50 K between the source zone and growth zone. After that, furnace was cooled down to room temperature at a rate of 10 K/hr. Thus the material has been found to be converted into the form of crystals at the cooler end of the ampoule. The grown crystals of dark red color as shown in Figure-1were collected after breaking the ampoule.

To optimize the temperature gradient of 50 K between the source zone and the growth zone, several runs were taken. The process was initially started with the temperature gradient of 100 K between both the zones. This gradient was than reduced to 10 K after investigating the results. Thus finally after six runs, the gradient was set to 50 K that resulted in to formation of small crystals. The selection of upper temperature and the gradient of temperature between the growth and source zone were made on the basis of an extensive literature survey. All six runs with their corresponding temperatures are tabulated in the Table -1. This optimized temperature gradient is useful in maintaining the partial vapor pressure of the constituent elements inside the closed volume of ampoule so that a reaction in vapor phase occurs and at a suitable surface site of inner walls of the ampoule, nucleation proceed to simulate further growth of crystals.

For X-ray diffraction (XRD) work, several small crystals were finely ground with the help of an agate mortar and filtered through 106-micron sieve to obtain grains of nearly equal size. The X-ray diffractograms were taken with Philips X-ray diffrractometer (model: PW1820) employing CuKα radiation. The energy dispersive analysis by X-Ray (EDAX) has been carried out at SICART-Vallabh Vidyanagar, for determination of the stoichiometric proportion of Zn and Te.

Results and Discussion

The crystals of ZnTe were grown by Physical Vapor Transport (PVT) Technique. The X-ray diffractogram obtained for ZnTe is shown in Figure-2 The sharp patterns indicate the good crystalline structure of the grown compound. The values of lattice parameters a, b and c, unit cell volume (V) and X-ray density (ρ) determined from x-ray diffractogram are presented in table – 2 which are very well matched with the values of JCPDS data. The crystal structure is found to be cubic. The X-ray data for ZnSe was used for estimation of particle size using Scherrer's formula given by-

$$t = \frac{K\lambda}{\beta_{2\theta} \cos\theta_0}$$

where t is the crystallite thickness as measured perpendicular to the reflecting plane, *K* is the Scherrer constant whose value is taken to be unity assuming the particles to be spherical, and λ is the wavelength of X-ray radiation, $\beta_{2\theta}$ the half intensity measured in radians and θ_0 is the Bragg angle. The (h k l) values corresponding to prominent reflection d-values, half width, peak intensities and particle size for ZnTe crystals are shown in Table - 3.

Conslusion

Crystals of ZnTe were grown by Physical Vapor Transport (PVT) Technique. The temperature difference between the source zone and the growth zone has been varied from 100 K to 50 K and it has been found that at 50 K difference in these temperatures resulted in to small, dark red crystals of ZnTe. The EDAX study gives a confirmation that crystals are nearer to stoichiomatrically perfect one. The X-ray diffraction analysis confirms a cubic structure of the as grown crystals and all structural parameters that have been determined are in good agreement with the standard JCPDS.

Initial Material: ZnTe (10 gram)

Run No.	Ampoule Dimensions			Temperature Distribution			Growth Time	Result
	OD (mm)	ID (mm)	LENGTH (mm)	Source Zone (K)	Growth Zone (K)	Diff. (K)	(Hour)	
1	25	22	250	1173	1073	100	168	Ingots
2	25	22	250	1173	1083	90	168	Ingots
3	25	22	250	1173	1093	80	168	Ingots
4	25	22	250	1173	1103	70	168	Ingots
5	25	22	250	1173	1113	60	168	Ingots
6	25	22	250	1173	1123	50	168	Crystals of **4mm×4mm×3mm** Size(App.)

Table - 1: Temperature distribution of various runs taken for crystal growth

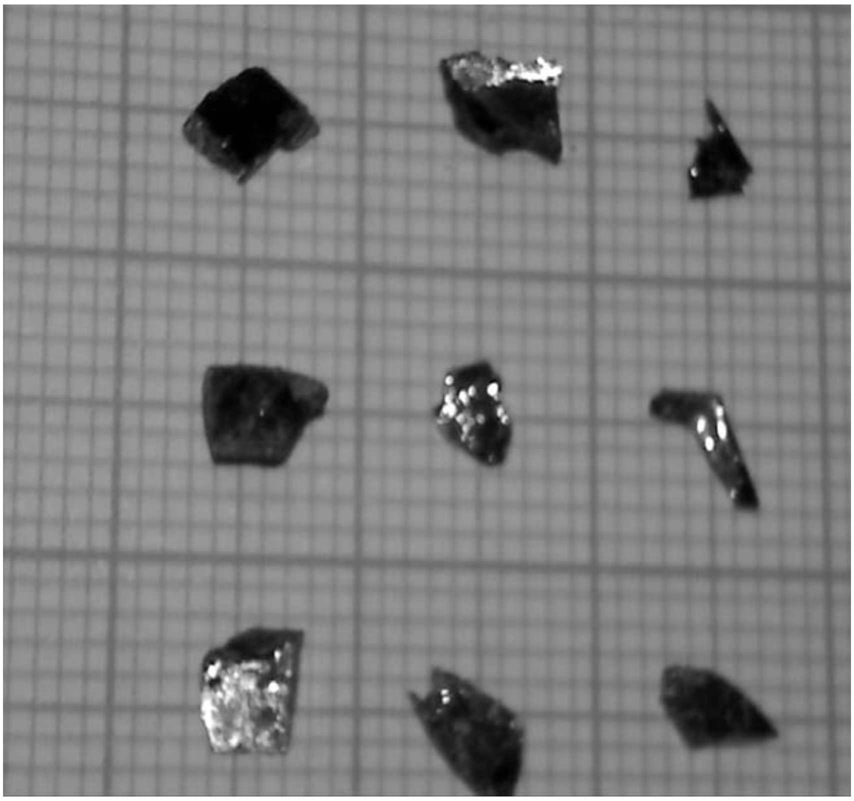

Figure -1: Photograph of as grown crystals of ZnTe

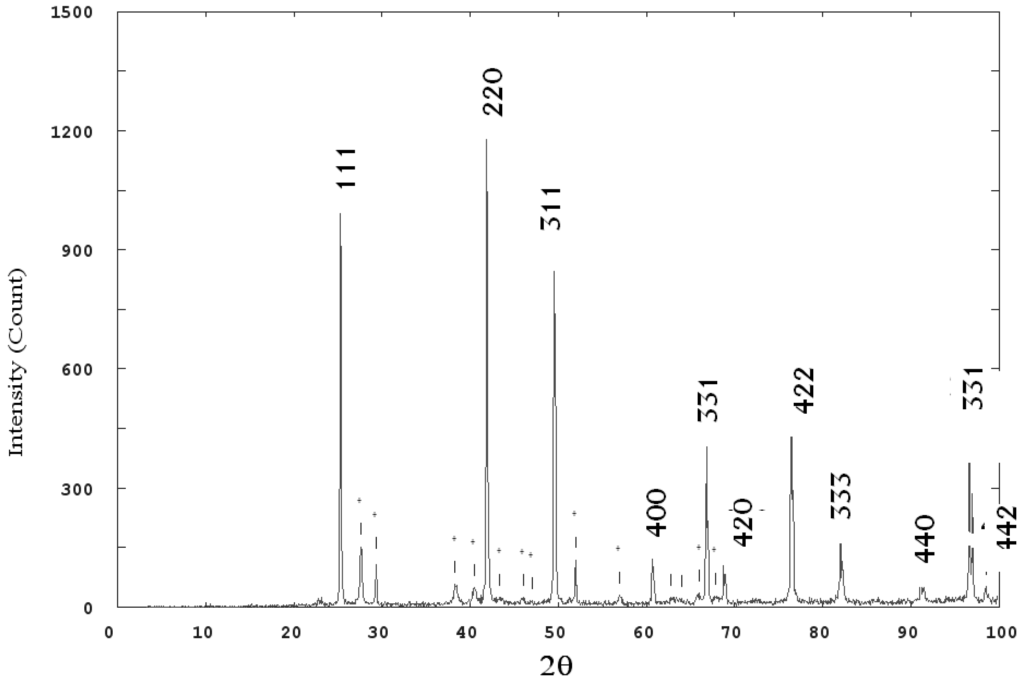

Figure -2: X-ray diffractogram of ZnTe crystals

Parameters	JCPDS data (PDF No. 150746)	Present Work
a =b=c (Å)	6.1026	6.0975
Unit cell Volume V $(Å)^3$	227.27	226.70
X-ray density ρ (gm. cm^{-3})	5.64	5.65

Table -2: Crystallographic data of ZnTe crystals grown using PVT technique

(h k l)	d-spacing (Å)	Peak Width (°2θ)	Peak Intensity (Counts/second)	Particle size (Å)
(1 1 1)	3.5234	0.21	1281.2	387.86
(2 2 0)	2.1573	0.21	1473.61	405.19
(3 1 1)	1.8402	0.28	1019.3	312.56
(4 0 0)	1.5263	0.35	138.28	263.04
(4 2 2)	1.2456	0.42	549.37	240.76
(3 3 3)	1.1748	0.28	232.79	375.67
(4 4 0)	1.0790	0.21	106.06	540.41
(5 3 1)	1.0315	0.21	511.37	569.07
(4 4 2)	1.0171	0.21	41.03	579.47

Table - 3: X-ray diffraction data for ZnTe crystals grown by PVT technique

Reference

1. Wu-Yih Uen, Shium-Yi Chou, Hwa-Yuhshin Sen-Mao Liao, Shan-Ming Lan Material Science and Enaginering, **B106,** 27-32 (2004)
2. Nishito M., Hayashida K., Guo Q., Ogawa H. Applied Surface Science, **223,** 169-170 (2001)
3. Takahicro Ishizaki, Nagahiro Saito, Osamu Takai, SAhuichi Asakwra, Kaori Goto, Akio Fuwa Elactrochimica Acta **50**, 3509-3516 (2005)
4. PVS Meyers, Proceedings of 7th Commission European Communities Conference on Photovoltaic Solar Energy, Reidel, Dordrecht, Netherlands, p. 1121 (1986)
5. Ashai T., Yabe T., Sato K., Arakawa A. Journal of Alloys and compounds **371**, 2-5 (2004)
6. Q. Wu. Hewitt, X.C. Zhang Applied Physics Letters **77**, 176 (2000)
7. Herrmann M. , Sakai K., Tani M., Fukasawa R. Proceedings of 8th International Conference on Terahertz Electronics p.185 (2000)
8. Takahash H., Hosoda M. Applied Physics Letters **77**, 1085 (2000)
9. Marketech International Inc.www.mkt-intl.com
10. Cardley Crystals Inc.www.cardley-crystals.com
11. Ching –Hua Su and Yi-Gao Sha, Current Topics in Crystal Growth Res. (NASA-CR-204722) **2** (1995)
12. Lauck R. Muller-Vogt G. & Wenchi W., Journal of Crystal Growth **74**, 520 (1986)

13. Hartmaan H. Journal of Crystal Growth **42**, 144 (1977)

14. Catano A. & Kum Z.K. Journal of Crystal Growth **33**, 324 (1976)

15. Koyoma T., Yodo T., Aka H., Yamashita K. & Yamasakai T. Journal of Crystal Growrh **91**, 639 (1988)

16. Fujita S., Mimoto H., Takeba H. & Noguchi T. Journal of Crystal Growth **47**, 326 (1979)

'Prajna' - Journal of Pure & Applied Sciences, 16 (2008) 172-177

THERMOELECTRIC POWER OF TUNGSTEN DISELENIDE GROWN BY A DIRECT VAPOUR TRANSPORT TECHNIQUE

Deepa Makhija, Mayur Patel, M.S. Jani and P.R. Jakhmola
Department of Physics, Sardar Patel University, Vallabh Vidyanagar - 388 120

Abstract

Single crystals of tungsten diselenide have been grown by direct vapour transport technique using a two zone furnace. The elemental composition and structure of grown crystals were confirmed using the energy dispersive analysis of X-rays (EDAX) and XRD. The Hall effect and thermopower measurements on these as grown crystals reveal that the crystals are p-type in nature. The relation between the thermoelectric power (TEP) and the concentration of charge carriers was also investigated along with their effective mass and effective density of states.

Introduction

In recent years, much attention has been given to various transition metal dichalcogenides (TMDCs) because of their interesting semiconducting characteristics [1]. These layer type TMDCs are important solids since they display a whole spectrum of electronic properties covering semiconductors, metals, insulators and superconductors [2-4]. Such materials have been used as solid lubricants [5], schottky junctions [6], photovoltaic/photocatalytic solar energy converters [7] and catalysts in many industrial applications [8].

Looking to such diverse applications of TMDCs, we have chosen to study tungsten diselenide, an anisotropic semiconducting material, of this group. A large number of studies of WSe_2 have been reported in the literature. Successful growth of single crystals of WSe_2 has been reported by R. Kershaw [9] for the measurements of photoelectronic and electrical properties. Brixner [10] and Hicks [11] measured the galvanomagnetic properties of polycrystalline sintered bars of WSe_2 and they found that anisotropy of the material is largely governed by their structure.

In general, the thermoelectric effect offers a distinctive advantage over other methods for determining carrier concentration, even for low mobility materials [12]. Further, the study of thermoelectric power provides an independent method for determining the sign of charge carriers, density of the states and the position of Fermi level in the semiconductors [11].

The present work reports the electrical transport properties of tungsten diselenide crystals evaluated from the thermoelectric power measurements as a function of temperature and room temperature Hall effect measurements. The values of Fermi energy (E_F) and the scattering constants have been calculated from thermoelectric power measurements. Also, using the relationship between the thermoelectric power and the carrier concentration (obtained from Hall effect measurements), the effective mass of the majority charge carriers (m_h*) in WSe_2 crystals and density of states have been estimated. These informations are helpful in understanding the scattering mechanisms in this semiconducting compound.

Experimental

The single crystals of tungsten diselenide were grown by direct vapour transport technique [13, 14] using a two zone furnace. The compound was prepared from the stoichiometric mixture of W (99.99 % pure) and Se (99.9 % pure). The total charge used in this experiment was about 10 gms. The ampoule containing the stoichiometric mixture as mentioned above was evacuated at a pressure of 10^{-5} Torr. It was shaken well for proper mixing of the powder. The ampoule was then placed in a two zone horizontal furnace. The source zone of the furnace was maintained at 1080^0C while the growth zone was kept at 1060^0C. The temperature inside the furnace was increased slowly at the rate of 50^0C/hr, till it attained the required temperatures. This slow heating was necessary to avoid any possibility of explosion due to the strongly exothermic reaction between the elements. The ampoule was kept in the furnace for seven days and thereafter the furnace was allowed to cool down slowly to room temperature. The ampoule containing the crystals was broken carefully and crystals of WSe_2 were taken out in the form of thin platelets having opaque appearance with perfectly shining surfaces.

The chemical and structural characterizations of the grown crystals were done by Energy Dispersive Analysis of X-rays (EDAX) and X-ray diffraction (XRD) technique.

The Thermoelectric power measurements on the sample of WSe_2 having dimensions 6x5x0.03 mm^3 were carried out in the temperature range 323K to 393K. The TEP measurements were made by using the thermoelectric power set up developed in our laboratory. This experimental set up consists of two blocks viz. (i) sample holder with heaters with suitable pick up probes and (ii) Electronic circuits controlling temperature and temperature gradient across the sample. The crystals of WSe_2 were kept on a mica sheet base to facilitate obtaining two junctions at different temperatures. The temperature difference between the two junctions (ΔT) could be controlled by the temperature controller. This temperature difference was kept constant (10K) as the temperatures of both the junctions increased from 323K to 393K.

Results and Discussion

The crystals of WSe_2 grown in the present investigation were found in the form of thin platelets having opaque appearance with perfectly shining surfaces. From EDAX analysis, it is observed that the crystals possess near stoichiometric elemental composition and X-ray analysis showed that all crystals possess single phase of 2H structure.

The variation of thermoelectric power S of WSe_2 crystals as a function of temperature in the range 323K to 393K is shown in figure 1. The sign of thermoelectric power (TEP) is found to be positive over the entire temperature range. It is observed that the thermoelectric power increases with temperature, indicating the typical semiconducting behaviour of the tungsten diselenide crystals [15].

To analyze the temperature dependence of the thermoelectric power S of a p-type semiconductor, the expression given by Mohanchandra and Uchil [16] and Goldsmid H.J. [17] has been used. This is given as,

$$S = -\frac{k}{e}\left[A + \frac{E_F}{kT}\right]. \quad \ldots\ldots\ldots\ldots\ldots\ldots\ldots\ldots\ldots\ldots (1)$$

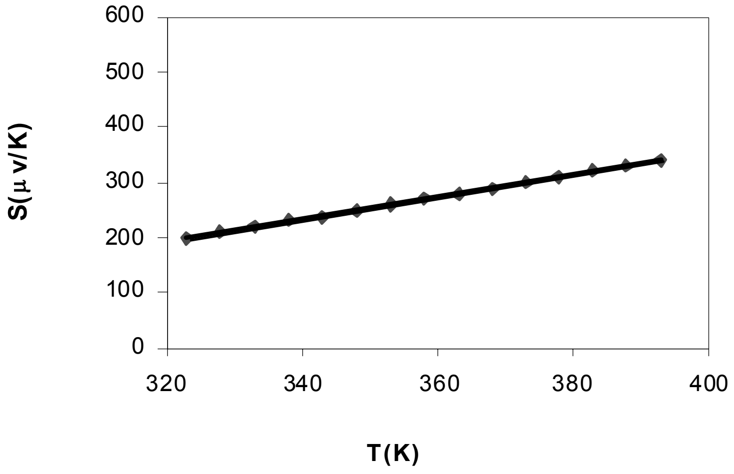

Fig. 1: Variation of thermoelectric power with temperature for WSe_2 single crystal in the temperature range 323K to 393K

where k is the Boltzmann constant, e is the electronic charge, $A = \left(\frac{5}{2} - s\right)$ is the constant that varies from 0 to 4 depending on the scattering process, *s* is the scattering parameter and E_F is the separation of the Fermi level from the top of the valance band.

The carrier concentration in the crystals essentially depends upon E_F. For a small temperature range, E_F can be considered as fairly constant and hence, from equation (1), if the thermoelectric power S can be plotted against reciprocal of temperature (T^{-1}), to give a straight line. Such a graph for present results is shown in figure 2. From the values of slope and intercept, E_F and A have been calculated and are found to be 0.254 eV and 1.2 respectively. The scattering parameter *s* comes out to be 1.3, which is close to 1.5, a value associated with the defect scattering [15, 18].

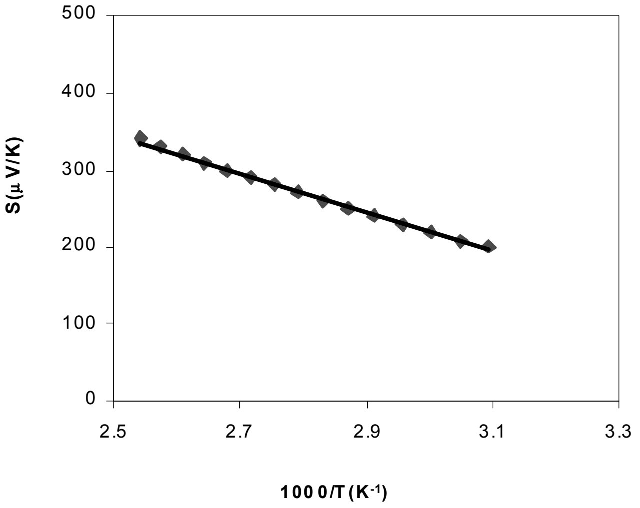

Fig. 2: Variation of thermoelectric power with inverse of temperature for WSe$_2$ single crystal in the temperature range 323K to 393K

The fairly constant value of E_F implies that the carrier concentration p is not substantially changing with temperature. Therefore, equation (1) can be expressed as

$$S = -\frac{k}{e}\left[A + \ln\left(\frac{N_A}{p}\right)\right] \text{ .... (3)}$$

where N_A is the effective density of states and is given by the relation

$$N_A = 2\left[\frac{2\pi m_h^* kT}{h^2}\right]^{\frac{3}{2}} \text{ . ...(4)}$$

where m_h^* is the effective mass of holes and *h* is the Plank's constant. Using the value of carrier concentration ($p=1.1 \times 10^{17}cm^{-3}$) obtained from Hall effect measurements, the effective density of states N_A can be calculated with the help of the formula [19],

$$p = N_A \exp\left(-\frac{E_F}{kT}\right). \qquad (5)$$

The value of effective density of state is found to be around $2.036\times10^{27}m^{-3}$. Substituting the value of effective density of states in equation (4), the effective mass of holes $m_h^*$was calculated and found to be around 1.66×10^{-27} kg.

Conclusion

The single crystals of WSe_2 grown by a direct vapour transport technique are found to be p-type semiconducting in nature. The value of scattering parameter is 1.3 which shows that the defect scattering dominates the charge transport mechanism in tungsten diselenide crystals.

References

1. Wilson J.A. and Yoffe A.D., Adv. Phys. **18**,193 (1969)
2. Lee P.A., Ed., Optical and electrical properties of layered semiconductors, D. Reidel Publ. Company, Dordrecht, Holland/Boston, USA (1976)
3. Levy, F., Ed., Intercalated layered materials, D. Reidel Publishing Company, Dordrecht/ Holland/Boston-USA (1979)
4. Tributsch H., Z. Naturforsch. **A32**, 972 (1977)
5. Subbarao C.V. and Sunandana C.S., in J.M. Honing and C.N. Rao (eds), Preparation and characterization of materials, Academic Press, London p. 269 (1981)
6. Spah R., Lux-Steiner M., Obergfell M., Bucher E. and Wagner S., Appl. Phys. Lett. **47**, 871 (1985)
7. Tributsch, J. Electrochem. Soc. **125**, 1086 (1978)
8. Weisser O. and Landa S., Sulphide Catalysts, their preparation and applications, Pergamon, Oxford (1973)
9. Kershaw R., Vlasse M., and Wold A., Inorg. Chem. **6**, 1599 (1967)
10. Brixner L.H., J. Inorg. Nucl. Chem., **22**, 257 (1962)
11. Hicks W.T., J. Electrochem. Soc. **6**, 1058 (1964)
12. Brixner L.H., J. Electrochem. Soc. **110**, 289 (1963)
13. Agarwal M.K., Patel P.D. and Gupta S.K., Journal of Crystal Growth **129**, 559 (1993)

14. Srivastava R. et al., J. Electrochem.Soc. **5(7)**, 537 (1989)

15. Solanki G.K., Gujarathi D.N., Deshpande M.P. Lakshminarayana D. and Agrawal M.K., Cryst. Res. Technology **43(2)**, 179 (2008)

16. Mahanchandra K.P. and Uchil J., Thin Solid Films, **305**,124 (1997)

17. Goldsmid H.J., Application in Thermoelectricity, Methuen Monograph, London (1950)

18. Perluzzo G., Lakhani A.A. and Jandl S., Solid State Communication, **35**, 301 (1980)

19. Patel J.B., Parmar M.N., Deshpande M.P., Solanki G.K. and Agarwal M.K., Journal of Pure & Applied Physics **43**, 527 (2005)